

IMPROVING OPERATIONAL PERFORMANCE OF ANTENNAS ON
COMPLEX PLATFORMS BY ARRANGING THEIR PLACEMENTS

A THESIS SUBMITTED TO
THE GRADUATE SCHOOL OF NATURAL AND APPLIED SCIENCES
OF
MIDDLE EAST TECHNICAL UNIVERSITY

BY

CAN BAYSEFEROĞULLARI

IN PARTIAL FULFILLMENT OF THE REQUIREMENTS
FOR
THE DEGREE OF MASTER OF SCIENCE
IN
ELECTRICAL AND ELECTRONICS ENGINEERING

DECEMBER 2010

Approval of the thesis:

**IMPROVING OPERATIONAL PERFORMANCE OF ANTENNAS ON
COMPLEX PLATFORMS BY ARRANGING THEIR PLACEMENTS**

submitted by **CAN BAYSEFEROĞULLARI** in partial fulfillment of the requirements for the degree of **Master of Science in Electrical and Electronics Engineering Department, Middle East Technical University** by,

Prof. Dr. Canan Özgen _____
Dean, Graduate School of **Natural and Applied Sciences**

Prof. Dr. İsmet Erkmen _____
Head of Department, **Electrical and Electronics Engineering**

Prof. Dr. Gülbin Dural _____
Supervisor, **Electrical and Electronics Engineering Dept., METU**

Examining Committee Members:

Prof. Dr. Tuncay Birand _____
Electrical and Electronics Engineering Dept., METU

Prof. Dr. Gülbin Dural _____
Electrical and Electronics Engineering Dept., METU

Prof. Dr. Sencer Koç _____
Electrical and Electronics Engineering Dept., METU

Prof. Dr. Özlem Aydın Çivi _____
Electrical and Electronics Engineering Dept., METU

M.Sc. Hacı Pınarbaşı _____
ASELSAN AŞ

Date: 14/12/2010

I hereby declare that all information in this document has been obtained and presented in accordance with academic rules and ethical conduct. I also declare that, as required by these rules and conduct, I have fully cited and referenced all material and results that are not original to this work.

Name, Last name : CAN BAYSEFEROĞULLARI

Signature :

ABSTRACT

IMPROVING OPERATIONAL PERFORMANCE OF ANTENNAS ON COMPLEX PLATFORMS BY ARRANGING THEIR PLACEMENTS

Bayseferoğulları, Can

M.Sc., Department of Electrical and Electronics Engineering

Supervisor: Prof. Dr. Gülbin Dural

December 2010, 139 pages

The aim of this thesis is to improve the operational performance of the communication antennas mounted on complex platforms such as aircrafts and warships by arranging placements of these antennas.

Towards this aim, primarily, in order to gain insight on the influence of geometrically simple structures composing the platform on antenna performance, a quarter wavelength monopole antenna placed at the center of a finite square ground plane is studied by using uniform Geometrical Theory of Diffraction (GTD). Besides, the change of far field radiation pattern and complex diffraction functions due to the variation of the width of a square ground plane is examined.

Secondly, electromagnetic analysis of two Ultra High Frequency (UHF) antennas mounted on geometrically simple structures composing simplified F-4 aircraft is

carried out by using transient solver of Computer Simulation Technology (CST) Microwave Studio[®] (MWS), in order to conceive the influence of each structure on antenna performance. Then, electromagnetic analysis of these antennas mounted on simplified and original F-4 aircrafts is performed, in order to determine the optimal location of the lower UHF antenna (newly installed antenna) for the operational performance of this antenna to be optimum in terms of electromagnetic coupling and far field radiation pattern.

Finally, electromagnetic analysis of the communication antennas mounted on a warship is performed by using transient solver of CST MWS[®], in order to determine the optimal locations of these antennas for the operational performance of these antennas to be optimum in terms of electromagnetic coupling and far field radiation pattern.

Keywords: Operational performance of antennas, electromagnetic coupling, far field radiation pattern, complex platforms, antenna placement.

ÖZ

KARMAŞIK PLATFORMLAR ÜZERİNDEKİ ANTENLERİN ÇALIŞMA PERFORMANSLARININ YERLEŞİMLERİNİN DÜZENLENEREK İYİLEŞTİRİLMESİ

Bayseferoğulları, Can

Yüksek Lisans, Elektrik ve Elektronik Mühendisliği Bölümü

Tez Yöneticisi: Prof. Dr. Gülbin Dural

Aralık 2010, 139 sayfa

Bu tezin amacı, uçaklar ve savaş gemileri gibi karmaşık platformlar üzerine monte edilen haberleşme antenlerinin yerleşimlerini düzenleyerek, bu antenlerin çalışma performanslarını iyileştirmektir.

Bu amaç doğrultusunda, öncelikle, platformu oluşturan basit geometrik yapıların anten performansı üzerindeki etkisine yönelik kavrayış kazanabilmek için, sonlu kare iletken düzlemin merkezine yerleştirilen çeyrek dalga boyu uzunluğundaki monopol anten, düzgün Geometrik Saçınım Kuramı (GTD) tekniği kullanılarak incelenmiştir. Ayrıca antenin, uzak alan ışınım örüntüsünün ve karmaşık kırınım fonksiyonlarının, kare iletken düzlemin boyutlarına bağlı olarak değişimleri incelenmiştir.

İkinci olarak, basitleştirilmiş F-4 uçağını oluşturan her bir basit geometrik yapının anten performansı üzerindeki etkisini kavrayabilmek için, uçağın temel yapısını oluşturan gövde üzerine bu geometrik yapılar sırayla monte edilip, her seferinde oluşan yapı üzerine yerleştirilen iki UHF antenin elektromanyetik analizi, CST MWS[®] yazılımının “Transient Solver” çözücüsü kullanılarak gerçekleştirilmiştir. Ondan sonra, esas F-4 uçağına yeni yerleştirilen alt UHF anteni için, bu antenin çalışma performansının elektromanyetik bağlaşım ve uzak alan ışımaya örüntüsü açısından optimum olmasına yönelik, platform üzerinde en uygun konumun belirlenmesi amacıyla, basitleştirilmiş ve esas F-4 uçakları üzerine monte edilen bu UHF antenlerin elektromanyetik analizi gerçekleştirilmiştir.

Son olarak, bir savaş gemisi üzerine monte edilen haberleşme antenleri için, bu antenlerin çalışma performanslarının elektromanyetik bağlaşım ve uzak alan ışımaya örüntüsü açısından optimum olmasına yönelik, platform üzerinde en uygun konumların belirlenmesi amacıyla, bu savaş gemisi üzerindeki haberleşme antenlerinin elektromanyetik analizi, CST MWS[®] yazılımının “Transient Solver” çözücüsü kullanılarak gerçekleştirilmiştir.

Anahtar kelimeler: Antenlerin çalışma performansları, elektromanyetik bağlaşım, uzak alan ışımaya örüntüsü, karmaşık platformlar, anten yerleşimi.

ACKNOWLEDGEMENTS

I would like to express my greatest gratitude to my supervisor Prof. Dr. Gülbin Dural, for her guidance, support, insight, understanding and tolerance throughout this thesis study.

I wish to thank Prof. Dr. Tuncay Birand, for his precious ideas and suggestions throughout this thesis study.

I appreciate my friend and colleague Ali Dinçer for his help on writing MATLAB[®] computer program of uniform GTD in Chapter 2.

I wish to tender my thanks to Dr. Uğur Dalı for encouraging me to get involved in the study of antennas mounted on the warship.

I wish to thank my friends and colleagues Mustafa Ural and Gönenç Afacan who never let me lose my motivation and energy, regardless of any circumstance.

I am also grateful for ASELSAN Inc. for providing the necessary platform for my research and computational activities.

I would also like to thank TÜBİTAK for supporting financially this thesis work.

My deepest and dearest gratitude goes to my family and to my love Elçin Ülker for their endless encouragement and love.

TABLE OF CONTENTS

| | |
|-------------------------|------|
| ABSTRACT | iv |
| ÖZ | vi |
| ACKNOWLEDGEMENTS | viii |
| TABLE OF CONTENTS | ix |
| LIST OF TABLES | xi |
| LIST OF FIGURES..... | xii |

CHAPTERS

| | |
|--|----|
| 1. INTRODUCTION..... | 1 |
| 2. ANALYSIS OF A MONOPOLE ANTENNA ON A SQUARE GROUND PLANE..... | 4 |
| 2.1. A Brief Introduction to GO and GTD | 5 |
| 2.2. Determination of Far Field Radiation Pattern of a Quarter Wavelength Monopole Mounted on a Finite Square Ground Plane by the Use of Uniform GTD and GO | 7 |
| 2.2.1. Examination of the Change of Far Field Radiation Pattern of the Monopole Antenna and Complex Diffraction Functions Due to the Variation of the Width of a Finite Square Ground Plane..... | 15 |
| 3. ANALYSIS OF ANTENNAS MOUNTED ON F-4 AIRCRAFT | 31 |
| 3.1. Analysis of Antennas on the Main Fuselage..... | 38 |
| 3.2. Analysis of Antennas on the Main Fuselage and Nose..... | 45 |
| 3.3. Analysis of Antennas on the Main Fuselage, Nose and Wings | 57 |
| 3.4. Analysis of Antennas on the Simplified F-4 Aircraft | 70 |
| 3.5. Analysis of Antennas on the Original F-4 Aircraft..... | 82 |
| 4. ANALYSIS OF ANTENNAS MOUNTED ON WARSHIP..... | 90 |

| | | |
|--------|---|-----|
| 4.1. | Analysis of HF Antennas | 94 |
| 4.2. | Analysis of VHF and V/UHF Antennas..... | 111 |
| 4.2.1. | Coupling between V/UHF 1 and V/UHF 2 Antennas..... | 113 |
| 4.2.2. | Coupling between V/UHF 1 and VHF 1 Antennas..... | 113 |
| 4.2.3. | Coupling between V/UHF 1 and VHF 2 Antennas..... | 114 |
| 4.2.4. | Coupling between V/UHF 2 and VHF 1 Antennas..... | 115 |
| 4.2.5. | Coupling between V/UHF 2 and VHF 2 Antennas..... | 116 |
| 4.2.6. | Coupling between VHF 1 and VHF 2 Antennas..... | 117 |
| 4.2.7. | The Optimal Placement Plan for VHF and V/UHF Antennas | 118 |
| 4.3. | The Optimal Placement Plan for HF, VHF and V/UHF Antennas | 132 |
| 5. | CONCLUSIONS AND FUTURE STUDIES | 134 |
| 6. | REFERENCES..... | 138 |

LIST OF TABLES

TABLES

| | |
|---|-----|
| Table 4-1 Properties of the Communication Antennas Mounted on the Warship . | 91 |
| Table 4-2 The Interaction Matrix of HF, VHF and V/UHF Antennas..... | 92 |
| Table 4-3 Mean Values of Coupling Levels for the First Seven Plans..... | 101 |
| Table 4-4 Mean Values of Coupling Levels for the Last Four Plans..... | 102 |
| Table 4-5 Results of Percentage of Coverage of HF Antennas for Plan 9..... | 111 |
| Table 4-6 Mean Values of Coupling Levels for Four Placement Plans..... | 122 |
| Table 4-7 Results of Percentage of Coverage of VHF and V/UHF Antennas for Plan 4..... | 129 |

LIST OF FIGURES

FIGURES

| | |
|--|----|
| Figure 2-1 $\lambda/4$ Monopole Antenna Mounted on the Center of a Finite Square Ground Plane..... | 7 |
| Figure 2-2 Radiation Mechanisms of the Direct, Reflected and Diffracted Fields.. | 9 |
| Figure 2-3 The Normalized Amplitude Pattern of the Total Field in the Principal Plane of Observation Calculated by the Written MATLAB [®] Computer Program | 13 |
| Figure 2-4 The Experimental and the Theoretical Normalized Amplitude Patterns of a $\lambda/4$ Monopole Antenna on Infinite and Finite Square Ground Planes in the Principal Plane of Observation Obtained by Balanis..... | 14 |
| Figure 2-5 The Normalized Amplitude Pattern of the Total Field ($w = 0.61$ m)... | 16 |
| Figure 2-6 The Magnitude of the Diffraction Function from Edge 1 ($w = 0.61$ m) | 16 |
| Figure 2-7 The Magnitude of the Diffraction Function from Edge 2 ($w = 0.61$ m) | 17 |
| Figure 2-8 The Normalized Amplitude Pattern of the Total Field ($w = 1.22$ m)... | 17 |
| Figure 2-9 The Magnitude of the Diffraction Function from Edge 1 ($w = 1.22$ m) | 18 |
| Figure 2-10 The Magnitude of the Diffraction Function from Edge 2 ($w = 1.22$ m) | 18 |
| Figure 2-11 The Normalized Amplitude Pattern of the Total Field ($w = 2.44$ m). | 19 |
| Figure 2-12 The Magnitude of the Diffraction Function from Edge 1 ($w = 2.44$ m) | 19 |
| Figure 2-13 The Magnitude of the Diffraction Function from Edge 2 ($w = 2.44$ m) | 20 |
| Figure 2-14 The Normalized Amplitude Pattern of the Total Field ($w = 10$ m).... | 20 |
| Figure 2-15 The Magnitude of the Diffraction Function from Edge 1 ($w = 10$ m) | 21 |
| Figure 2-16 The Magnitude of the Diffraction Function from Edge 2 ($w = 10$ m) | 21 |
| Figure 2-17 The Normalized Amplitude Pattern of the Total Field ($w = 100$ m).. | 22 |

| | |
|---|----|
| Figure 2-18 The Magnitude of the Diffraction Function from Edge 1 ($w = 100$ m) | 22 |
| | |
| Figure 2-19 The Magnitude of the Diffraction Function from Edge 2 ($w = 100$ m) | 23 |
| | |
| Figure 2-20 $\lambda/4$ Monopole above a Finite Square Ground Plane ($w = 0.61$ m)..... | 27 |
| Figure 2-21 $\lambda/4$ Monopole above a Finite Square Ground Plane ($w = 1.22$ m)..... | 27 |
| Figure 2-22 $\lambda/4$ Monopole above a Finite Square Ground Plane ($w = 2.44$ m)..... | 28 |
| Figure 2-23 The Far Field Radiation Pattern of the Electric Field ($w = 0.61$ m)... | 28 |
| Figure 2-24 The Far Field Radiation Pattern of the Electric Field ($w = 1.22$ m)... | 29 |
| Figure 2-25 The Far Field Radiation Pattern of the Electric Field ($w = 2.44$ m)... | 29 |
| Figure 3-1 The Location of the Upper UHF Antenna on F-4 Aircraft..... | 32 |
| Figure 3-2 First Location of the Lower UHF Antenna Denoted as Antenna #7 | 32 |
| Figure 3-3 Second Location of the Lower UHF Antenna Denoted as Antenna #10 | 33 |
| | |
| Figure 3-4 Third Location of the Lower UHF Antenna Denoted as Antenna #11 | 33 |
| Figure 3-5 Fourth Location of the Lower UHF Antenna Denoted as Antenna #12 | 34 |
| | |
| Figure 3-6 The Simplified F-4 Model Built Based on the Original F-4 Model..... | 35 |
| Figure 3-7 Four Different Structures on which Antenna Analysis Performed | 36 |
| Figure 3-8 The Lower (#7) and Upper (#1) UHF Antennas on the Main Fuselage | 39 |
| Figure 3-9 Coupling ($S_{1,7}$) between the Lower and Upper UHF Antennas..... | 39 |
| Figure 3-10 Polar Radiation Pattern of the Lower UHF Antenna (#7) in x-y Plane | 40 |
| | |
| Figure 3-11 Polar Radiation Pattern of the Lower UHF Antenna (#7) in x-z Plane | 41 |
| | |
| Figure 3-12 Polar Radiation Pattern of the Lower UHF Antenna (#7) in y-z Plane | 41 |
| | |
| Figure 3-13 3D Radiation Pattern of the Lower UHF Antenna (#7) | 42 |
| Figure 3-14 3D Radiation Pattern of the Lower UHF Antenna (#7) | 42 |
| Figure 3-15 The Lower (#7) and Upper (#1) UHF Antennas on the Main Fuselage and the Nose | 46 |

| | |
|--|----|
| Figure 3-16 The Lower (#10) and Upper (#1) UHF Antennas on the Main Fuselage and the Nose | 46 |
| Figure 3-17 The Lower (#11) and Upper (#1) UHF Antennas on the Main Fuselage and the Nose | 46 |
| Figure 3-18 The Lower (#12) and Upper (#1) UHF Antennas on the Main Fuselage and the Nose | 46 |
| Figure 3-19 Coupling Levels – $S_{1,7}$, $S_{1,10}$, $S_{1,11}$ and $S_{1,12}$ | 47 |
| Figure 3-20 Polar Radiation Patterns of the Lower UHF Antenna in x-y Plane.... | 49 |
| Figure 3-21 Polar Radiation Patterns of the Lower UHF Antenna in x-z Plane.... | 50 |
| Figure 3-22 Polar Radiation Patterns of the Lower UHF Antenna in y-z Plane.... | 50 |
| Figure 3-23 3D Radiation Pattern of the Lower UHF Antenna (#7) | 51 |
| Figure 3-24 3D Radiation Pattern of the Lower UHF Antenna (#7) | 51 |
| Figure 3-25 3D Radiation Pattern of the Lower UHF Antenna (#10) | 52 |
| Figure 3-26 3D Radiation Pattern of the Lower UHF Antenna (#10) | 52 |
| Figure 3-27 3D Radiation Pattern of the Lower UHF Antenna (#11) | 53 |
| Figure 3-28 3D Radiation Pattern of the Lower UHF Antenna (#11) | 53 |
| Figure 3-29 3D Radiation Pattern of the Lower UHF Antenna (#12) | 54 |
| Figure 3-30 3D Radiation Pattern of the Lower UHF Antenna (#12) | 54 |
| Figure 3-31 The Lower (#7) and Upper (#1) UHF Antennas on the Main Fuselage, the Nose and the Wings..... | 58 |
| Figure 3-32 The Lower (#10) and Upper (#1) UHF Antennas on the Main Fuselage, the Nose and the Wings | 58 |
| Figure 3-33 The Lower (#11) and Upper (#1) UHF Antennas on the Main Fuselage, the Nose and the Wings | 58 |
| Figure 3-34 The Lower (#12) and Upper (#1) UHF Antennas on the Main Fuselage, the Nose and the Wings | 58 |
| Figure 3-35 Coupling Levels – $S_{1,7}$, $S_{1,10}$, $S_{1,11}$ and $S_{1,12}$ | 59 |
| Figure 3-36 Polar Radiation Patterns of the Lower UHF Antenna in x-y Plane.... | 61 |
| Figure 3-37 Polar Radiation Patterns of the Lower UHF Antenna in x-z Plane.... | 62 |
| Figure 3-38 Polar Radiation Patterns of the Lower UHF Antenna in y-z Plane.... | 62 |
| Figure 3-39 3D Radiation Pattern of the Lower UHF Antenna (#7) | 63 |

| | |
|--|----|
| Figure 3-40 3D Radiation Pattern of the Lower UHF Antenna (#7) | 63 |
| Figure 3-41 3D Radiation Pattern of the Lower UHF Antenna (#10) | 64 |
| Figure 3-42 3D Radiation Pattern of the Lower UHF Antenna (#10) | 64 |
| Figure 3-43 3D Radiation Pattern of the Lower UHF Antenna (#11) | 65 |
| Figure 3-44 3D Radiation Pattern of the Lower UHF Antenna (#11) | 65 |
| Figure 3-45 3D Radiation Pattern of the Lower UHF Antenna (#12) | 66 |
| Figure 3-46 3D Radiation Pattern of the Lower UHF Antenna (#12) | 66 |
| Figure 3-47 The Lower (#7) and Upper (#1) UHF Antennas on the Simplified F-4 Aircraft | 70 |
| Figure 3-48 The Lower (#10) and Upper (#1) UHF Antennas on the Simplified F-4 Aircraft | 70 |
| Figure 3-49 The Lower (#11) and Upper (#1) UHF Antennas on the Simplified F-4 Aircraft | 71 |
| Figure 3-50 The Lower (#12) and Upper (#1) UHF Antennas on the Simplified F-4 Aircraft | 71 |
| Figure 3-51 Coupling Levels – $S_{1,7}$, $S_{1,10}$, $S_{1,11}$ and $S_{1,12}$ | 72 |
| Figure 3-52 Polar Radiation Patterns of the Lower UHF Antenna in x-y Plane.... | 74 |
| Figure 3-53 Polar Radiation Patterns of the Lower UHF Antenna in x-z Plane.... | 74 |
| Figure 3-54 Polar Radiation Patterns of the Lower UHF Antenna in y-z Plane.... | 75 |
| Figure 3-55 3D Radiation Pattern of the Lower UHF Antenna (#7) | 75 |
| Figure 3-56 3D Radiation Pattern of the Lower UHF Antenna (#7) | 76 |
| Figure 3-57 3D Radiation Pattern of the Lower UHF Antenna (#10) | 76 |
| Figure 3-58 3D Radiation Pattern of the Lower UHF Antenna (#10) | 77 |
| Figure 3-59 3D Radiation Pattern of the Lower UHF Antenna (#11) | 77 |
| Figure 3-60 3D Radiation Pattern of the Lower UHF Antenna (#11) | 78 |
| Figure 3-61 3D Radiation Pattern of the Lower UHF Antenna (#12) | 78 |
| Figure 3-62 3D Radiation Pattern of the Lower UHF Antenna (#12) | 79 |
| Figure 3-63 The Lower (#7) and Upper (#1) UHF Antennas on the Original F-4 Aircraft | 82 |
| Figure 3-64 The Lower (#10) and Upper (#1) UHF Antennas on the Original F-4 Aircraft | 83 |

| | |
|--|-----|
| Figure 3-65 The Lower (#11) and Upper (#1) UHF Antennas on the Original F-4 Aircraft | 83 |
| Figure 3-66 The Lower (#12) and Upper (#1) UHF Antennas on the Original F-4 Aircraft | 83 |
| Figure 3-67 Coupling Levels – $S_{1,7}$, $S_{1,10}$, $S_{1,11}$ and $S_{1,12}$ | 84 |
| Figure 3-68 3D Radiation Pattern of the Lower UHF Antenna (#7) | 87 |
| Figure 3-69 3D Radiation Pattern of the Lower UHF Antenna (#7) | 88 |
| Figure 3-70 3D Radiation Pattern of the Lower UHF Antenna above Infinite Ground Plane..... | 88 |
| Figure 4-1 The Warship on which Analysis of Antennas Performed | 90 |
| Figure 4-2 Placement Plan 1 for HF Antennas | 95 |
| Figure 4-3 Placement Plan 2 for HF Antennas | 95 |
| Figure 4-4 Placement Plan 3 for HF Antennas | 96 |
| Figure 4-5 Placement Plan 4 for HF Antennas | 96 |
| Figure 4-6 Placement Plan 5 for HF Antennas | 97 |
| Figure 4-7 Placement Plan 6 for HF Antennas | 97 |
| Figure 4-8 Placement Plan 7 for HF Antennas | 98 |
| Figure 4-9 Placement Plan 8 for HF Antennas | 98 |
| Figure 4-10 Placement Plan 9 for HF Antennas | 99 |
| Figure 4-11 Placement Plan 10 for HF Antennas | 99 |
| Figure 4-12 Placement Plan 11 for HF Antennas | 100 |
| Figure 4-13 Coupling Levels for the First Seven Placement Plans..... | 101 |
| Figure 4-14 Coupling Levels for the Last Four Placement Plans | 102 |
| Figure 4-15 3D Radiation Pattern of HF 1 Antenna at 6 MHz – Plan 9 | 104 |
| Figure 4-16 3D Radiation Pattern of HF 2 Antenna at 6 MHz – Plan 9 | 105 |
| Figure 4-17 3D Radiation Pattern of HF 1 Antenna at 18 MHz – Plan 9 | 105 |
| Figure 4-18 3D Radiation Pattern of HF 2 Antenna at 18 MHz – Plan 9 | 106 |
| Figure 4-19 3D Radiation Pattern of HF 1 Antenna at 30 MHz – Plan 9 | 106 |
| Figure 4-20 3D Radiation Pattern of HF 2 Antenna at 30 MHz – Plan 9 | 107 |
| Figure 4-21 3D Radiation Pattern of HF 1 Antenna at 6 MHz – Above Infinite Ground Plane..... | 107 |

| | |
|--|-----|
| Figure 4-22 3D Radiation Pattern of HF 2 Antenna at 6 MHz – Above Infinite Ground Plane..... | 108 |
| Figure 4-23 3D Radiation Pattern of HF 1 Antenna at 18 MHz – Above Infinite Ground Plane..... | 108 |
| Figure 4-24 3D Radiation Pattern of HF 2 Antenna at 18 MHz – Above Infinite Ground Plane..... | 109 |
| Figure 4-25 3D Radiation Pattern of HF 1 Antenna at 30 MHz – Above Infinite Ground Plane..... | 109 |
| Figure 4-26 3D Radiation Pattern of HF 2 Antenna at 30 MHz – Above Infinite Ground Plane..... | 110 |
| Figure 4-27 Placement Plan 1 for VHF and V/UHF Antennas..... | 111 |
| Figure 4-28 Placement Plan 2 for VHF and V/UHF Antennas..... | 112 |
| Figure 4-29 Placement Plan 3 for VHF and V/UHF Antennas..... | 112 |
| Figure 4-30 Placement Plan 4 for VHF and V/UHF Antennas..... | 112 |
| Figure 4-31 Coupling Levels between V/UHF 1 and V/UHF 2 Antennas | 113 |
| Figure 4-32 Coupling Levels between V/UHF 1 and VHF 1 Antennas | 114 |
| Figure 4-33 Coupling Levels between V/UHF 1 and VHF 2 Antennas | 115 |
| Figure 4-34 Coupling Levels between V/UHF 2 and VHF 1 Antennas | 116 |
| Figure 4-35 Coupling Levels between V/UHF 2 and VHF 2 Antennas | 117 |
| Figure 4-36 Coupling Levels between VHF 1 and VHF 2 Antennas | 118 |
| Figure 4-37 3D Radiation Pattern of V/UHF 1 Antenna at 150 MHz – Plan 4 (1 st Angle of View)..... | 124 |
| Figure 4-38 3D Radiation Pattern of V/UHF 1 Antenna at 150 MHz – Plan 4 (2 nd Angle of View)..... | 125 |
| Figure 4-39 3D Radiation Pattern of V/UHF 1 Antenna at 300 MHz – Plan 4 (1 st Angle of View)..... | 125 |
| Figure 4-40 3D Radiation Pattern of V/UHF 1 Antenna at 300 MHz – Plan 4 (2 nd Angle of View)..... | 126 |
| Figure 4-41 3D Radiation Pattern of V/UHF 1 Antenna at 150 MHz – Above Infinite Ground Plane..... | 126 |

| | |
|--|-----|
| Figure 4-42 3D Radiation Pattern of V/UHF 1 Antenna at 300 MHz – Above Infinite Ground Plane | 127 |
| Figure 4-43 3D Radiation Pattern of VHF 1 Antenna at 150 MHz – Plan 4 (1 st Angle of View)..... | 127 |
| Figure 4-44 3D Radiation Pattern of VHF 1 Antenna at 150 MHz – Plan 4 (2 nd Angle of View)..... | 128 |
| Figure 4-45 3D Radiation Pattern of VHF 1 Antenna at 150 MHz – Above Infinite Ground Plane..... | 128 |
| Figure 4-46 Polar Radiation Pattern of V/UHF 1 Antenna in y-z Plane – Plan 4 (at 150 MHz) | 131 |
| Figure 4-47 Polar Radiation Pattern of V/UHF 1 Antenna in y-z Plane – Plan 4 (at 300 MHz) | 131 |
| Figure 4-48 Polar Radiation Pattern of VHF 1 Antenna in y-z Plane – Plan 4 (at 150 MHz) | 132 |
| Figure 4-49 The Optimal Placement Plan for HF, VHF and V/UHF Antennas .. | 133 |

CHAPTER 1

INTRODUCTION

There are many communication, navigation and identification systems which may have antennas mounted on aircrafts or ships. Among these systems, especially the operational frequency bands of the communication systems placed in the same platform generally coincide with each other and these communication systems may operate at the same time.

Due to the electromagnetic coupling between the antennas of the communication systems, Electromagnetic Interference (EMI) can occur between these systems. This EMI problem results in degradation of the operational performance of these systems, which is unacceptable for ensuring intra-system Electromagnetic Compatibility (EMC) within the platform. In order to resolve this problem, it is crucial to decrease the electromagnetic coupling between the communication antennas whose operational frequency bands coincide with each other. Therefore, decreasing the electromagnetic coupling between these antennas as much as possible by arranging their placements on the platform is the primary criterion for improving the operational performance of these antennas.

In addition, antennas may interact with their platforms which are usually conducting structures resulting in strong scattered fields degrading the performance of the antennas. Because of this, although the electromagnetic coupling levels between the related communication antennas are minimal, the far

field radiation characteristics of the antennas may be far beyond the desired properties. Therefore, at the locations, where the electromagnetic coupling levels between the related communication antennas are minimal, whether the far field radiation pattern of each antenna on the platform has sufficient directivity values in the region where the antenna has to operate efficiently shall be investigated.

On the subject of antenna placement on platforms, Afacan [1] carried out simulations of antennas mounted on F-4 aircraft by using transient solver of Computer Simulation Technology (CST) Microwave Studio[®] (MWS). As a result of these simulations, he obtained electromagnetic coupling levels between the antennas and obtained the radiation patterns of these antennas for different locations. Besides, he performed antenna coupling measurements on a 1:10 down-scaled F-4 aircraft model, in order to examine the accuracy of the results obtained from the simulations. Finally, he observed that there is a very good agreement between the coupling results of simulations and those of measurements.

In this thesis study, the optimal locations of the antennas of the communication systems mounted on F-4 aircraft and warship are determined on the basis of the reduction of electromagnetic coupling and the sufficiency of far field radiation patterns, in order to improve the operational performance of these antennas among the predetermined possible locations. Within this context;

- In Chapter 2, in order to examine the influence of the physical characteristics of geometrically simple structures composing the platform on performance of antennas, first, far field radiation pattern of a quarter wavelength monopole antenna mounted on a finite square ground plane is studied by means of uniform Geometrical Theory of Diffraction (GTD) and Geometrical Optics (GO) high frequency asymptotic techniques. Besides, the change of far field radiation pattern of the antenna and complex diffraction functions due to the variation of the width of a finite square ground plane is examined. Motivation of this study is to gain insight about

the basic scattering mechanisms as much as being familiar with the effect of the planar conducting platforms on performance of the antennas.

- In Chapter 3, electromagnetic analysis of two Ultra High Frequency (UHF) antennas mounted on simplified and original F-4 aircrafts is carried out by using transient solver of CST MWS[®], in order to determine the optimal location of the lower UHF antenna (newly installed antenna) for the operational performance of this antenna to be optimum in terms of the reduction of electromagnetic coupling and the sufficiency of far field radiation pattern. Towards this aim, in order to conceive how the electromagnetic coupling between UHF antennas and the far field radiation patterns of the lower UHF antenna are affected due to the geometrically simple structures composing simplified F-4 aircraft and the locations of UHF antennas, electromagnetic analysis of these UHF antennas mounted on geometrically simple structures is also performed.
- In Chapter 4, electromagnetic analysis of High Frequency (HF), Very High Frequency (VHF) and Very/Ultra High Frequency (V/UHF) antennas mounted on warship is performed by using transient solver of CST MWS[®], in order to determine the optimal locations of these antennas for the operational performance of these antennas to be optimum in terms of the reduction of electromagnetic coupling and the sufficiency of far field radiation patterns. Moreover, the influences of the structural components such as mainmast, topmast, main yard and bridge of warship, the locations of these antennas and the sea on the electromagnetic coupling between the related antennas and the far field radiation patterns of VHF and V/UHF antennas are examined.
- Finally, the general conclusions obtained within the scope of this thesis study are summarized in Chapter 5. Besides, future studies which can be carried out based on this thesis study are discussed.

CHAPTER 2

ANALYSIS OF A MONOPOLE ANTENNA ON A SQUARE GROUND PLANE

In order to succeed in improving the operational performance of antennas mounted on platforms such as aircrafts and ships which are composed of complex geometrical structures, it is important to examine the influence of basic structural components composing the platform on antenna performance.

Basic structural components composing platforms such as aircrafts and ships analyzed in this thesis are generally planar, cylindrical and conical structures. Therefore, so as to comprehend the effect of platform structure and size on performance of antennas and to determine antenna placement properly for obtaining the best performance of antennas, primarily, it is crucial to understand how performance of antennas mounted on geometrically simple conducting platforms is affected due to the physical characteristics of these structures. In this chapter, far field radiation pattern of a quarter wavelength monopole antenna mounted on a finite square ground plane is examined in the principal planes, by means of uniform GTD and GO which are high frequency asymptotic techniques, used to analyze radiation and scattering mechanisms from electrically large structures. Because, a conducting plane is considered to be a good representative to understand the basic scattering mechanisms from planar conducting structures such as wings of an aircraft, ship platforms etc.

In the scope of this study, also, the change of far field radiation pattern (elevation plane pattern, in the principal planes) of the antenna and complex diffraction functions due to the variation of the width of a finite square ground plane is examined. Before handling this problem, basics of GO and uniform GTD were studied. Also, to be able to solve this problem by using uniform GTD, straight edge diffraction of electromagnetic wave incident normally and obliquely on the edge was studied.

2.1. A Brief Introduction to GO and GTD

GO is a high frequency technique used to examine electromagnetic wave propagation of incident, reflected and refracted rays. However, GO has a major deficiency that diffraction mechanism can not be treated with the use of GO.

In order to come up with this deficiency, GTD, developed by Keller [2, 3] and enhanced by Kouyoumjian and Pathak [4-7], which is a high frequency asymptotic technique, is used to determine electromagnetic wave propagation of diffracted rays that are generated by electromagnetic waves incident on the edges, corners, vertices of the radiating or scattering object of interest and electromagnetic waves grazing boundary surfaces of this object [3]. Keller's diffraction functions of GTD include singularities along the incident and reflection shadow boundaries, whereas the diffraction functions of uniform GTD are continuous along these shadow boundaries [8].

Diffraction is a local phenomenon at high frequencies, such as reflection and refraction, and it is based on the following two matters [8]:

1. The geometrical shape of the radiating or scattering object at the point of diffraction (edge, vertex, curved surface).

2. The amplitude, phase and polarization of the incident electromagnetic wave at the point of diffraction.

At an observation point, the total field is dependent on all diffracted rays and equal to the sum of all of the rays passing through this point. The field intensity at an observation point within the shadow region is dependent on diffracted rays penetrating into the shadow region. The diffracted field established by a generalization of Fermat's Principle [3, 4] is triggered at points on the surface of the radiating or scattering object that generate a discontinuity in the incident GO field at incident and reflection shadow boundaries.

The phase of the field on a ray is supposed to be equal to the product of the optical length of the ray from the reference point determined and the wave number of the medium. Besides, the amplitude of the field on a ray is supposed to vary according to the principle of conservation of energy in a narrow tube of rays.

Based on the electromagnetic wave incident on the radiating or scattering object and a convenient diffraction coefficient which is a dyadic for electromagnetic fields, the initial value of the field on a diffracted ray is determined. This is similar to the approach that reflected fields are established by the use of the reflection coefficient.

The rays travel through the paths such that the optical distance between the source and the observation point is extremum (usually a minimum), which results rays to propagate along straight lines within homogeneous media and along geodesics on smooth surfaces of the object of interest.

2.2. Determination of Far Field Radiation Pattern of a Quarter Wavelength Monopole Mounted on a Finite Square Ground Plane by the Use of Uniform GTD and GO

Far field radiation pattern of a quarter wavelength ($\lambda/4$) monopole antenna mounted on the center of a finite square ground plane, whose sidelength is w , is determined in the principal planes (y - z or x - z planes), by means of uniform GTD and GO [8]. Moreover, the change of far field radiation pattern (elevation plane pattern, in the principal planes) of the monopole antenna and complex diffraction functions due to the variation of the width of a finite square ground plane is examined. The geometry of the problem is shown in Figure 2-1.

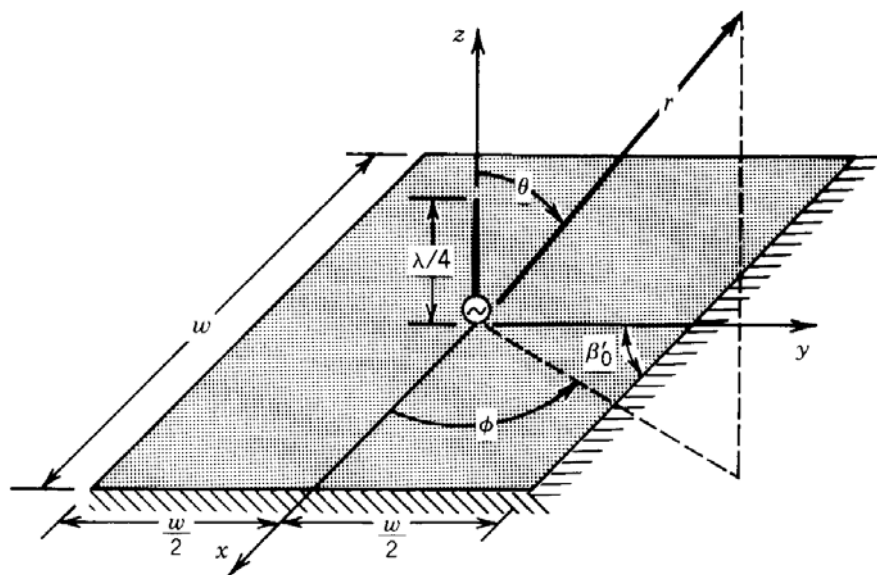


Figure 2-1 $\lambda/4$ Monopole Antenna Mounted on the Center of a Finite Square Ground Plane [8]

The formulations of the diffracted fields, diffraction functions and coefficients, which are used in the scope of the solution of this problem, are based on the formulations included in the section [8], named as “Geometrical Theory of Diffraction: Edge Diffraction”, involving mainly the subsections of straight edge diffraction of electromagnetic wave incident normally and obliquely on the edge.

Besides, in order to perform all computations of the diffracted fields, diffraction functions and coefficients existing within the solution of this problem, a MATLAB[®] computer program was written on the basis of the FORTRAN computer subroutine [8], namely Wedge Diffraction Coefficient (WDC), computing the normalized (with respect to square root of λ) wedge diffraction coefficients based on the formulations included in the subsection [8] of straight edge diffraction of electromagnetic wave incident obliquely on the edge.

The total field at an observation point is the sum of the total GO field, which comprises of the direct and reflected fields, and diffracted fields from the edges of the square ground plane. The radiation mechanisms of the direct, reflected fields and diffracted fields from the two edges, perpendicular to the principal plane including the observation point, are indicated in Figure 2-2.

It is obvious that among all diffracted fields from these two edges, only the diffracted fields from two points contribute to the total field at an observation point in the principal plane. These two points exist at the intersection of these edges with the principal plane of observation.

In order to obtain the incident and reflected fields, the ground plane is assumed to be infinite in extent. By the use of the coordinate system seen in Figure 2-1 and the image theory [8], the total GO field of the $\lambda/4$ monopole antenna mounted on the ground plane is written as [9]:

$$E_{\theta G}(r, \theta) = E_0 \left[\frac{\cos\left(\frac{\pi}{2} \cos \theta\right)}{\sin \theta} \right] \frac{e^{-j\beta r}}{r}, \quad 0 \leq \theta \leq \pi/2 \quad (2-1)$$

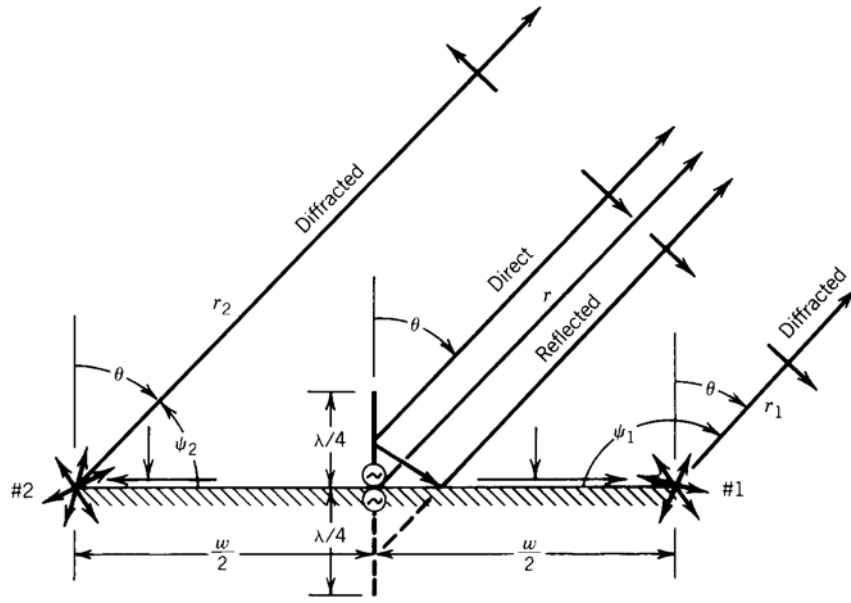


Figure 2-2 Radiation Mechanisms of the Direct, Reflected and Diffracted Fields [8]

The diffracted fields from edges 1 and 2 are obtained by the use of the formulations included in the subsection [8] of straight edge diffraction of electromagnetic wave incident obliquely on the edge.

With reference to the geometry in Figure 2-2, the direct field is incident normally ($\beta'_0 = \pi/2$) on the diffraction points occurring at the intersection of two edges with the principal plane of observation and therefore, the diffracted field from edge 1 is written as:

$$E_{\theta_1}^d(\theta) = E^i(Q_1)D_h(L, \xi_1^\pm, \beta'_0 = \pi/2, n=2)A_1(w, r_1)e^{-j\beta r_1} \quad (2-2)$$

It is assumed that the total field arises from the base of the monopole antenna. This is a good approach that concurs well with measurements. Therefore,

$$E^i(Q_1) = \frac{1}{2}E_{\theta G} \left(r = \frac{w}{2}, \theta = \frac{\pi}{2} \right) = \frac{E_0}{2} \frac{e^{-j\beta w/2}}{w/2} \quad (2-3)$$

$$D_h \left(L, \xi_1^\pm, \beta'_0 = \frac{\pi}{2}, n=2 \right) = D^i(L, \xi_1^-, n=2) + D^r(L, \xi_1^+, n=2) \quad (2-4)$$

Due to the fact that the waveform of the incident wave is spherical and observations are conducted in the far field region, the distance parameter L and spatial attenuation factor $A_1(w, r_1)$ are stated as:

$$L = s' \sin^2 \beta'_0 \Big|_{\substack{s'=w/2 \\ \beta'_0=\pi/2}} = \frac{w}{2} \quad (2-5)$$

$$A_1(w, r_1) = \frac{\sqrt{s'}}{s} \Big|_{\substack{s'=w/2 \\ s=r_1}} = \frac{\sqrt{w/2}}{r_1} \quad (2-6)$$

The angle of incidence ψ_0 from the base of the monopole antenna to the diffraction point Q_1 is zero degrees. Thus,

$$\xi_1^- = \psi_1 - \psi_0 = \psi_1 = \theta + \frac{\pi}{2} = \xi_1 \quad (2-7)$$

$$\xi_1^+ = \psi_1 + \psi_0 = \psi_1 = \theta + \frac{\pi}{2} = \xi_1 \quad (2-8)$$

Accordingly,

$$\begin{aligned} D_h\left(L, \xi_1^\pm, \beta'_0 = \frac{\pi}{2}, n = 2\right) &= 2D^i\left(\frac{w}{2}, \theta + \frac{\pi}{2}, n = 2\right) \\ &= 2D^r\left(\frac{w}{2}, \theta + \frac{\pi}{2}, n = 2\right) \end{aligned} \quad (2-9)$$

The diffracted field from edge 1 is written as:

$$\begin{aligned} E_{\theta 1}^d(\theta) &= \frac{E_0}{2} \frac{e^{-j\beta w/2}}{w/2} 2D^{i,r}\left(\frac{w}{2}, \theta + \frac{\pi}{2}, n = 2\right) \frac{\sqrt{w/2}}{r_1} e^{-j\beta r_1} \\ &= E_0 \left[\frac{e^{-j\beta w/2}}{\sqrt{w/2}} D^{i,r}\left(\frac{w}{2}, \theta + \frac{\pi}{2}, n = 2\right) \right] \frac{e^{-j\beta r_1}}{r_1} \end{aligned} \quad (2-10)$$

$$E_{\theta 1}^d(\theta) = E_0 V_B^{i,r}\left(\frac{w}{2}, \theta + \frac{\pi}{2}, n = 2\right) \frac{e^{-j\beta r_1}}{r_1} \quad (2-11)$$

By the use of a similar method, the diffracted field from edge 2 is written, with reference to the geometry in Figure 2-2, as:

$$E_{\theta 2}^d(\theta) = -E_0 \left[\frac{e^{-j\beta w/2}}{\sqrt{w/2}} D^{i,r}\left(\frac{w}{2}, \xi_2, n = 2\right) \right] \frac{e^{-j\beta r_2}}{r_2} \quad (2-12)$$

$$E_{\theta 2}^d(\theta) = -E_0 V_B^{i,r}\left(\frac{w}{2}, \xi_2, n = 2\right) \frac{e^{-j\beta r_2}}{r_2} \quad (2-13)$$

Where,

$$\xi_2 = \psi_2 = \begin{cases} \frac{\pi}{2} - \theta & 0 \leq \theta \leq \frac{\pi}{2} \\ \frac{5\pi}{2} - \theta & \frac{\pi}{2} < \theta < \pi \end{cases} \quad (2-14)$$

For the observations conducted in the far field region, the distance parameters (r_1 and r_2) are expressed as:

$$\text{For phase terms } \begin{cases} r_1 \cong r - \frac{w}{2} \cos\left(\frac{\pi}{2} - \theta\right) = r - \frac{w}{2} \sin \theta \\ r_2 \cong r + \frac{w}{2} \cos\left(\frac{\pi}{2} - \theta\right) = r + \frac{w}{2} \sin \theta \end{cases} \quad (2-15)$$

$$\text{For amplitude terms } r_1 \cong r_2 \cong r \quad (2-16)$$

Thus, the diffracted fields from edges 1 and 2 are written as:

$$E_{\theta 1}^d(\theta) = E_0 V_B^{i,r} \left(\frac{w}{2}, \theta + \frac{\pi}{2}, n = 2 \right) e^{j(\beta w/2) \sin \theta} \frac{e^{-j\beta r}}{r} \quad (2-17)$$

$$E_{\theta 2}^d(\theta) = -E_0 V_B^{i,r} \left(\frac{w}{2}, \xi_2, n = 2 \right) e^{-j(\beta w/2) \sin \theta} \frac{e^{-j\beta r}}{r} \quad (2-18)$$

On the other hand, there are diffractions due to the waves incident obliquely on the other two edges of the square ground plane, which are parallel to the principal plane of observation. Nevertheless, the diffracted field from these edges is principally cross-polarized to the incident field and the diffracted field generated in the principal plane, which is composed of E_ϕ component. The cross-polarized E_ϕ components composing the diffracted fields from these two edges neutralize each other and therefore, there is principally an E_θ component in the principal plane of observation.

As a result, the total field in the principal plane of observation is equal to the sum of the diffracted fields from edges 1 and 2 and the total GO field. The amplitude pattern of the total field, which is normalized with respect to maximum amplitude value in the principal plane of observation, is calculated for a $\lambda/4$ monopole

antenna mounted on the center of a finite square ground plane, whose sidelength w is 1.22 m (4.067λ), at 1 GHz frequency by the use of the written MATLAB[®] computer program. This amplitude pattern shown in Figure 2-3 is compared with the experimental and theoretical (GO and GTD) normalized amplitude patterns in Figure 2-4 [8].

Farfield Radiation Pattern of the Total E-Field in the Principal Plane (Polar Form) vs Theta

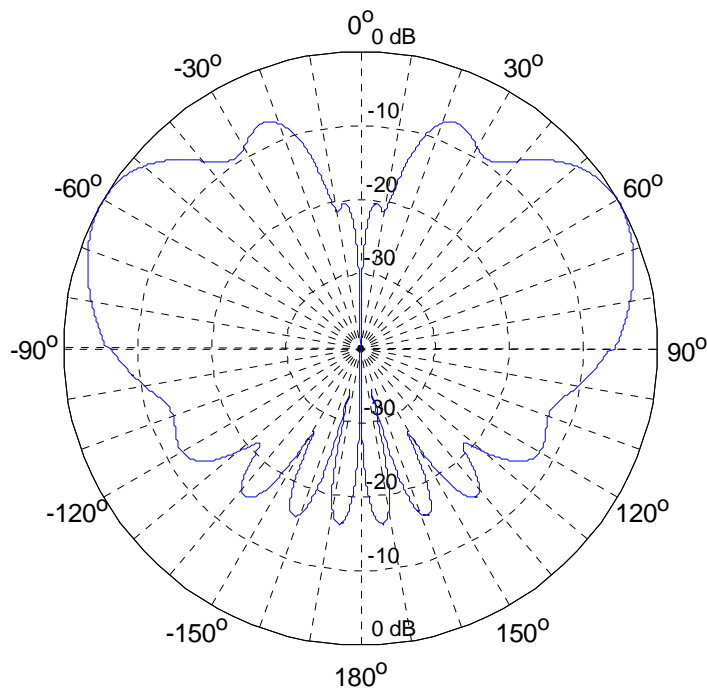


Figure 2-3 The Normalized Amplitude Pattern of the Total Field in the Principal Plane of Observation Calculated by the Written MATLAB[®] Computer Program

It is observed that the normalized amplitude pattern calculated by the written MATLAB[®] computer program is exactly the same as the theoretical (GO and GTD) normalized amplitude pattern obtained by Balanis, as expected. Also, there is a very good agreement between the normalized amplitude pattern calculated by

the written MATLAB[®] computer program and the experimental normalized amplitude pattern obtained by Balanis.

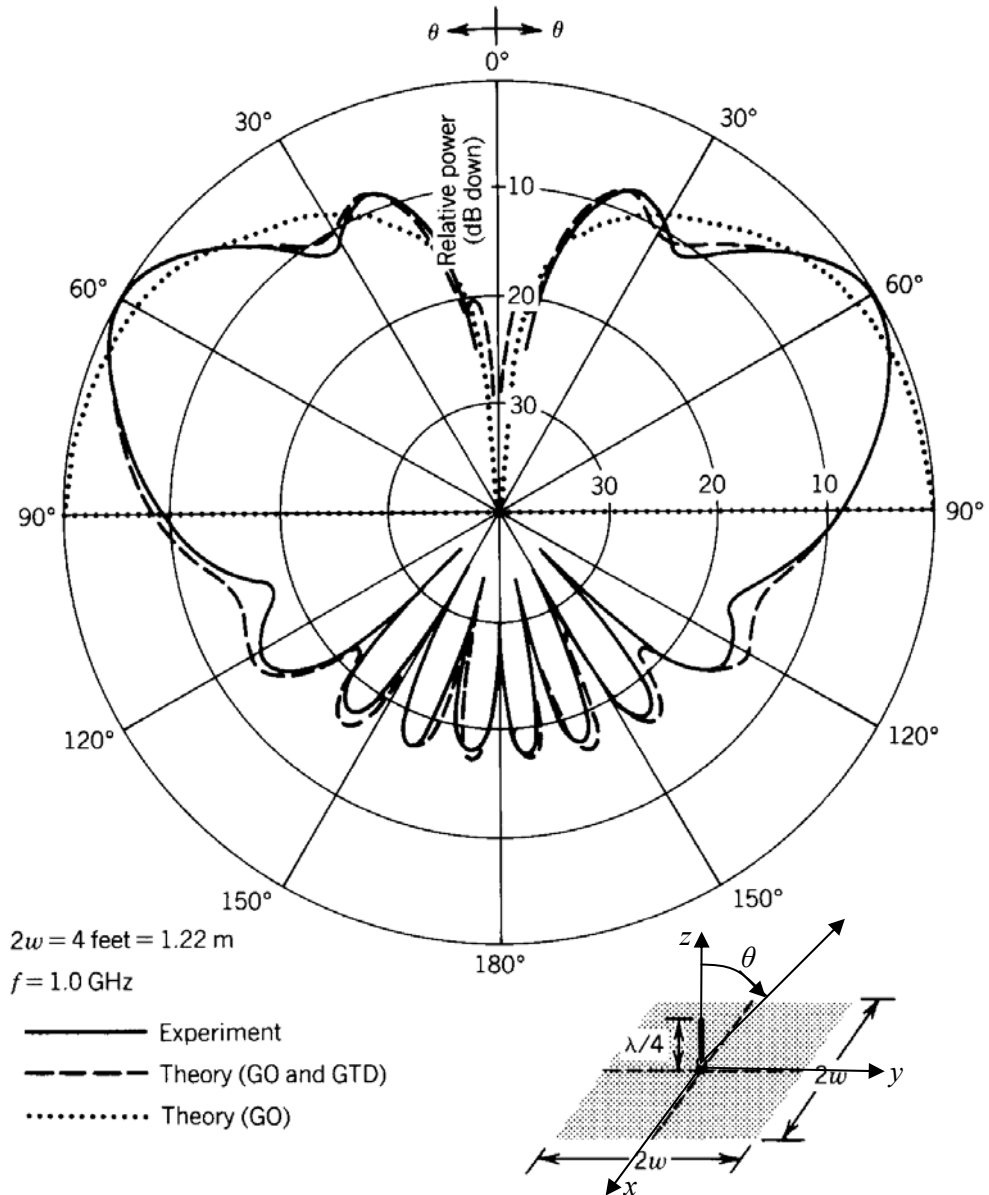


Figure 2-4 The Experimental and the Theoretical Normalized Amplitude Patterns of a $\lambda/4$ Monopole Antenna on Infinite and Finite Square Ground Planes in the Principal Plane of Observation Obtained by Balanis [8]

2.2.1. Examination of the Change of Far Field Radiation Pattern of the Monopole Antenna and Complex Diffraction Functions Due to the Variation of the Width of a Finite Square Ground Plane

In this subsection of the thesis, the change of far field radiation pattern (elevation plane pattern, in the principal planes) of the monopole antenna and complex diffraction functions due to the variation of the width of a finite square ground plane is examined.

In the first part of this study, this examination is carried out by the use of the written MATLAB[®] computer program. First of all, five different sidelengths for the width of a finite square ground plane on which a quarter wavelength ($\lambda/4$) monopole antenna mounted are defined, so that it can be observed how the normalized amplitude pattern of the total field and complex diffraction functions in the principal plane of observation, at 1 GHz frequency, change while the size of a square ground plane is varying from electrically small to electrically large. These five different sidelengths are specified as $w = 0.61$ m (2.033λ), 1.22 m (4.067λ), 2.44 m (8.133λ), 10 m (33.333λ), 100 m (333.333λ).

The normalized amplitude patterns of the total fields and the magnitudes of complex diffraction functions ($|V_B^{i,r}|$ produced by diffractions from edge 1 and edge 2) in the principal plane of observation, at 1 GHz frequency, obtained for these five different sidelengths by using the written MATLAB[®] computer program are demonstrated in Figures 2-5 to 2-19.

Farfield Radiation Pattern of the Total E-Field in the Principal Plane (Polar Form) vs Theta

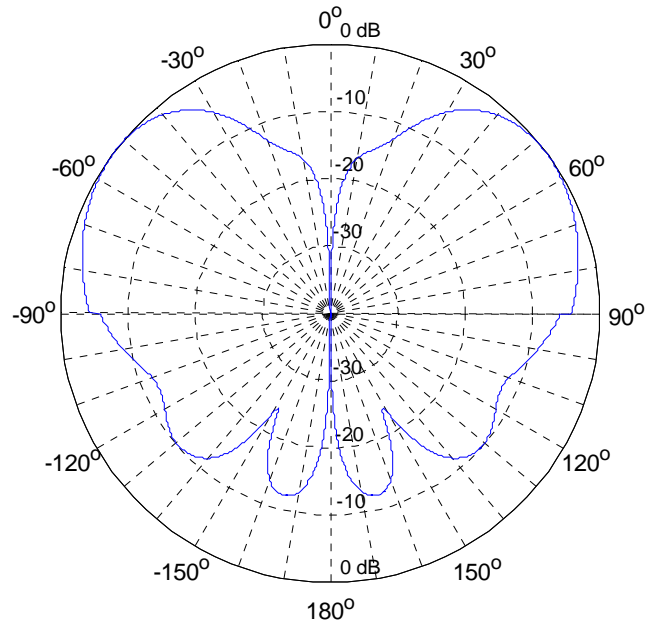


Figure 2-5 The Normalized Amplitude Pattern of the Total Field ($w = 0.61$ m)

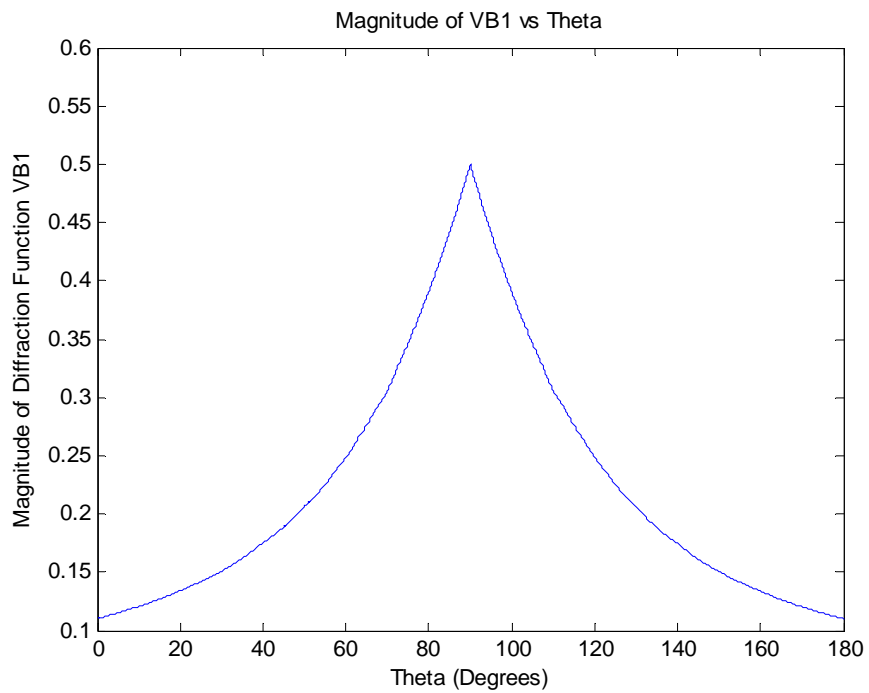


Figure 2-6 The Magnitude of the Diffraction Function from Edge 1 ($w = 0.61$ m)

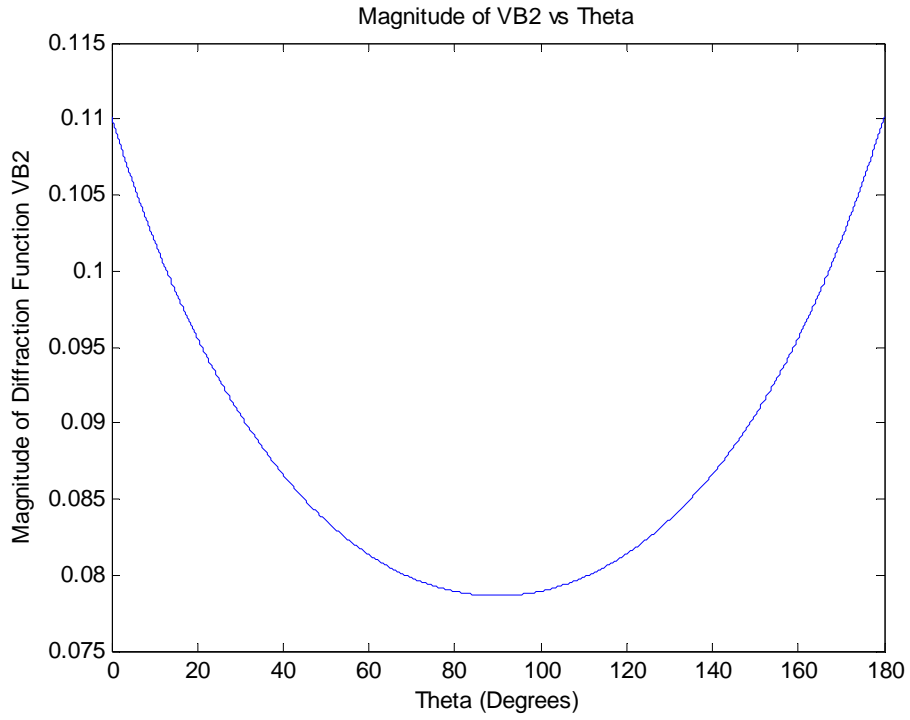


Figure 2-7 The Magnitude of the Diffraction Function from Edge 2 ($w = 0.61$ m)

Farfield Radiation Pattern of the Total E-Field in the Principal Plane (Polar Form) vs Theta

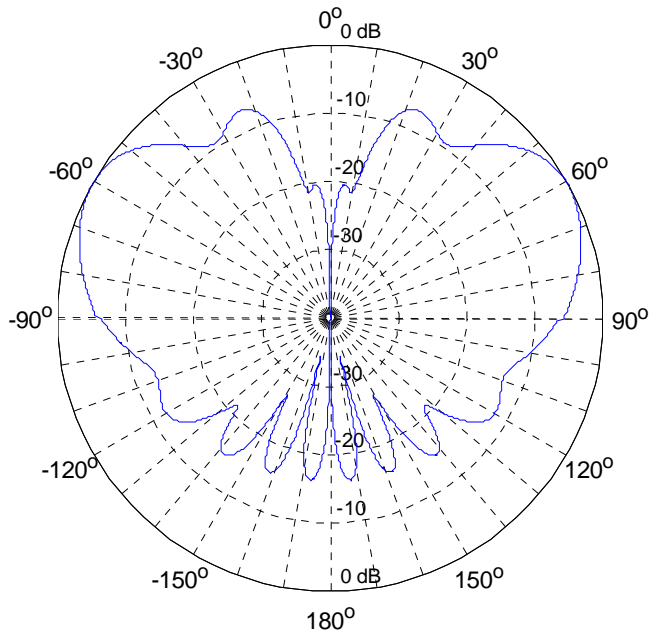


Figure 2-8 The Normalized Amplitude Pattern of the Total Field ($w = 1.22$ m)

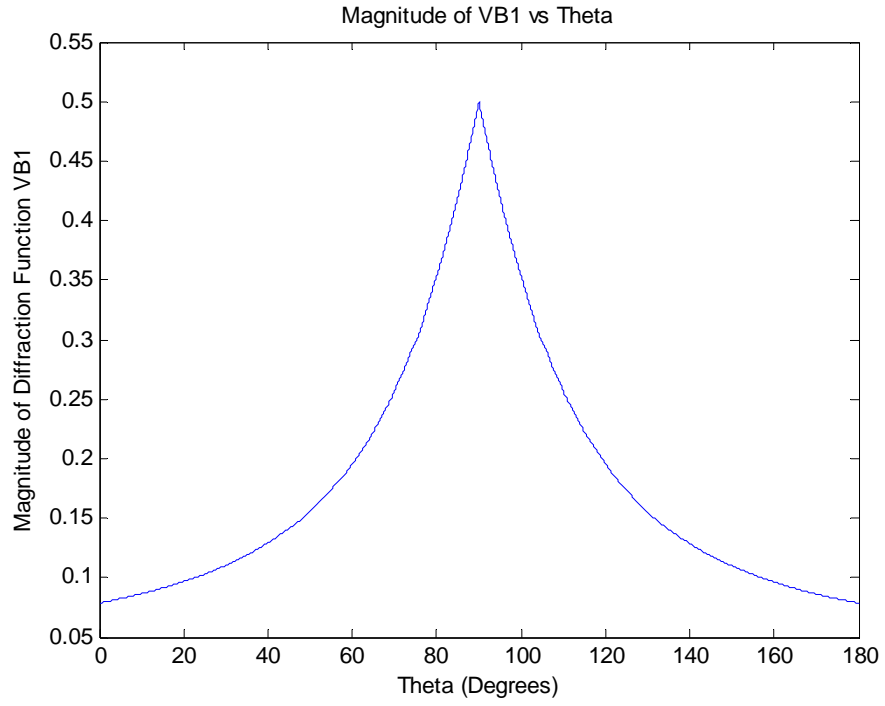


Figure 2-9 The Magnitude of the Diffraction Function from Edge 1 ($w = 1.22$ m)

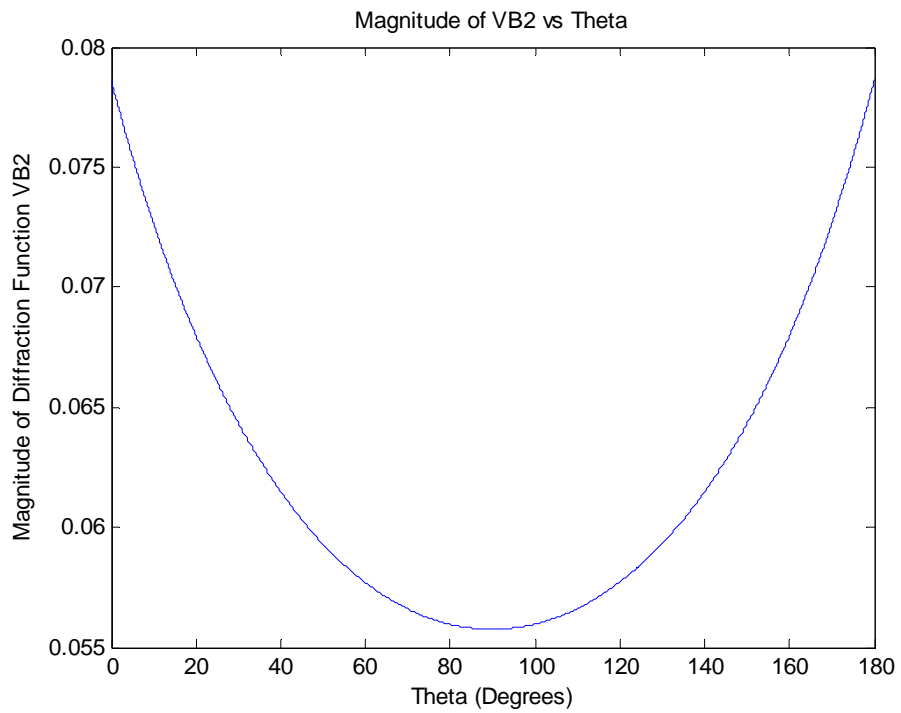


Figure 2-10 The Magnitude of the Diffraction Function from Edge 2 ($w = 1.22$ m)

Farfield Radiation Pattern of the Total E-Field in the Principal Plane (Polar Form) vs Theta

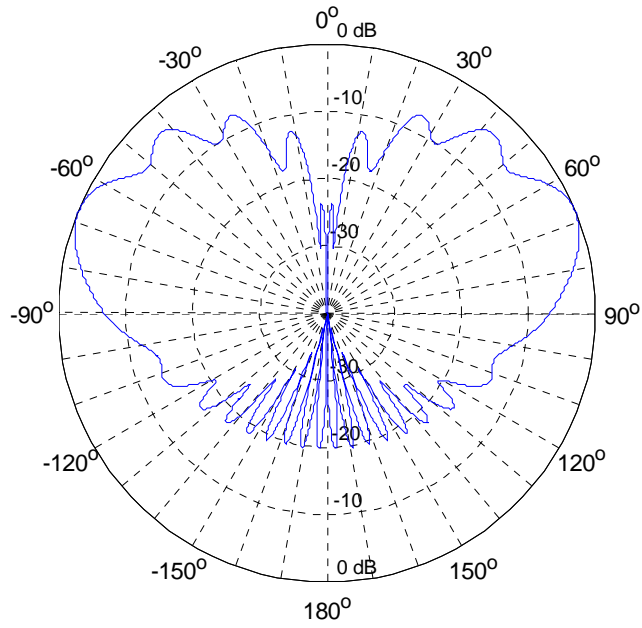


Figure 2-11 The Normalized Amplitude Pattern of the Total Field ($w = 2.44$ m)

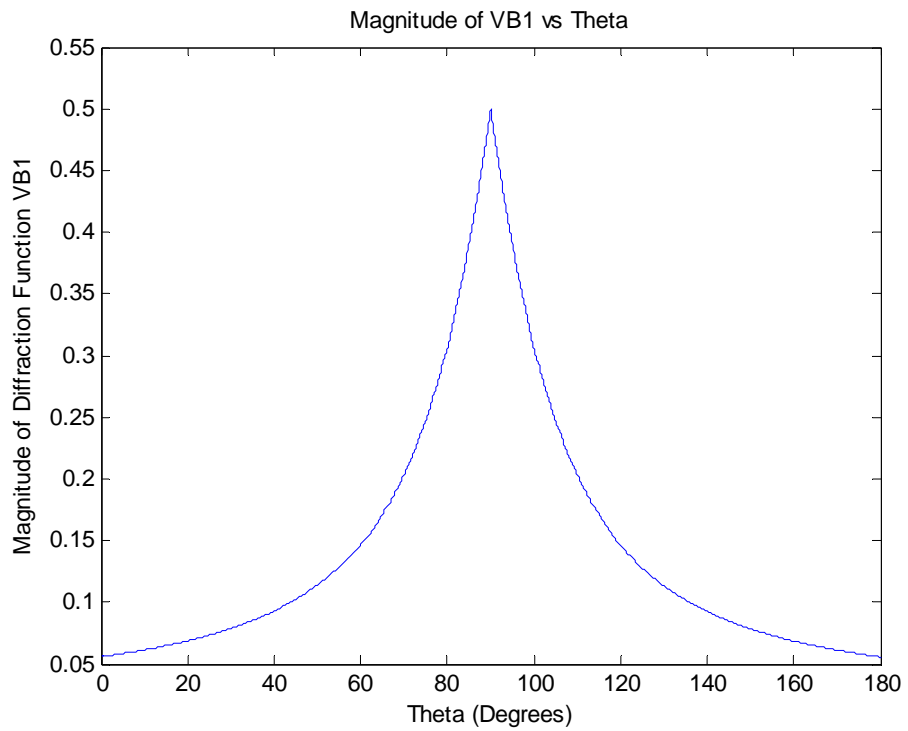


Figure 2-12 The Magnitude of the Diffraction Function from Edge 1 ($w = 2.44$ m)

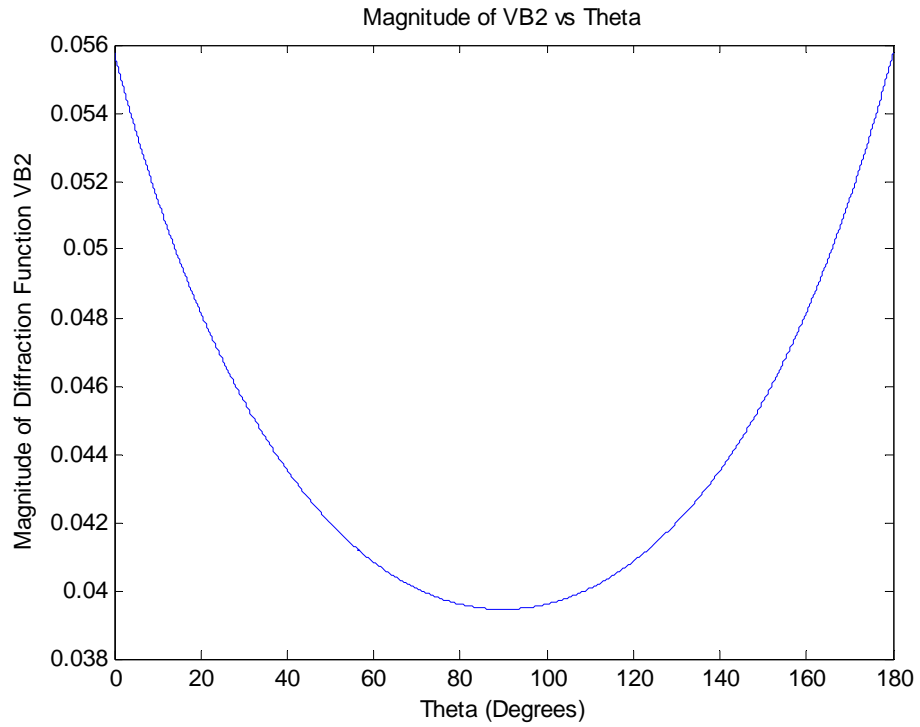


Figure 2-13 The Magnitude of the Diffraction Function from Edge 2 ($w = 2.44$ m)

Farfield Radiation Pattern of the Total E-Field in the Principal Plane (Polar Form) vs Theta

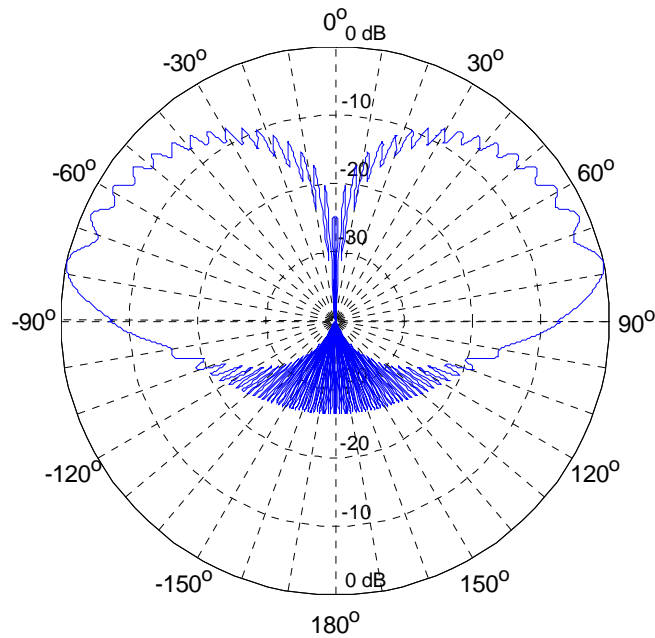


Figure 2-14 The Normalized Amplitude Pattern of the Total Field ($w = 10$ m)

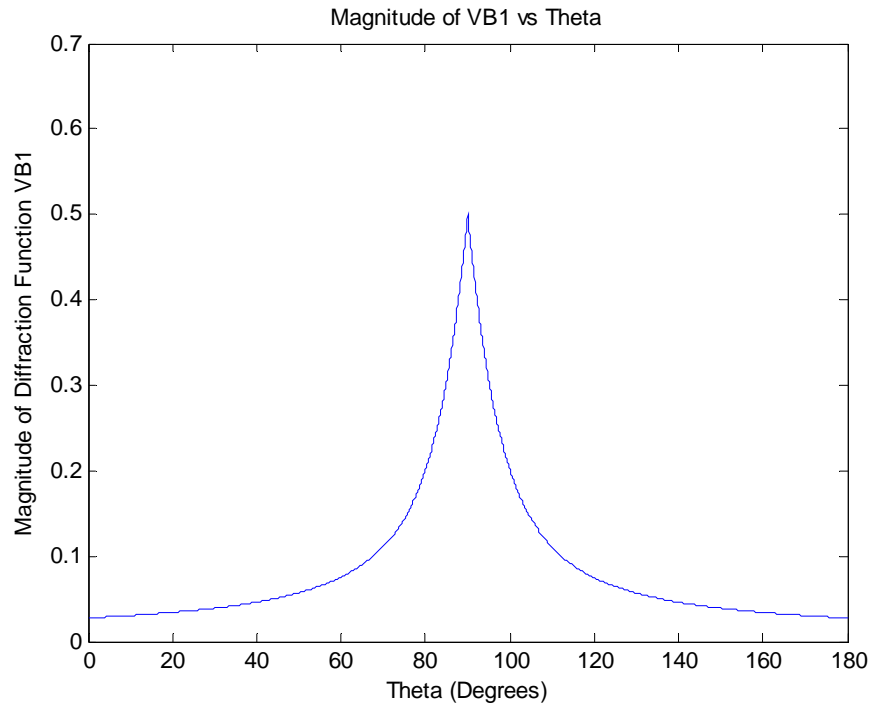


Figure 2-15 The Magnitude of the Diffraction Function from Edge 1 ($w = 10$ m)

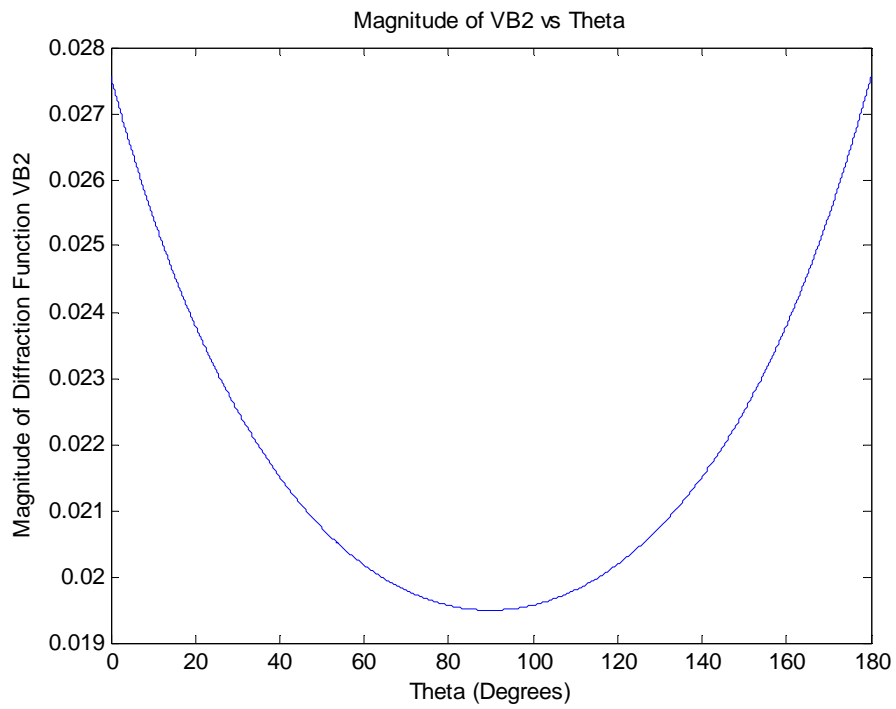


Figure 2-16 The Magnitude of the Diffraction Function from Edge 2 ($w = 10$ m)

Farfield Radiation Pattern of the Total E-Field in the Principal Plane (Polar Form) vs Theta

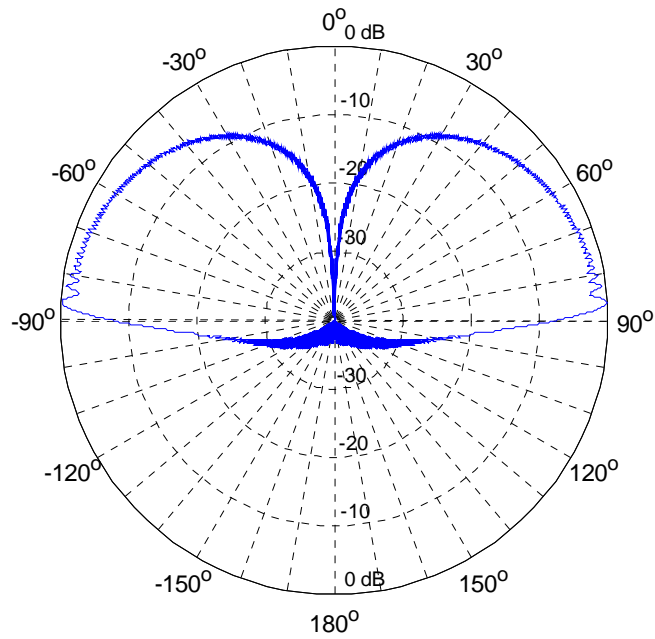


Figure 2-17 The Normalized Amplitude Pattern of the Total Field ($w = 100$ m)

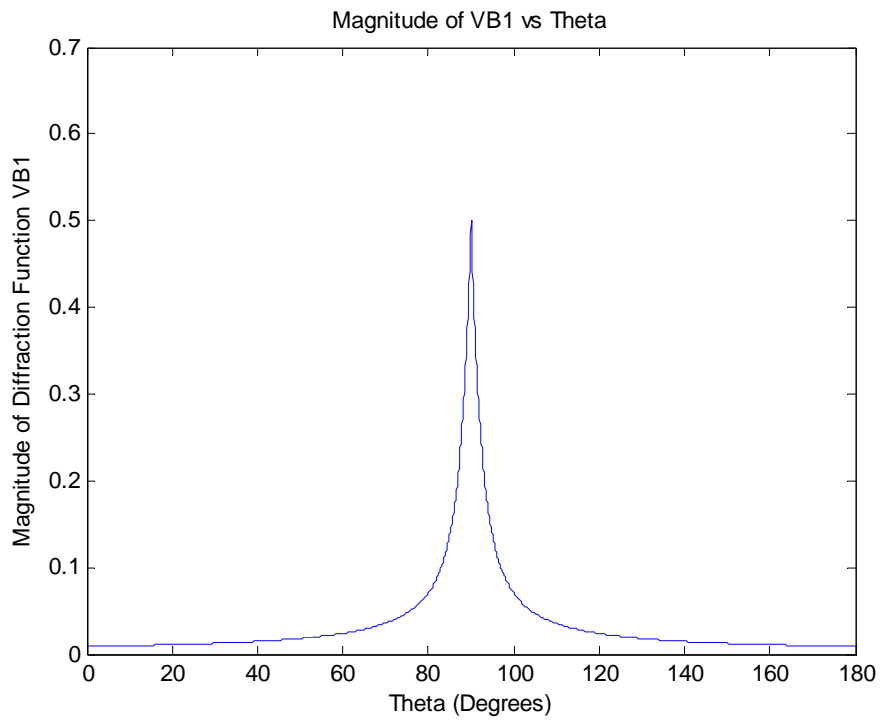


Figure 2-18 The Magnitude of the Diffraction Function from Edge 1 ($w = 100$ m)

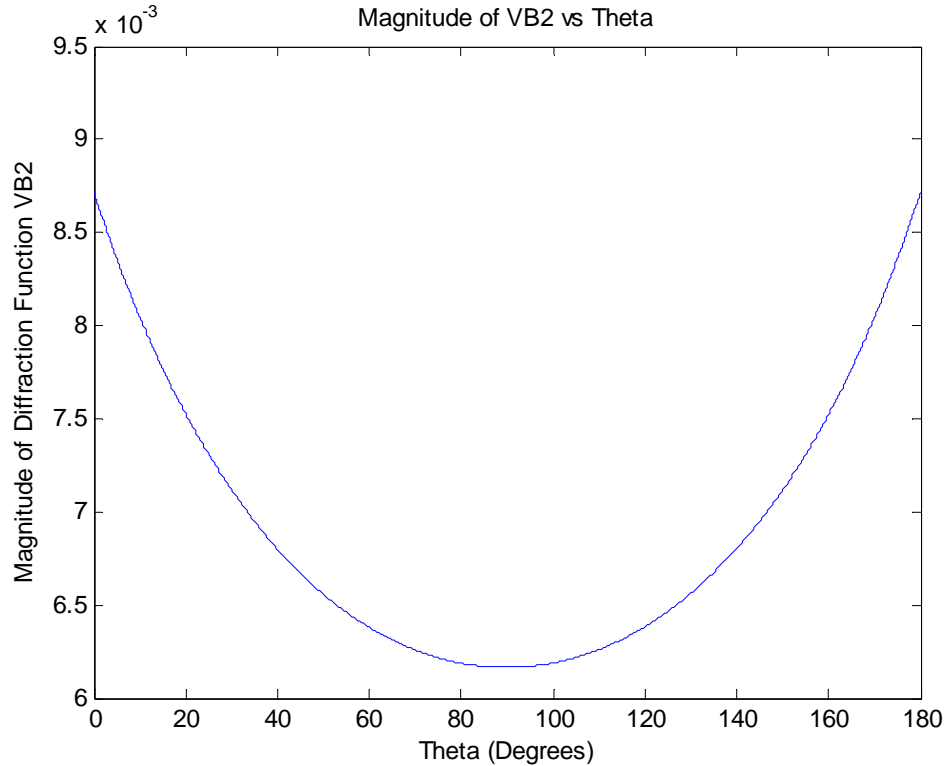


Figure 2-19 The Magnitude of the Diffraction Function from Edge 2 ($w = 100$ m)

In consequence of the examination performed for observing the change of the normalized amplitude pattern of the total field in the principal plane of observation due to the variation of the width of a finite square ground plane, it can be concluded that:

- As the sidelength of the square ground plane increases, the total field intensity in the region where θ is greater than 90° (the hemisphere below the square ground plane) decreases, as expected. This fact is due to the general decrease of the magnitudes of the diffraction functions from edges 1 and 2 as the sidelength of the square ground plane increases. Thus, the total field happens to be composed of mainly GO field and the normalized amplitude pattern of the total field happens to resemble the amplitude

pattern of the total GO field as the size of the square ground plane becomes electrically very large.

- As the sidelength of the square ground plane increases, the angle between $\theta = 0^\circ$ and the main lobe direction increases and the main lobe direction converges to $\theta = 90^\circ$, as expected.
- As the sidelength of the square ground plane increases, the number of sidelobes increases in the regions where θ is both greater and less than 90° . However, the amplitude difference between two adjacent sidelobes and undulations formed in the amplitude pattern, in the region where θ is less than 90° , happen to vanish, as the size of the square ground plane becomes electrically very large. Also, the amplitudes of the sidelobes in the region where θ is greater than 90° decrease, as the sidelength of the square ground plane increases.

In consequence of the examination performed for observing the change of the magnitudes of the diffraction functions from edges 1 and 2 in the principal plane of observation due to the variation of the width of a finite square ground plane, it can be concluded that:

- As the sidelength of the square ground plane increases, the magnitudes of the diffraction functions from edges 1 and 2 decrease predominantly.
- According to the radiation mechanisms shown in Figure 2-2, since the angle of incidence from the base of the monopole antenna to the diffraction points is 0° , the incident and reflection shadow boundaries coincide each other at $\theta = 90^\circ$ in the principal plane of observation for both edges 1 and 2. Therefore, since the observation point at $\theta = 90^\circ$, in the right side of the Figure 2-2, corresponds to the incident/reflection shadow boundary for edge 1, the magnitude of the diffraction function from edge 1 is maximum and equals to 0.5 at $\theta = 90^\circ$ for all sidelengths. On the other hand, since the observation point at $\theta = 90^\circ$, in the right side of the Figure 2-2, corresponds

to the line in the reverse direction of the incident/reflection shadow boundary for edge 2, the magnitude of the diffraction function from edge 2 is minimum at $\theta = 90^\circ$ for all sidelengths.

- As the observation point goes away from $\theta = 90^\circ$, in the right side of the Figure 2-2, the magnitude of the diffraction function from edge 1 decreases rapidly and it decreases more rapidly for larger sidelengths.
- As the observation point goes away from $\theta = 90^\circ$, in the right side of the Figure 2-2, the magnitude of the diffraction function from edge 2 increases gradually.

In the second part of this study, the normalized amplitude patterns of the total fields in the principal plane of observation shown in Figures 2-5, 2-8 and 2-11, at 1 GHz frequency, obtained for three different sidelengths, specified as $w = 0.61, 1.22, 2.44$ m, by using the written MATLAB[®] computer program are compared with the far field radiation patterns (polar plots of elevation plane patterns) of the total electric fields obtained for the same structures stated above by using the transient solver of the electromagnetic simulation software, named as CST MWS[®].

CST MWS[®] is an electromagnetic simulation software used for analysis of electromagnetic problems and design of the structures such as antennas, waveguides and resonators etc. in the high frequency range. Also, the transient solver of CST MWS[®] is used for the electromagnetic analysis of antennas located on the aircraft and the ship, which is performed in the scope of this thesis. Both for the simulations performed for the electromagnetic analysis of antennas located on the aircraft and the ship and the simulations performed for the analysis of the far field radiation pattern of a $\lambda/4$ monopole antenna above a finite square ground plane, the modeling of the structures handled in the simulations and simulation settings are carried out properly by taking into account the factors such as accuracy, simulation time and simulation complexity.

The geometries with three different ground plane sidelengths, specified as $w = 0.61, 1.22, 2.44$ m, modeled in the simulations are shown in Figures 2-20, 2-21 and 2-22, respectively.

First of all, the length of the $\lambda/4$ monopole antenna is specified as 7.5 cm for all simulations, since the analysis of the far field radiation pattern is performed at the frequency of 1 GHz. Afterwards, the thickness of the finite square ground plane is chosen as zero so that the structure modeled in CST MWS[®] is the same as the one in the written MATLAB[®] computer program, and also in Figure 2-4.

Besides, the calculation domain including the whole structure modeled and electromagnetic properties of the material surrounding the structure are specified for all simulations. The size and the boundaries of the calculation domain are determined by setting the boundary conditions as open (absorbing) boundary conditions operating like free space [10], since the structure modeled involves an antenna radiating into free space. The material surrounding the structure within the calculation domain is specified as free space (electrical conductivity, $\sigma = 0$; relative permittivity and permeability, $\epsilon_r = \mu_r = 1$).

The material of the $\lambda/4$ monopole antenna and the finite square ground plane is specified as Perfect Electric Conductor (PEC) for all simulations. Moreover, the $\lambda/4$ monopole antenna is excited with a discrete port having an impedance of 50 Ω , shown as a red cone in Figures 2-20, 2-21 and 2-22, for all simulations. After finishing modeling of the structures, the simulations are run. As a result of these simulations, the far field radiation patterns (polar plots of elevation plane patterns) of the total electric fields in the principal plane of observation (y-z plane), at the frequency of 1 GHz, are obtained for three different sidelengths specified above. These far field radiation patterns are demonstrated in Figures 2-23, 2-24 and 2-25. In these radiation patterns; the dark blue line indicates main lobe direction, light blue lines indicate 3 dB angular beamwidth and the green circle indicates the level of the highest sidelobe.

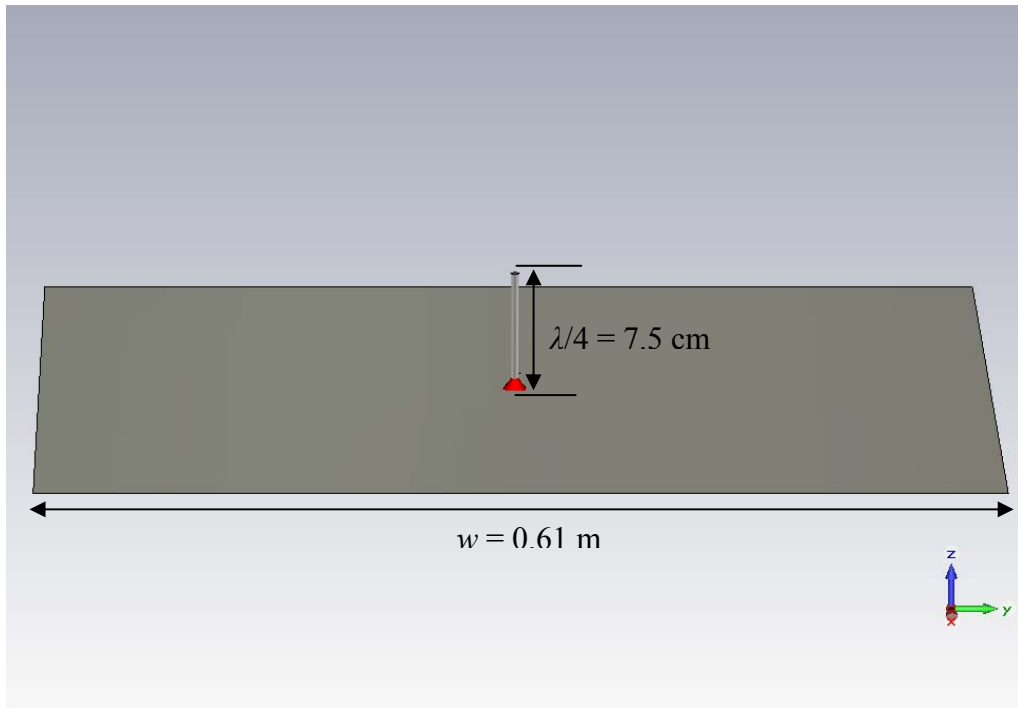


Figure 2-20 $\lambda/4$ Monopole above a Finite Square Ground Plane ($w = 0.61$ m)

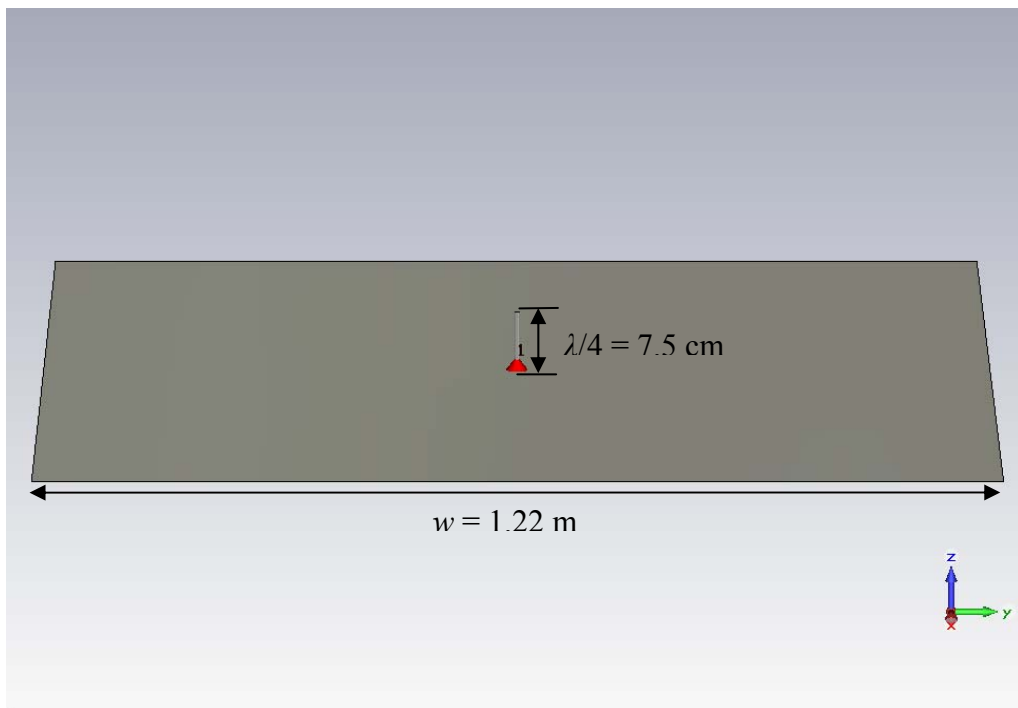


Figure 2-21 $\lambda/4$ Monopole above a Finite Square Ground Plane ($w = 1.22$ m)

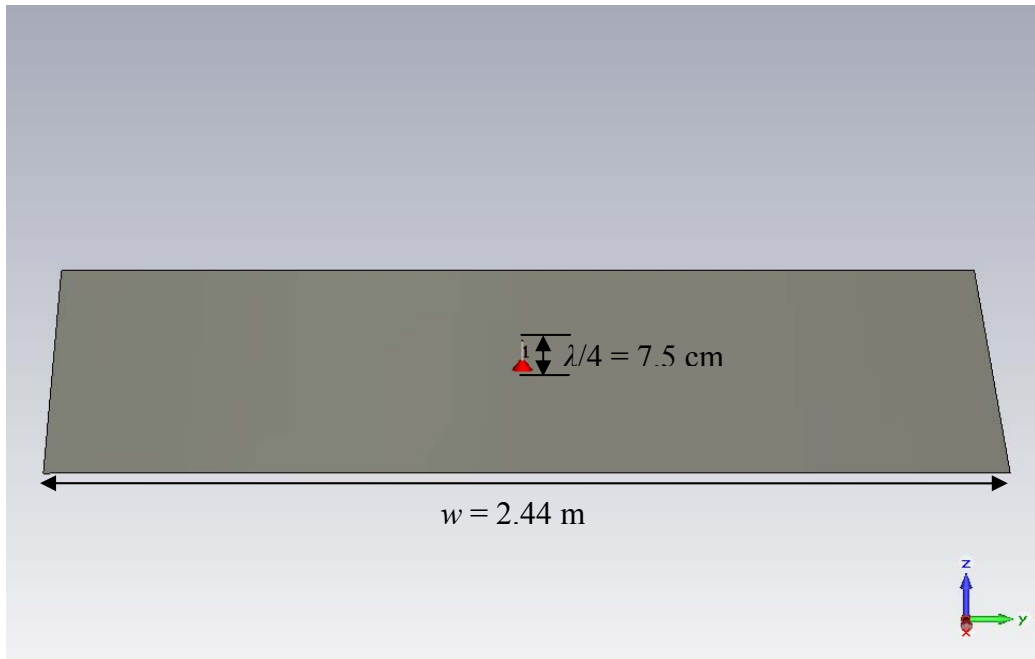


Figure 2-22 $\lambda/4$ Monopole above a Finite Square Ground Plane ($w = 2.44 \text{ m}$)

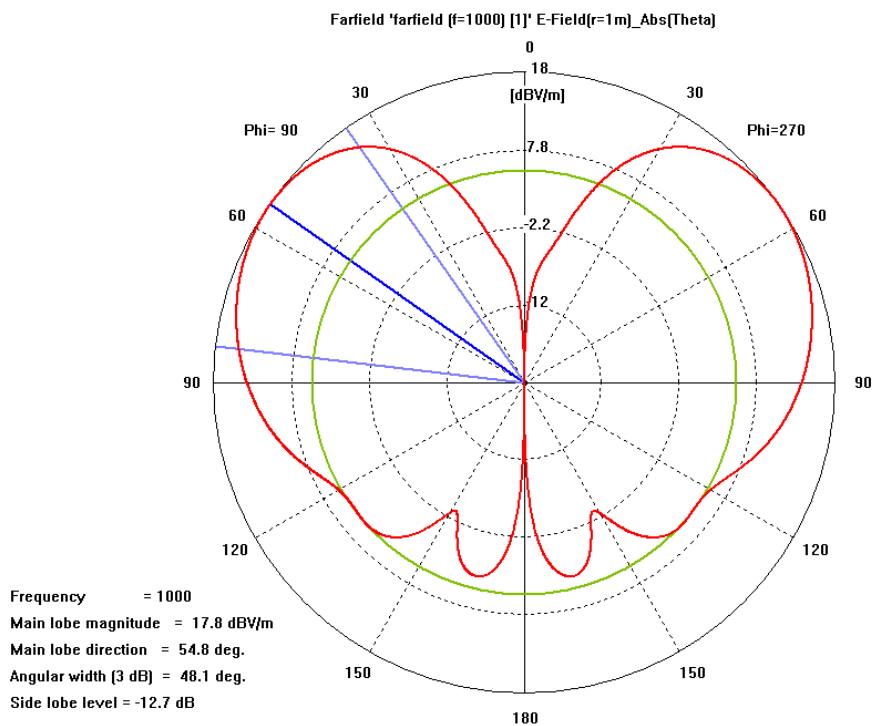


Figure 2-23 The Far Field Radiation Pattern of the Electric Field ($w = 0.61 \text{ m}$)

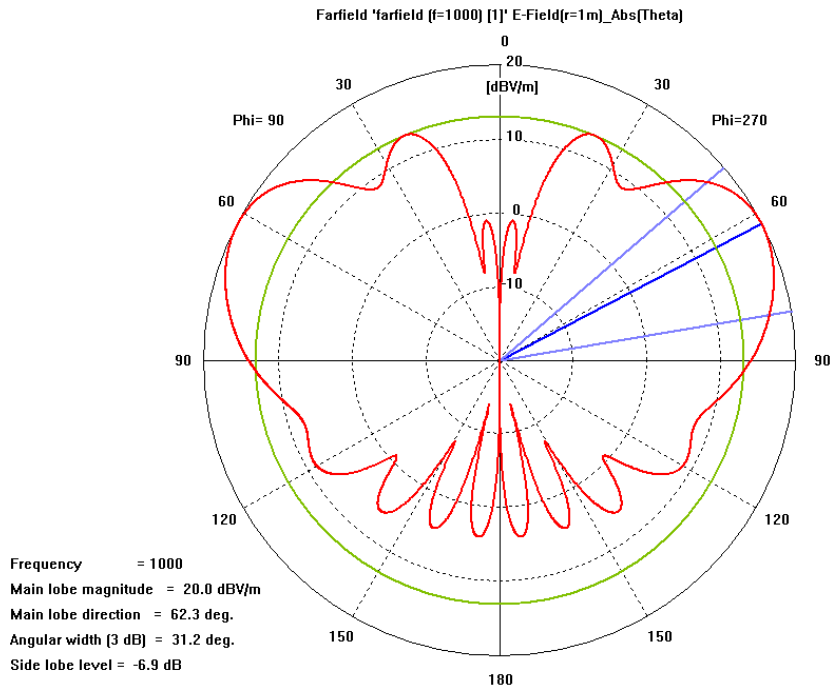


Figure 2-24 The Far Field Radiation Pattern of the Electric Field ($w = 1.22$ m)

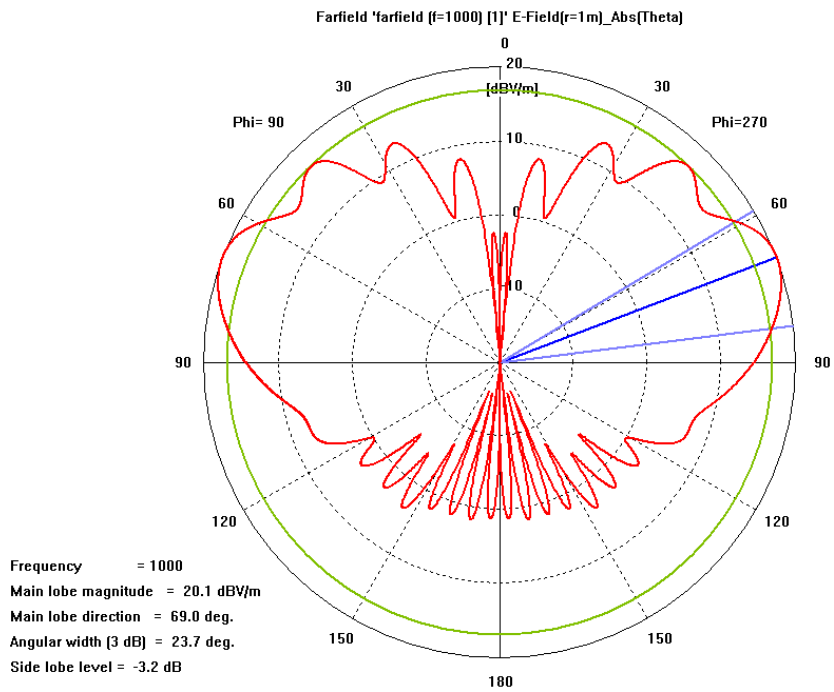


Figure 2-25 The Far Field Radiation Pattern of the Electric Field ($w = 2.44$ m)

In consequence of the comparison done between the normalized amplitude patterns of the total fields obtained by using the written MATLAB[®] computer program and the far field radiation patterns of the total electric fields obtained by using the transient solver of CST MWS[®], it can be concluded that:

- There is a very good agreement between the normalized amplitude patterns calculated by the written MATLAB[®] computer program and the far field radiation patterns obtained by using the transient solver of CST MWS[®].
- However, there is a slight difference between the normalized amplitude patterns calculated by the written MATLAB[®] computer program and the far field radiation patterns obtained by using the transient solver of CST MWS[®].
- This slight difference increases, as the sidelength of the square ground plane decreases due to the fact that the accuracy of the results obtained by the use of GO and uniform GTD techniques decreases, as the electrical size of the radiating or scattering object of interest becomes smaller. It can be noted that since the transient solver of CST MWS[®] is a full wave solver operating based on the numerical technique, named as Finite Integration Technique (FIT), it gives more accurate results than GO and uniform GTD techniques for electrically small radiating or scattering structures.
- It is observed that the far field radiation patterns obtained by using the transient solver of CST MWS[®] are quite accurate, since there is a very good agreement between the far field radiation pattern, shown in Figure 2-24, and the experimental normalized amplitude pattern, shown in Figure 2-4, obtained by Balanis [8].

CHAPTER 3

ANALYSIS OF ANTENNAS MOUNTED ON F-4 AIRCRAFT

In this chapter, electromagnetic analysis of antennas mounted on F-4 aircraft performed for improving the operational performance of antennas on the aircraft by arranging their placements is discussed.

In general, there are two monopole antennas operating in the UHF communication band (225 – 400 MHz) on F-4 aircrafts. One is usually located on the upper side of the fuselage of the aircraft and the other one is located on the lower side of the fuselage so that one provides sufficient coverage in the hemisphere above the aircraft and the other one provides sufficient coverage in the hemisphere below.

In the scope of this study, electromagnetic analysis of two UHF antennas mounted on F-4 aircraft is performed by using the transient solver of CST MWS[®], in order to determine the optimal location of the lower UHF antenna (newly installed antenna) for the operational performance of the lower UHF antenna to be optimum in terms of the reduction of electromagnetic coupling between UHF antennas and the sufficiency of far field radiation pattern of the lower UHF antenna. The location of the upper UHF antenna (existing antenna) is already definite, shown in Figure 3-1 as antenna #1, based on the original placement of upper UHF antennas mounted on F-4 aircrafts. On the other hand, for the lower UHF antenna, four different locations are specified on the lower side of the fuselage of the aircraft,

shown in Figures 3-2, 3-3, 3-4 and 3-5 as antennas #7, #10, #11 and #12, respectively, by taking into account the physical and operational constraints of the aircraft.

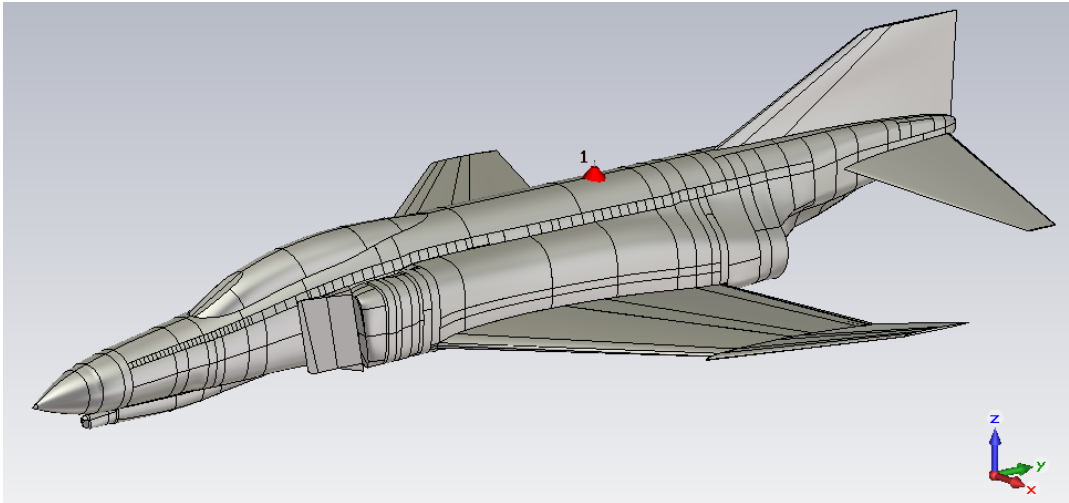


Figure 3-1 The Location of the Upper UHF Antenna on F-4 Aircraft

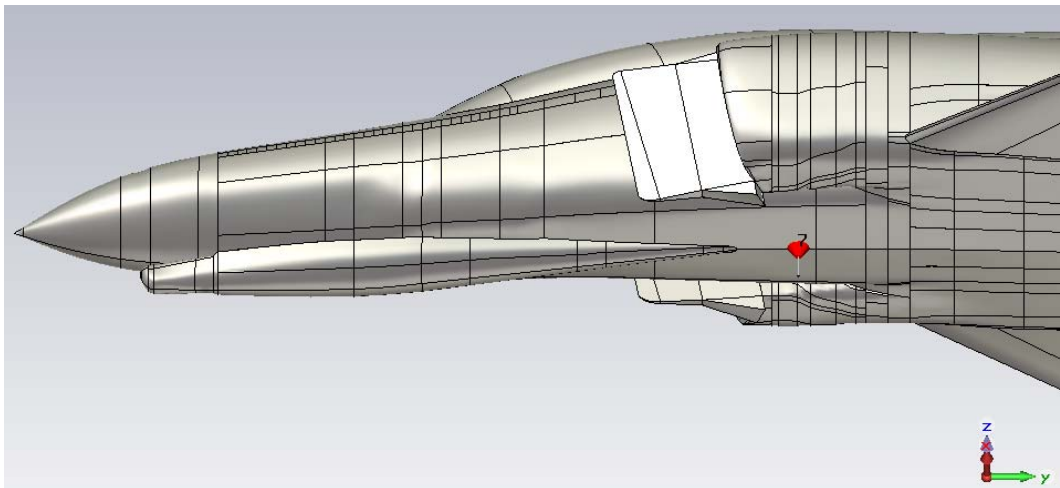


Figure 3-2 First Location of the Lower UHF Antenna Denoted as Antenna #7

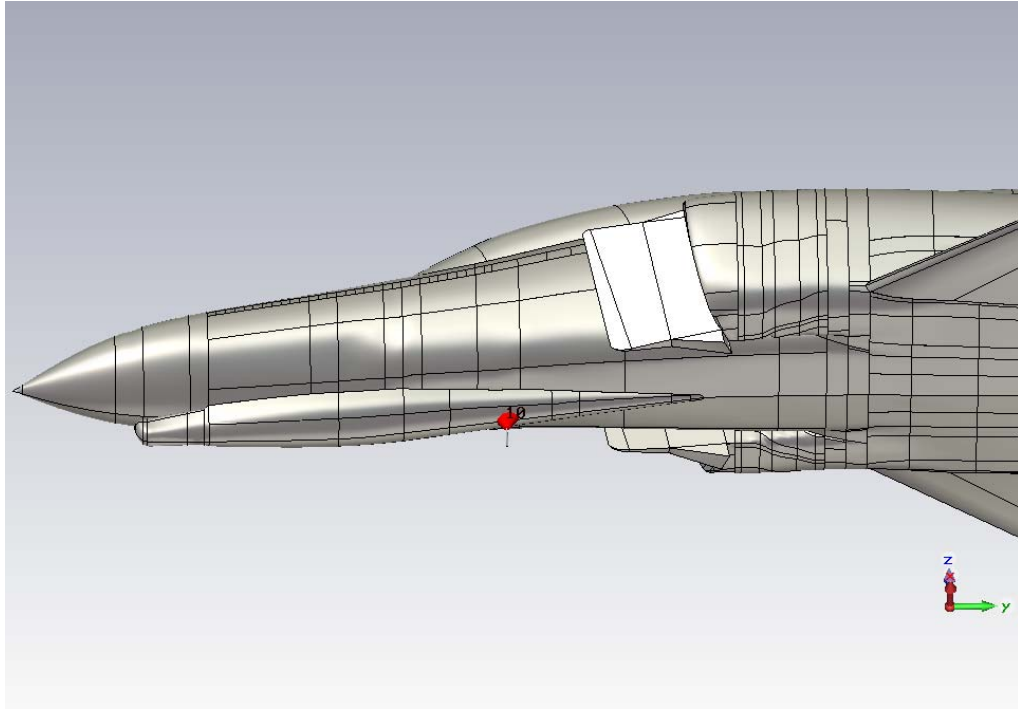


Figure 3-3 Second Location of the Lower UHF Antenna Denoted as Antenna #10

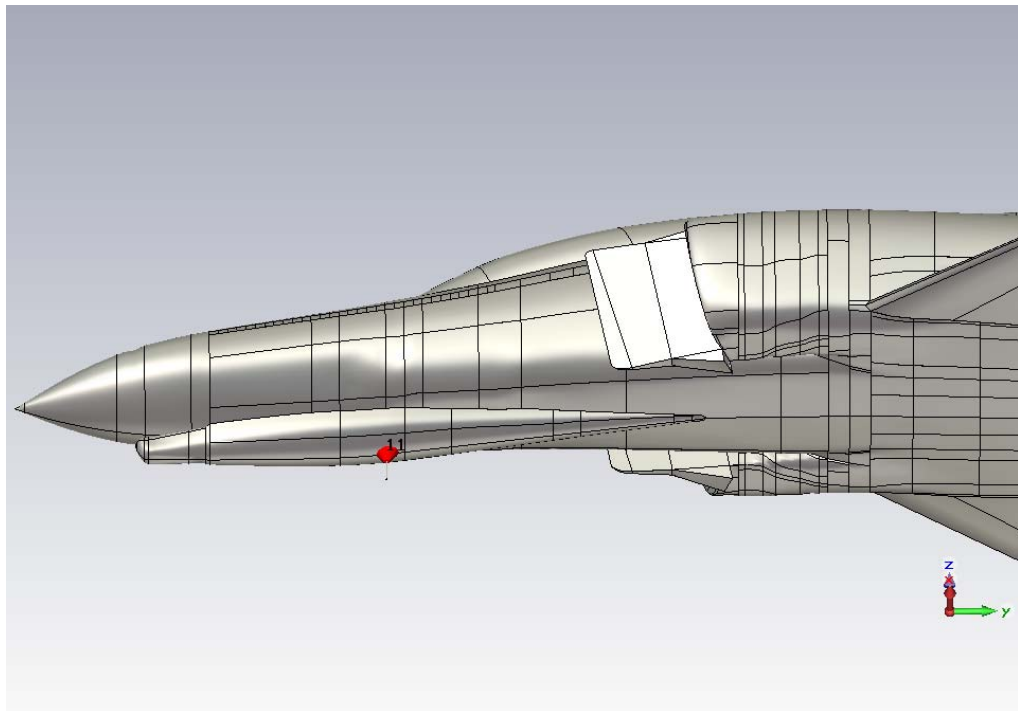


Figure 3-4 Third Location of the Lower UHF Antenna Denoted as Antenna #11

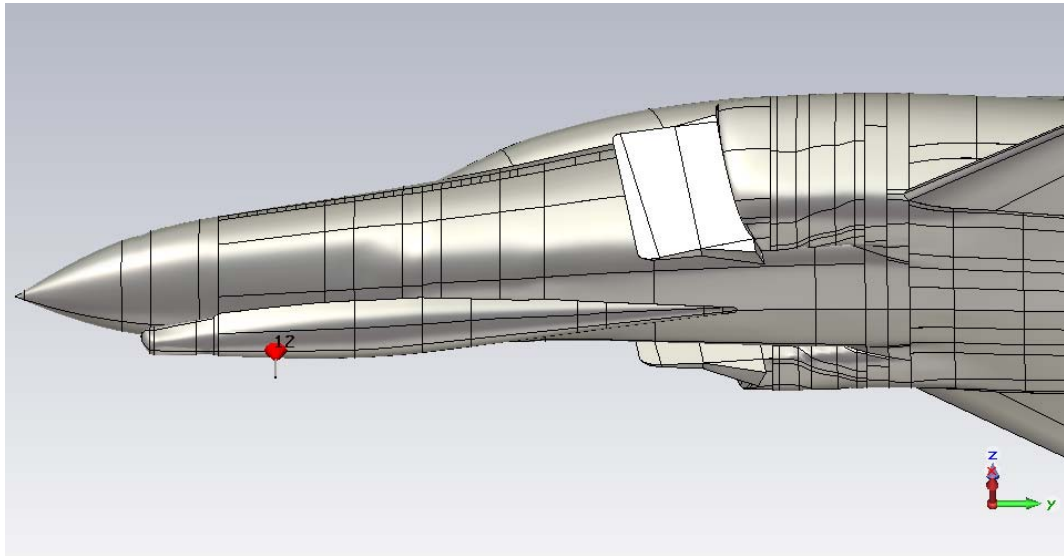


Figure 3-5 Fourth Location of the Lower UHF Antenna Denoted as Antenna #12

Since the location of the upper UHF antenna is on the centerline of the upper side of the fuselage, four different locations specified for the lower UHF antenna are chosen on the centerline of the lower side of the fuselage, so that the electromagnetic coupling ($S_{2,1}$) between the lower and upper UHF antennas is at a minimum level due to the fact that the angular separation between these two antennas is 180° [11]. Also, this placement of the antennas is compliant with the symmetry requirement of the aircraft.

The optimal location for the lower UHF antenna is determined among these four different locations depending on the following two criteria ensuring the operational performance of the antenna to be optimum:

1. Decreasing the electromagnetic coupling between the lower and upper UHF antennas as much as possible.
2. The far field radiation pattern of the antenna shall have sufficient directivity values in the region where the antenna has to operate efficiently.

In order to achieve the aim of this study on the basis of these two criteria, primarily, it is considerable to conceive how the electromagnetic coupling between the lower and upper UHF antennas and the far field radiation patterns of the lower UHF antenna are affected due to the structural components such as fuselage, nose, wings, tail, and vertical/horizontal stabilizers composing F-4 aircraft. Therefore, a new simplified F-4 aircraft model is built based on the original F-4 aircraft model by using the object creation tool of CST MWS[®]. This simplified F-4 model, shown in Figure 3-6, is composed of geometrically simple structures such as elliptical cylinder as the fuselage, cones as the nose and the tail, and planar polygons as wings and vertical/horizontal stabilizers.

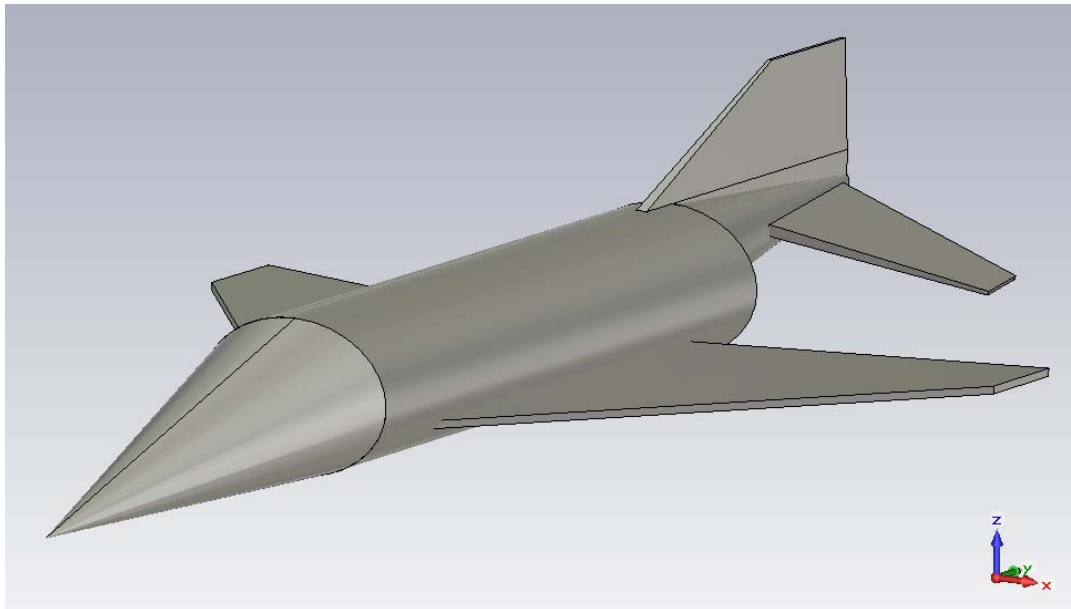


Figure 3-6 The Simplified F-4 Model Built Based on the Original F-4 Model

Towards the aim of this study, in order to conceive the influence of each geometrically simple structure composing the simplified F-4 model on the electromagnetic coupling between the lower and upper UHF antennas and the far field radiation patterns of the lower UHF antenna, primarily, electromagnetic

analysis of these antennas is carried out on four different structures which are constituted by adding each geometrically simple structure one by one. These structures are shown in Figure 3-7.

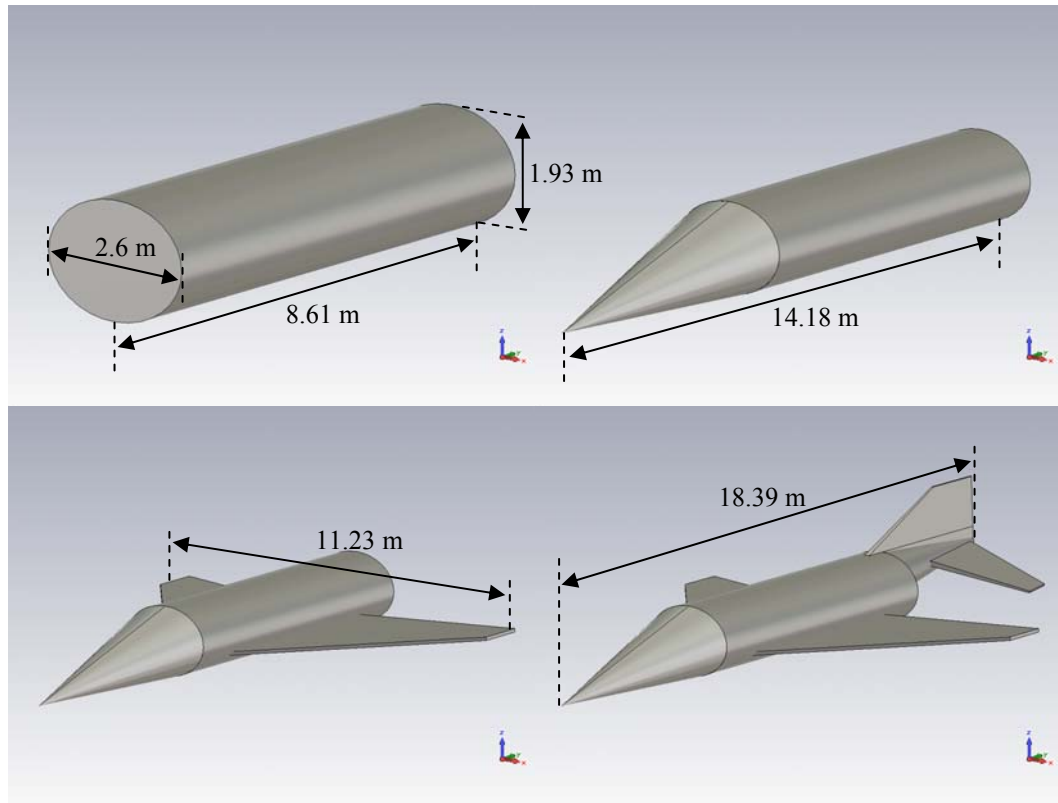


Figure 3-7 Four Different Structures on which Antenna Analysis Performed

As it is seen in Figure 3-7;

- First structure is composed only of the main fuselage of the aircraft.
- Second structure is composed of the main fuselage and nose of the aircraft.
- Third structure is composed of the main fuselage, nose and wings of the aircraft.
- Fourth structure is already the simplified F-4 aircraft model.

The locations of the lower and upper UHF antennas in this analysis are identical to the locations of these antennas in the analysis performed on the original F-4 model, shown in Figures 3-1, 3-2, 3-3, 3-4 and 3-5.

Within the scope of the analysis performed on these four structures, the electromagnetic coupling levels between the lower and upper UHF antennas and the far field radiation patterns of the lower UHF antenna are obtained for four different locations of the lower UHF antenna. By this way, the electromagnetic coupling levels and the far field radiation pattern obtained for each location of the lower UHF antenna in the analysis performed on each structure are compared with the corresponding results of the other three different locations obtained on the same structure in order to determine the optimal location for the lower UHF antenna on F-4 aircraft among these four different locations. After the electromagnetic analysis of the antennas performed on these four structures is completed, the same analysis is performed on the original F-4 model. Finally, since decreasing the electromagnetic coupling between the lower and upper UHF antennas as much as possible is the primary criterion for determining the optimal location of the lower UHF antenna, the electromagnetic coupling levels obtained for each location of the lower UHF antenna in the analysis performed on the simplified F-4 aircraft are compared with the corresponding results obtained in the analysis performed on the original F-4 aircraft and the location, that the electromagnetic coupling is minimum, is determined as the optimal location for the lower UHF antenna among these four different locations. In addition to this, at this optimal location whether the far field radiation pattern of the lower UHF antenna has sufficient directivity values in the region where the antenna has to operate efficiently is investigated.

For modeling the structures in the simulations of the electromagnetic analysis performed on four different structures and the original F-4 model, the following steps are applied:

- The lengths of the lower and upper UHF antennas are specified as 25 cm ($\lambda/4$ monopole antennas at the frequency of 300 MHz), since these antennas operate in the UHF communication band (225 – 400 MHz).
- The calculation domains including the structures modeled in the simulations and electromagnetic properties of the materials surrounding the structures are specified.
 - a. The sizes and the boundaries of the calculation domains are determined by setting the boundary conditions as open (absorbing) boundary conditions operating like free space [10], since the structures modeled involve antennas radiating into free space.
 - b. The materials surrounding the structures within the calculation domains are specified as free space (electrical conductivity, $\sigma = 0$; relative permittivity and permeability, $\epsilon_r = \mu_r = 1$).
- The materials of the lower and upper UHF antennas, four different structures and the original F-4 aircraft are specified as PEC.
- The lower and upper UHF antennas are excited with discrete ports having impedances of 50 Ω .

3.1. Analysis of Antennas on the Main Fuselage

As a result of the electromagnetic analysis of the lower and upper UHF antennas mounted on the main fuselage of the simplified F-4 model, the electromagnetic coupling levels between the lower and upper UHF antennas and the far field radiation patterns of the lower UHF antenna are obtained for the first location of the lower UHF antenna, shown in Figure 3-8 as antenna #7. Since the other three locations of the lower UHF antenna do not exist in the structure handled in this study, the analysis is performed only for the first location of the lower UHF antenna.

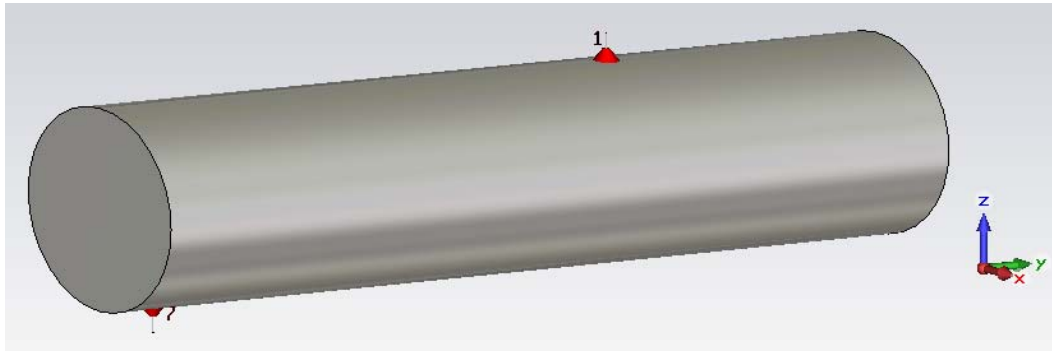


Figure 3-8 The Lower (#7) and Upper (#1) UHF Antennas on the Main Fuselage

The graph of the electromagnetic coupling levels ($S_{1,7}$) between the lower and upper UHF antennas over 225 – 400 MHz frequency band is given in Figure 3-9.

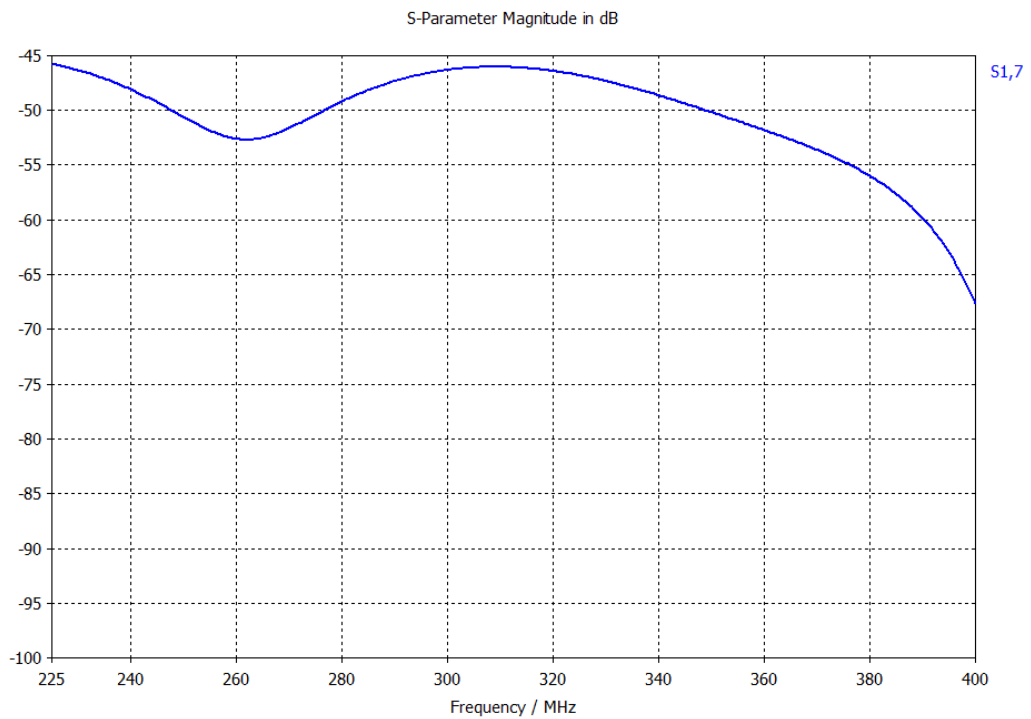


Figure 3-9 Coupling ($S_{1,7}$) between the Lower and Upper UHF Antennas

The mean value of the electromagnetic coupling levels ($S_{1,7}$) over 225 – 400 MHz frequency band is calculated as -50.58 dB.

Both for the analysis performed on the main fuselage and the other analysis performed on the other structures in this chapter, the far field radiation patterns (directivity plots) of the lower UHF antenna are obtained in x-y, x-z and y-z planes as polar radiation patterns. Also, the far field radiation patterns are obtained in 3D form. Since all of the structures modeled in the simulations of the analysis performed within this chapter are symmetrical with respect to y-z plane, polar radiation patterns obtained in x-y and x-z planes and 3D far field radiation patterns are also symmetrical with respect to y-z plane. Therefore, each 3D far field radiation pattern is given for two different angles of view in order to be able to observe the whole radiation pattern. Besides, all of the far field radiation patterns are obtained at the frequency of 300 MHz. The far field radiation patterns of the lower UHF antenna are given in Figures 3-10 to 3-14.

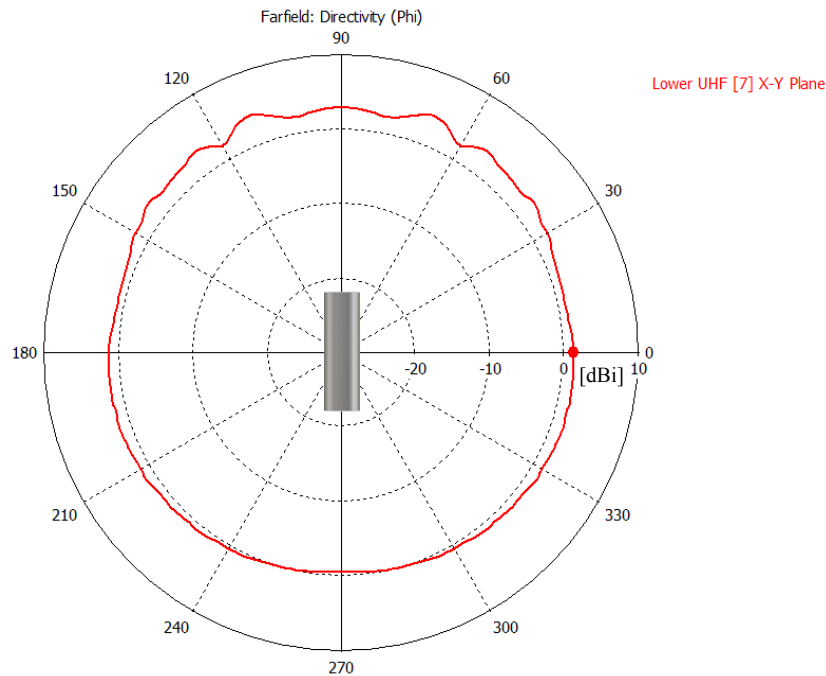


Figure 3-10 Polar Radiation Pattern of the Lower UHF Antenna (#7) in x-y Plane

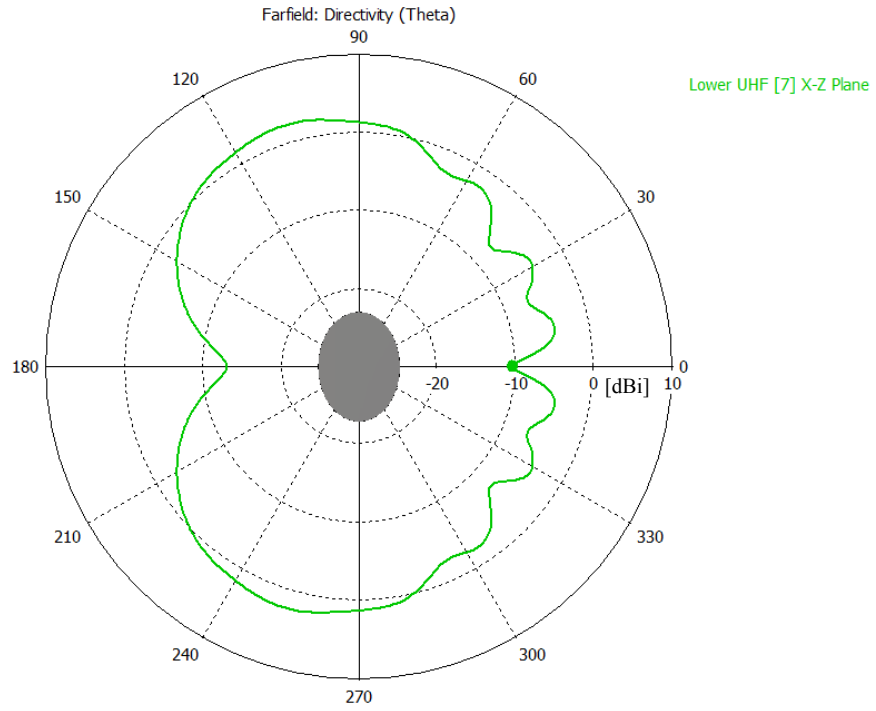


Figure 3-11 Polar Radiation Pattern of the Lower UHF Antenna (#7) in x-z Plane

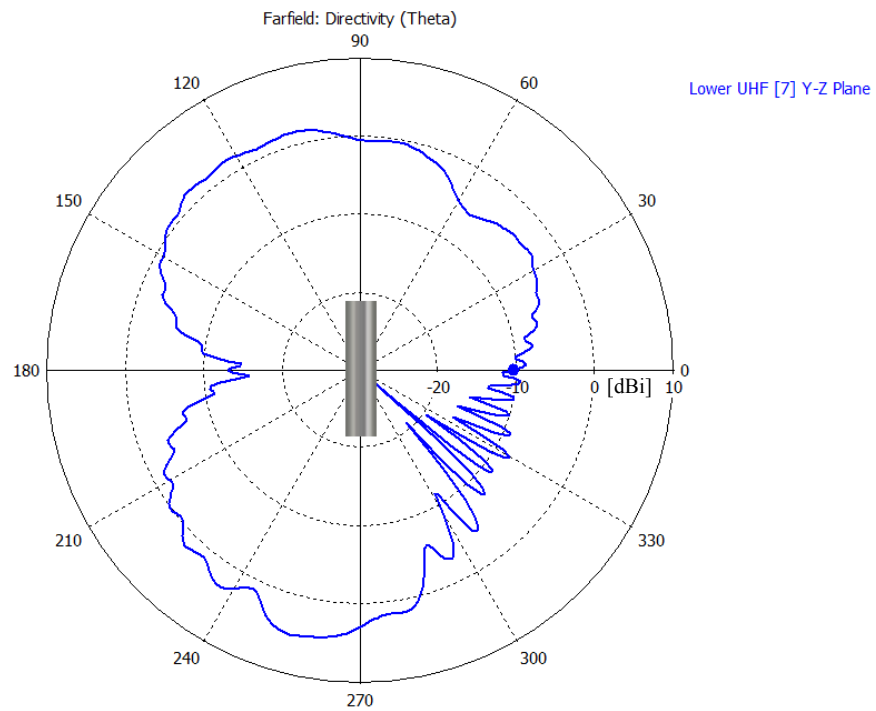


Figure 3-12 Polar Radiation Pattern of the Lower UHF Antenna (#7) in y-z Plane

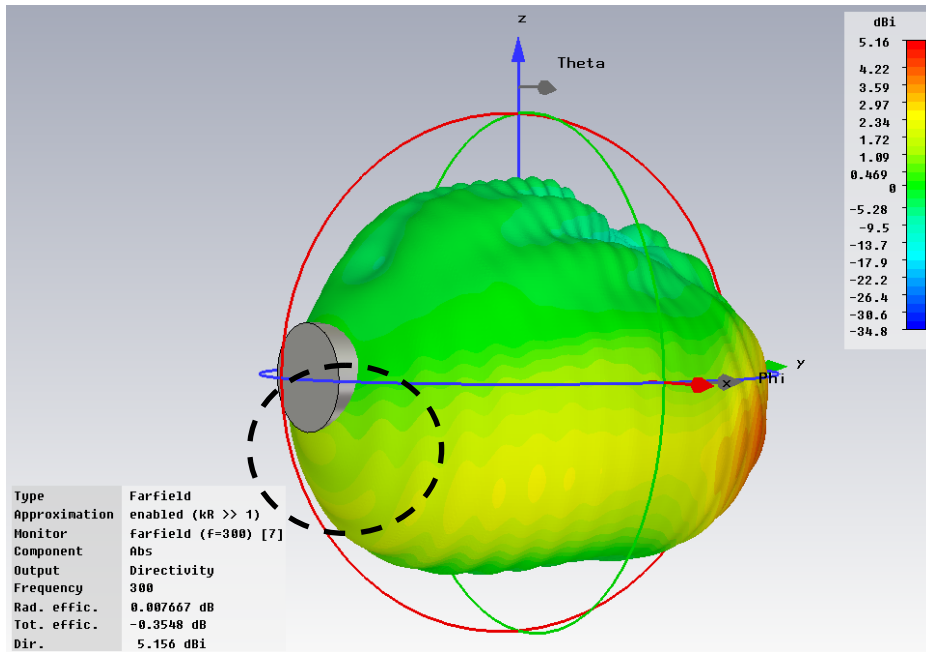


Figure 3-13 3D Radiation Pattern of the Lower UHF Antenna (#7)
 – 1st Angle of View

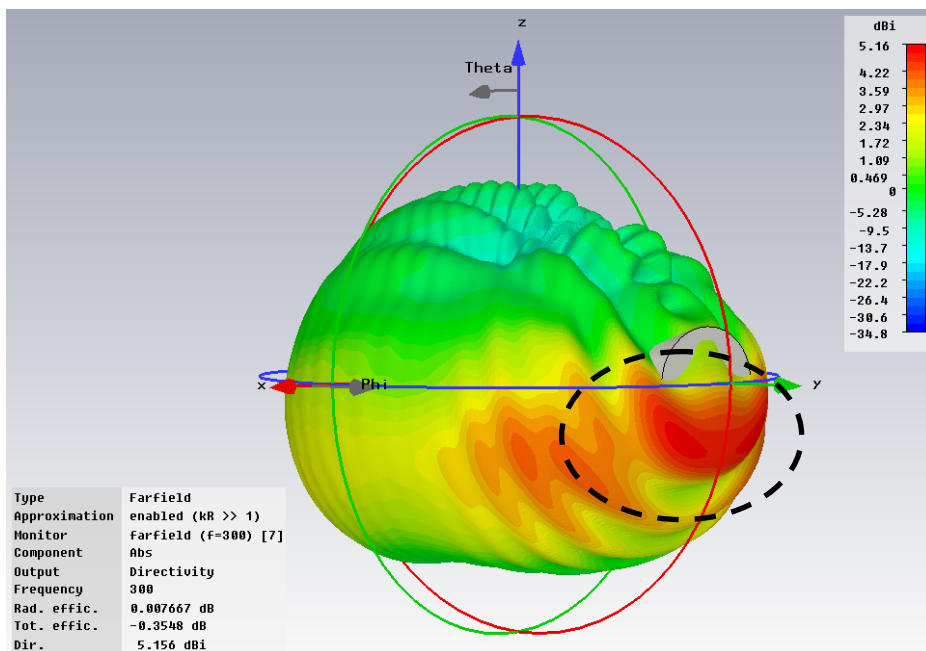


Figure 3-14 3D Radiation Pattern of the Lower UHF Antenna (#7)
 – 2nd Angle of View

Both in the analysis performed on the main fuselage and the other analysis performed on the other structures in this chapter;

- In polar radiation patterns of the lower UHF antenna obtained in x-z plane, the region where theta (θ) is greater than 0° and less than 180° corresponds to phi (Φ) = 180° plane. On the other hand, the region where θ is greater than 180° and less than 360° corresponds to $\Phi = 0^\circ$ plane.
- In polar radiation patterns of the lower UHF antenna obtained in y-z plane, the region where θ is greater than 0° and less than 180° corresponds to $\Phi = 270^\circ$ plane. On the other hand, the region where θ is greater than 180° and less than 360° corresponds to $\Phi = 90^\circ$ plane.

In consequence of the observation of the 3D radiation pattern and the polar radiation patterns of the lower UHF antenna in x-y, x-z and y-z planes, it can be concluded that:

- As it is shown in Figure 3-10, the directivity pattern in x-y plane is almost omnidirectional like the azimuth plane pattern of a monopole antenna above infinite ground plane, since the main fuselage on which the antennas mounted functions as a finite size ground plane. Besides, since the electrical distance between the lower UHF antenna and the back side of the main fuselage is longer than the electrical distance between this antenna and the front side, more power is directed towards the back of the main fuselage (the region where $60^\circ < \Phi < 120^\circ$) compared to the power directed towards the front (the region where $240^\circ < \Phi < 300^\circ$).
- As it is shown in Figure 3-11, in the region where $90^\circ < \theta < 270^\circ$ (in the hemisphere below the main fuselage), the directivity pattern in x-z plane resembles the elevation plane pattern of a monopole antenna above infinite ground plane, since the main fuselage functions as a finite size ground plane. On the other hand, in the region where $0^\circ < \theta < 90^\circ$ and

$270^\circ < \theta < 360^\circ$ (in the hemisphere above the main fuselage), directivity values of the polar radiation pattern are much lower than directivity values in the region where $90^\circ < \theta < 270^\circ$, due to the electromagnetic blockage caused by the main fuselage against the radiation of the lower UHF antenna towards the hemisphere above the main fuselage. In addition to this, in the region where $0^\circ < \theta < 90^\circ$ and $270^\circ < \theta < 360^\circ$, several sidelobes having lower directivity values are observed.

- As it is shown in Figure 3-12, in the region where $90^\circ < \theta < 270^\circ$, the directivity pattern in y-z plane resembles the elevation plane pattern of a monopole antenna above infinite ground plane, since the main fuselage functions as a finite size ground plane. Besides, since the electrical distance between the lower UHF antenna and the back side of the main fuselage is longer than the electrical distance between this antenna and the front side, more power is directed towards the region where $240^\circ < \theta < 270^\circ$ compared to the power directed towards the region where $90^\circ < \theta < 120^\circ$. On the other hand, in the region where $0^\circ < \theta < 90^\circ$ and $270^\circ < \theta < 360^\circ$, directivity values of the polar radiation pattern are much lower than directivity values in the region where $90^\circ < \theta < 270^\circ$, due to the electromagnetic blockage caused by the main fuselage against the radiation of the lower UHF antenna towards the hemisphere above the main fuselage. Also, since the electrical distance between the lower UHF antenna and the front side of the main fuselage is shorter than the electrical distance between this antenna and the back side, more power is directed towards the region where $0^\circ < \theta < 90^\circ$ compared to the power directed towards the region where $270^\circ < \theta < 360^\circ$. In addition to these, in the region where $0^\circ < \theta < 90^\circ$ and $270^\circ < \theta < 360^\circ$, many sidelobes having lower directivity values are observed.
- As it is shown in Figures 3-13 and 3-14, in the region where $90^\circ < \theta < 180^\circ$, the 3D directivity pattern resembles the 3D radiation pattern of a monopole antenna above infinite ground plane, since the main fuselage functions as a finite size ground plane. Besides, since the electrical

distance between the lower UHF antenna and the back side of the main fuselage is longer than the electrical distance between this antenna and the front side, more power is directed towards the region indicated with the dashed circle in Figure 3-14 compared to the power directed towards the region indicated with the dashed circle in Figure 3-13. On the other hand, in the region where $0^\circ < \theta < 90^\circ$, directivity values of the 3D radiation pattern are much lower than directivity values in the region where $90^\circ < \theta < 180^\circ$, due to the electromagnetic blockage caused by the main fuselage against the radiation of the lower UHF antenna towards the hemisphere above the main fuselage. Also, since the electrical distance between the lower UHF antenna and the front side of the main fuselage is shorter than the electrical distance between this antenna and the back side, more power is directed towards the region where $0^\circ < \theta < 90^\circ$ and $180^\circ < \Phi < 360^\circ$ compared to the power directed towards the region where $0^\circ < \theta < 90^\circ$ and $0^\circ < \Phi < 180^\circ$. In addition to these, in the region where $0^\circ < \theta < 90^\circ$, many sidelobes having lower directivity values are observed.

3.2. Analysis of Antennas on the Main Fuselage and Nose

As a result of the electromagnetic analysis of the lower and upper UHF antennas mounted on the main fuselage and the nose of the simplified F-4 model, the electromagnetic coupling levels between the lower and upper UHF antennas and the far field radiation patterns of the lower UHF antenna are obtained for four different locations of the lower UHF antenna, shown in Figures 3-15, 3-16, 3-17 and 3-18 as antennas #7, #10, #11 and #12, respectively.

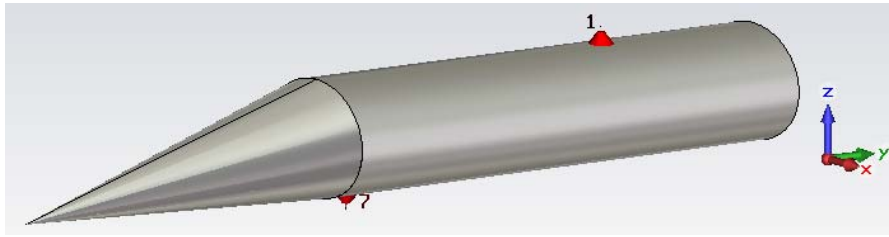


Figure 3-15 The Lower (#7) and Upper (#1) UHF Antennas on the Main Fuselage and the Nose

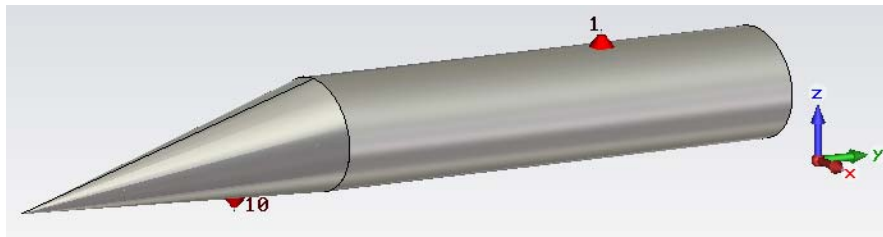


Figure 3-16 The Lower (#10) and Upper (#1) UHF Antennas on the Main Fuselage and the Nose

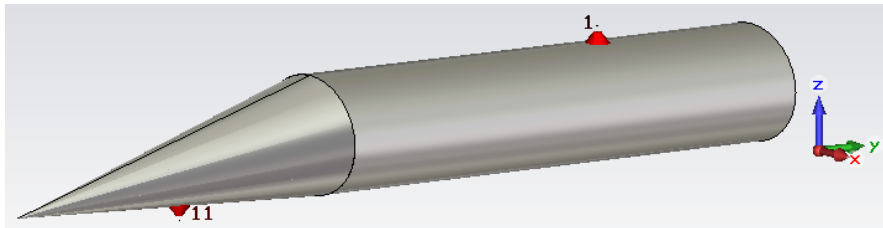


Figure 3-17 The Lower (#11) and Upper (#1) UHF Antennas on the Main Fuselage and the Nose

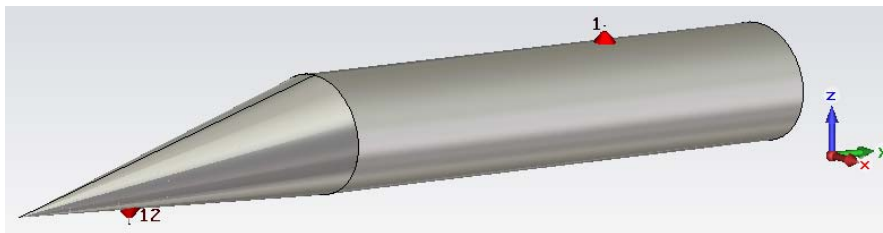


Figure 3-18 The Lower (#12) and Upper (#1) UHF Antennas on the Main Fuselage and the Nose

The plots of the electromagnetic coupling levels ($S_{1,7}$, $S_{1,10}$, $S_{1,11}$ and $S_{1,12}$) between the lower and upper UHF antennas, obtained for four different locations of the lower UHF antenna, over 225 – 400 MHz frequency band are given in Figure 3-19.

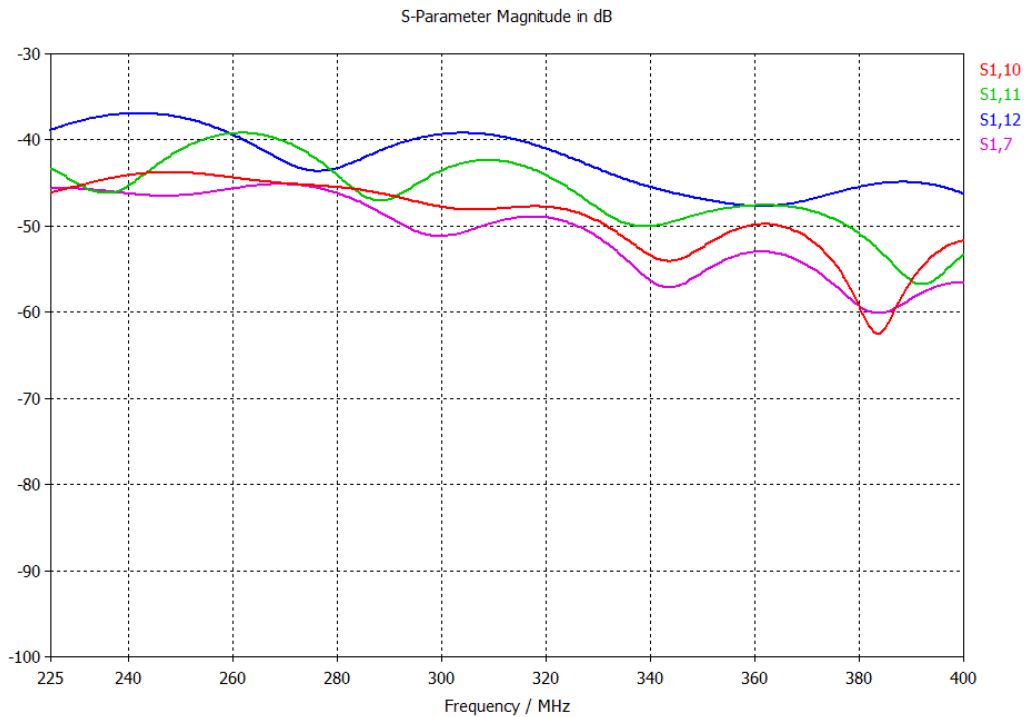


Figure 3-19 Coupling Levels – $S_{1,7}$, $S_{1,10}$, $S_{1,11}$ and $S_{1,12}$

The mean values of the electromagnetic coupling levels ($S_{1,7}$, $S_{1,10}$, $S_{1,11}$ and $S_{1,12}$) over 225 – 400 MHz frequency band are calculated as:

- The mean value of $S_{1,7}$: -50.91 dB
- The mean value of $S_{1,10}$: -48.99 dB
- The mean value of $S_{1,11}$: -46.2 dB
- The mean value of $S_{1,12}$: -42.43 dB

In consequence of the observation of Figure 3-19 and the mean values of the electromagnetic coupling levels, it can be concluded that:

- As the location of the lower UHF antenna changes from the first (antenna #7) to the fourth location (antenna #12) one by one, the mean value of the electromagnetic coupling levels between the lower and upper UHF antennas increases gradually due to the following factors:
 - a. The effectiveness of the electromagnetic blockage caused by the main fuselage and the nose against the radiation of the lower and upper UHF antennas towards each other decreases and the amount of power directed towards the hemisphere above the main fuselage and the nose increases. Because the thickness of the blocking structure above the corresponding lower UHF antenna decreases gradually.
 - b. The angle between the x-y plane, which the gains of the lower and upper UHF antennas above infinite ground plane are maximum ($\theta = 90^\circ$ plane), and the distance vector between the antennas decreases gradually.
 - c. Although the physical distance between the lower and upper UHF antennas increases, the mean value of the electromagnetic coupling levels between the antennas increases due to the fact that the effects of the electromagnetic blockage caused by the main fuselage and the nose and the angle between $\theta = 90^\circ$ plane and the distance vector between the antennas are much more dominant than the effect of the physical distance between the antennas.
- When the lower UHF antenna is at the first location (antenna #7), the mean value of the electromagnetic coupling levels between the lower and upper UHF antennas is minimum among the corresponding results of four different locations, since the electromagnetic blockage caused by the main fuselage and the nose is most effective and the angle between $\theta = 90^\circ$ plane and the distance vector between the antennas is maximum in this case.

- When the lower UHF antenna is at the fourth location (antenna #12), the mean value of the electromagnetic coupling levels between the lower and upper UHF antennas is maximum among the corresponding results of four different locations, since the electromagnetic blockage caused by the main fuselage and the nose is least effective and the angle between $\theta = 90^\circ$ plane and the distance vector between the antennas is minimum in this case.

The far field radiation patterns of the lower UHF antenna, which are obtained for four different locations of the lower UHF antenna, are given in Figures 3-20 to 3-30.

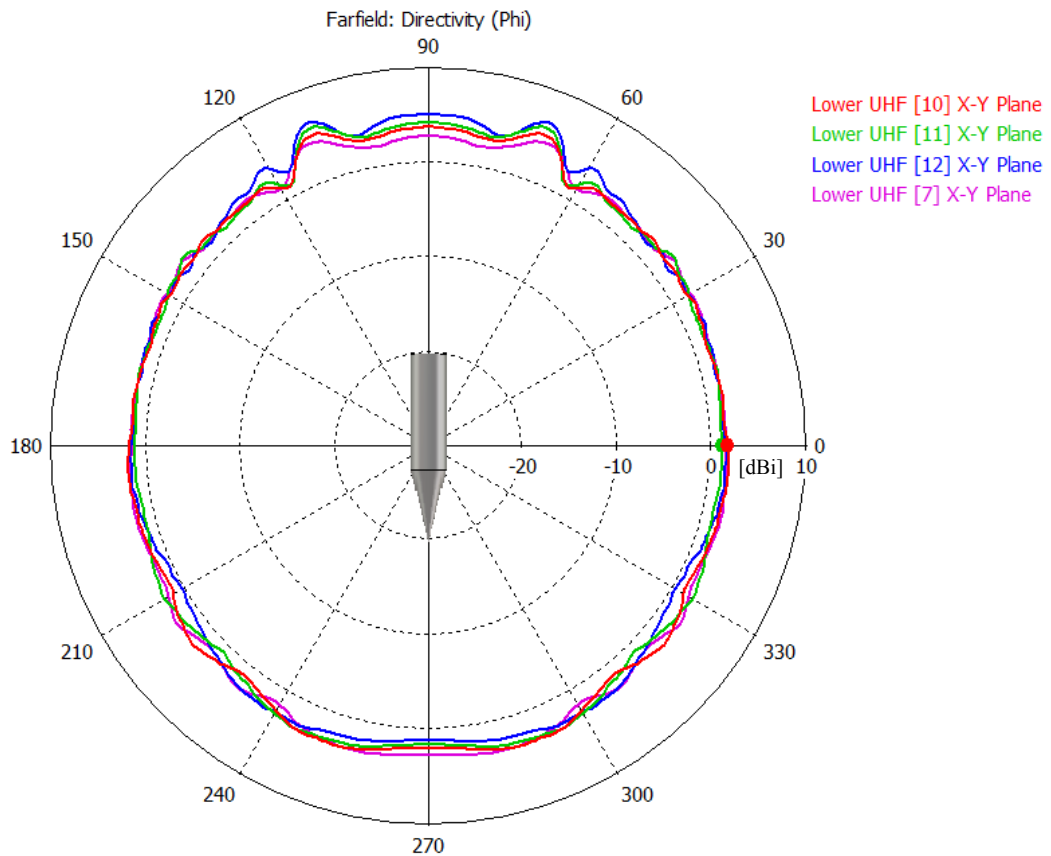


Figure 3-20 Polar Radiation Patterns of the Lower UHF Antenna in x-y Plane

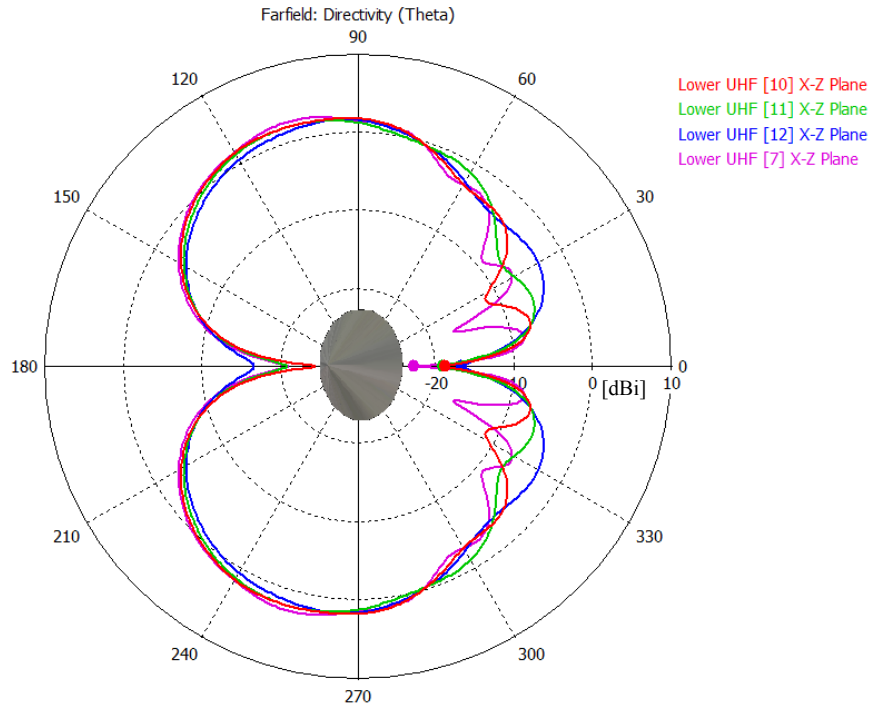


Figure 3-21 Polar Radiation Patterns of the Lower UHF Antenna in x-z Plane

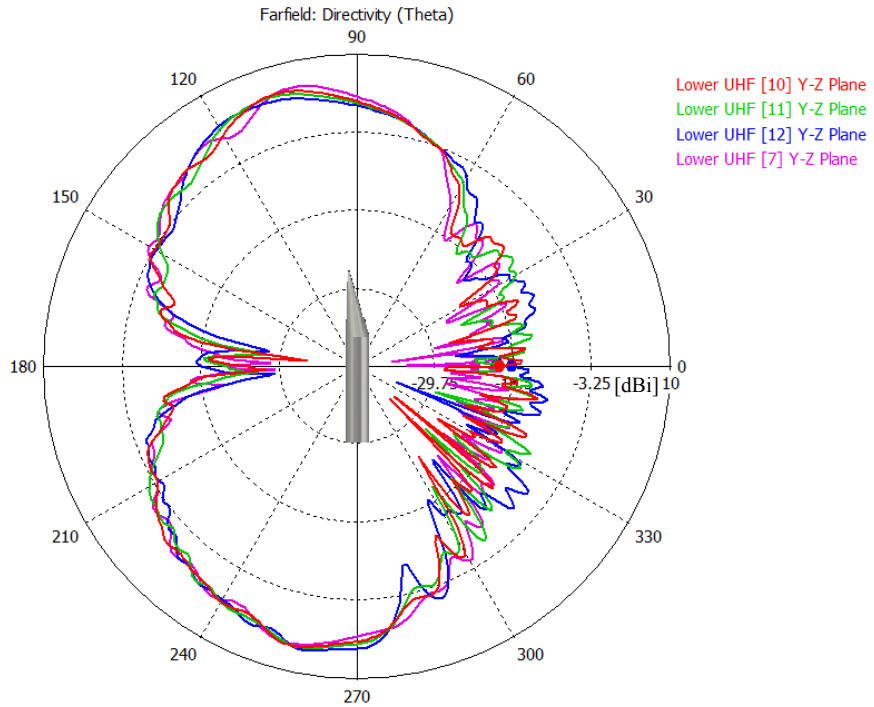


Figure 3-22 Polar Radiation Patterns of the Lower UHF Antenna in y-z Plane

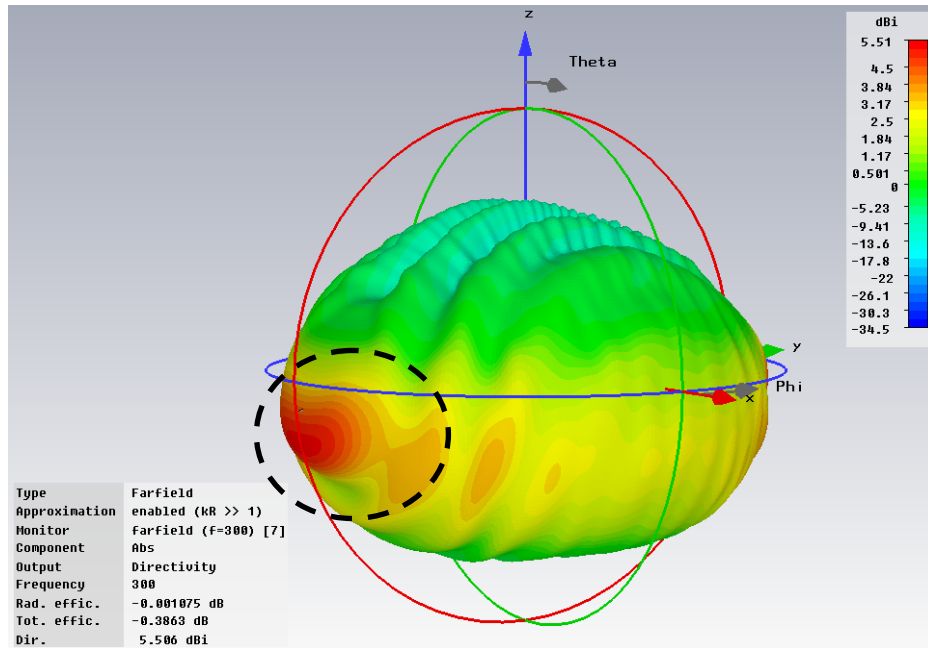


Figure 3-23 3D Radiation Pattern of the Lower UHF Antenna (#7)
 – 1st Angle of View

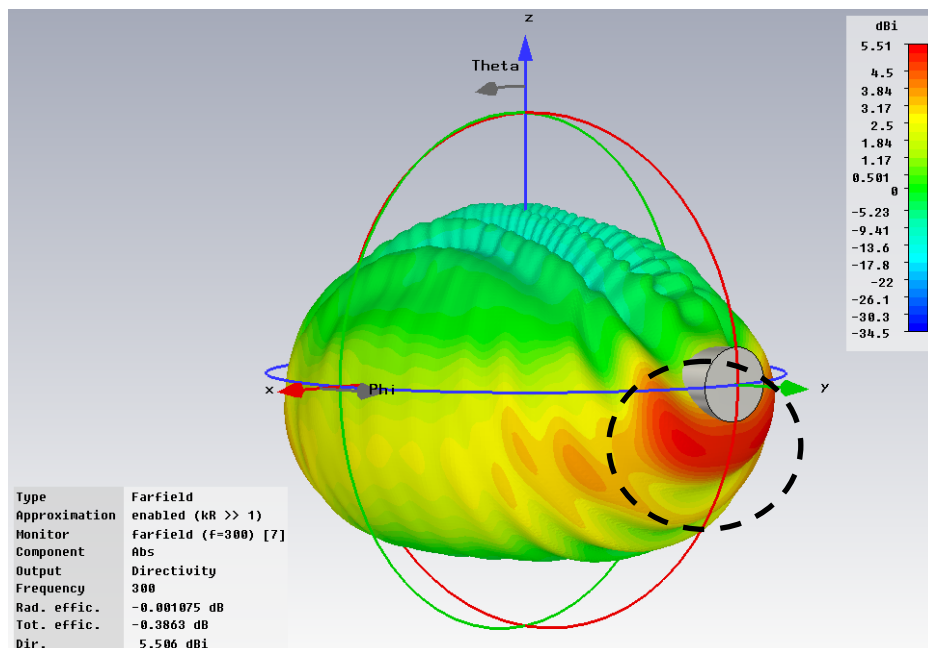


Figure 3-24 3D Radiation Pattern of the Lower UHF Antenna (#7)
 – 2nd Angle of View

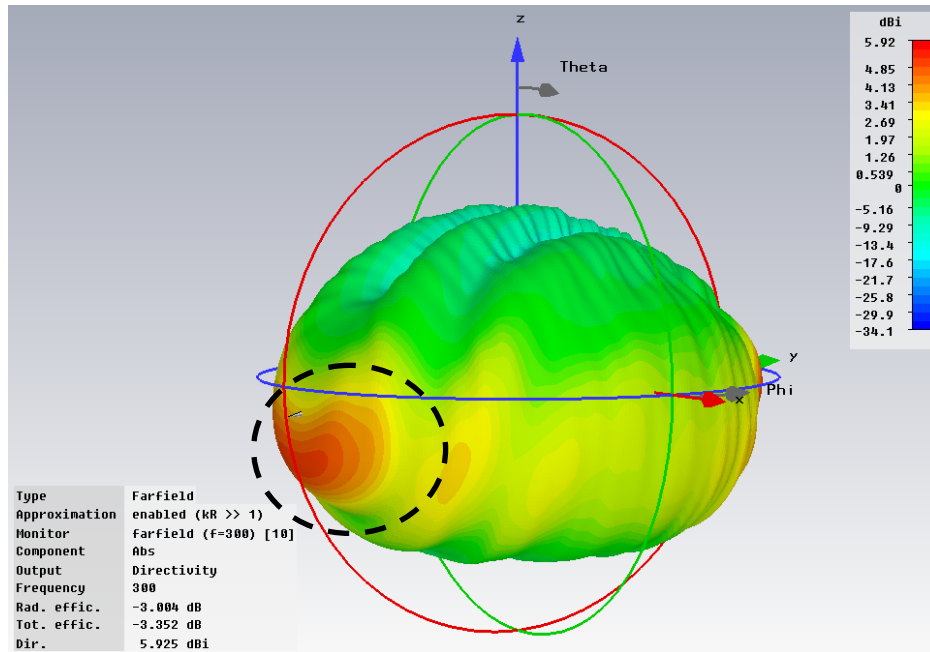


Figure 3-25 3D Radiation Pattern of the Lower UHF Antenna (#10)
 – 1st Angle of View

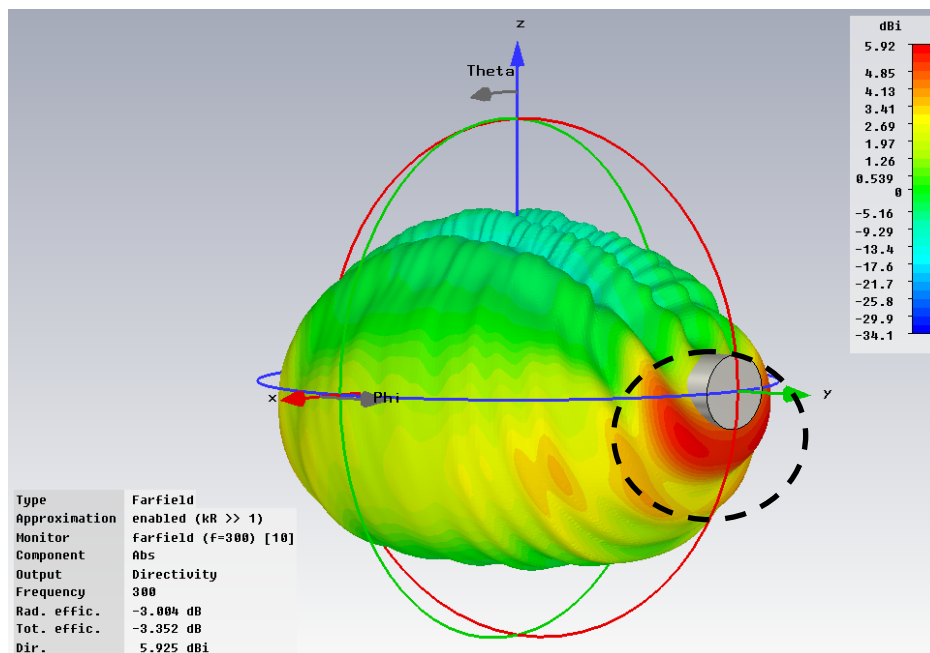


Figure 3-26 3D Radiation Pattern of the Lower UHF Antenna (#10)
 – 2nd Angle of View

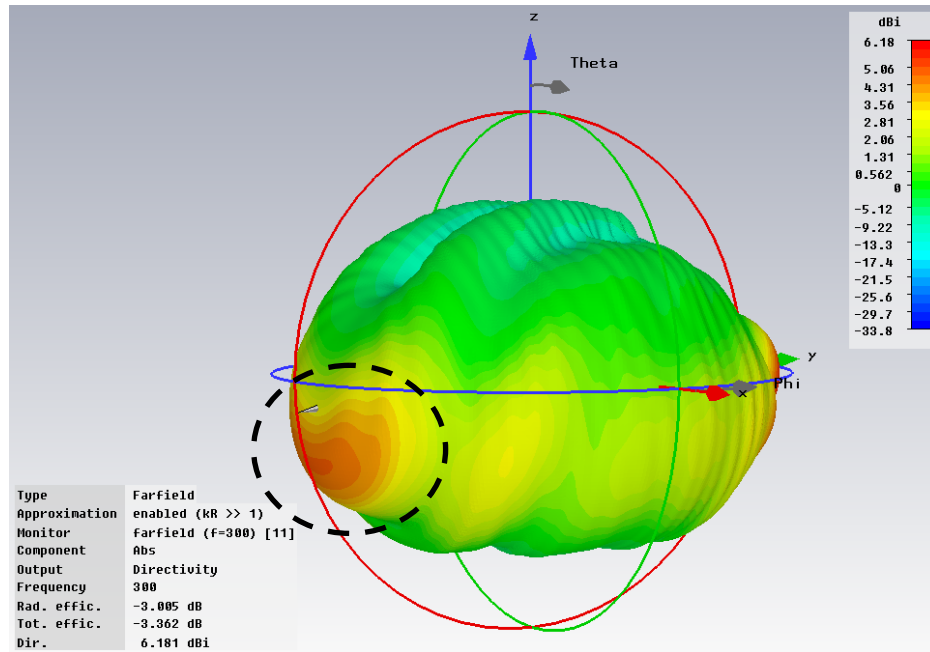


Figure 3-27 3D Radiation Pattern of the Lower UHF Antenna (#11)
 - 1st Angle of View

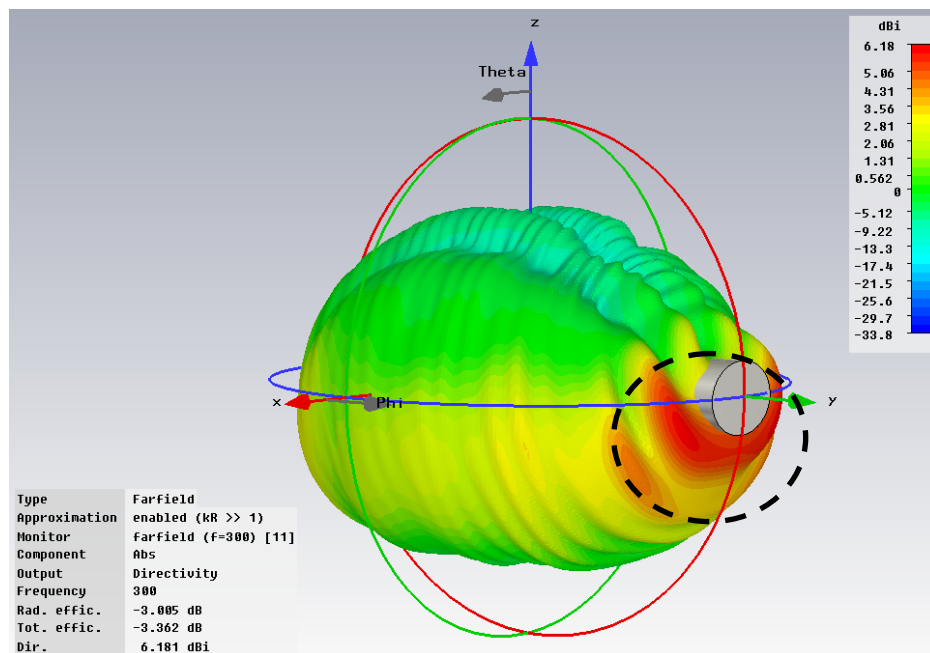


Figure 3-28 3D Radiation Pattern of the Lower UHF Antenna (#11)
 - 2nd Angle of View

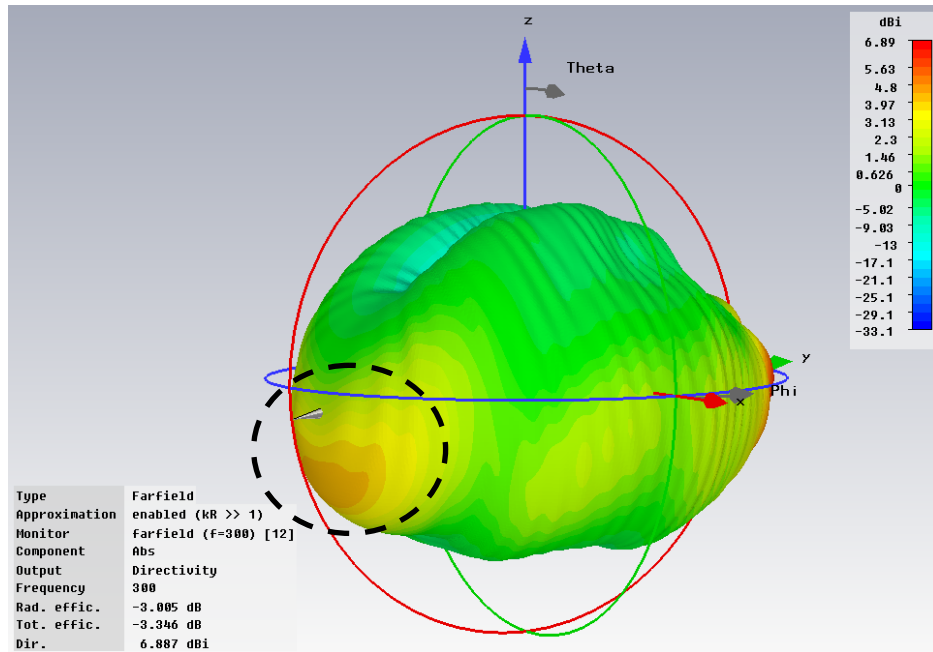


Figure 3-29 3D Radiation Pattern of the Lower UHF Antenna (#12)
 – 1st Angle of View

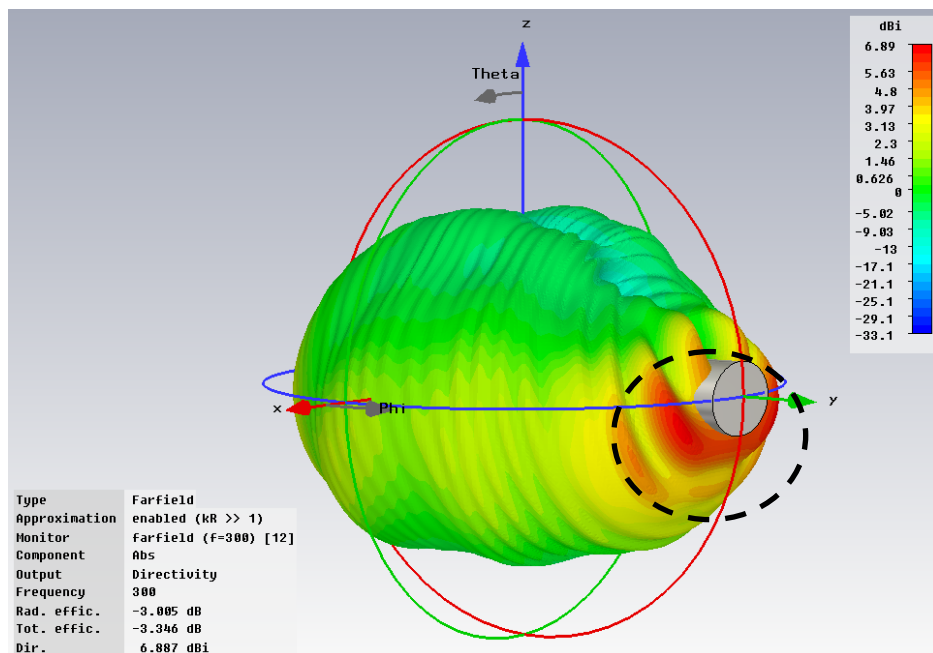


Figure 3-30 3D Radiation Pattern of the Lower UHF Antenna (#12)
 – 2nd Angle of View

In consequence of the observation of the 3D radiation patterns and the polar radiation patterns of the lower UHF antenna in x-y, x-z and y-z planes, which are obtained for four different locations of the lower UHF antenna, it can be concluded that:

- As it is shown in Figure 3-20, all directivity patterns in x-y plane are almost omnidirectional like the azimuth plane pattern of a monopole antenna above infinite ground plane, since the main fuselage and the nose on which the antennas mounted function as a finite size ground plane. Besides, as the location of the lower UHF antenna changes from the first (antenna #7) to the fourth location (antenna #12) one by one, since the electrical distance between the lower UHF antenna and the back side of the main fuselage increases and the electrical distance between this antenna and the tip of the nose decreases, the amount of power directed towards the back of the main fuselage (the region where $60^\circ < \Phi < 120^\circ$) increases and the amount of power directed towards the front of the nose (the region where $240^\circ < \Phi < 300^\circ$) decreases.
- As it is shown in Figure 3-21, in the region where $90^\circ < \theta < 270^\circ$, all directivity patterns in x-z plane resemble the elevation plane pattern of a monopole antenna above infinite ground plane, since the main fuselage and the nose function as a finite size ground plane. On the other hand, as the location of the lower UHF antenna changes from the first (antenna #7) to the fourth location (antenna #12) one by one, in the region where $0^\circ < \theta < 90^\circ$ and $270^\circ < \theta < 360^\circ$, directivity values of the polar radiation pattern increase (the amount of power directed towards the hemisphere above the main fuselage and the nose increases) and the number of sidelobes decreases, due to the decrease of the electromagnetic blockage effect (the thickness of the blocking structure above the corresponding lower UHF antenna decreases) caused by the main fuselage and the nose against the radiation of the lower UHF antenna towards the hemisphere above the main fuselage and the nose.

- As it is shown in Figure 3-22, in the region where $90^\circ < \theta < 270^\circ$, all directivity patterns in y-z plane resemble the elevation plane pattern of a monopole antenna above infinite ground plane, since the main fuselage and the nose function as a finite size ground plane. Besides, as the location of the lower UHF antenna changes from the first (antenna #7) to the fourth location (antenna #12) one by one, since the electrical distance between the lower UHF antenna and the back side of the main fuselage increases and the electrical distance between this antenna and the tip of the nose decreases, the amount of power directed towards the region where $255^\circ < \theta < 270^\circ$ increases and the amount of power directed towards the region where $90^\circ < \theta < 105^\circ$ decreases. On the other hand, as the location of the lower UHF antenna changes from the first (antenna #7) to the fourth location (antenna #12) one by one, in the region where $0^\circ < \theta < 90^\circ$ and $270^\circ < \theta < 360^\circ$, directivity values of the polar radiation pattern increase (the amount of power directed towards the hemisphere above the main fuselage and the nose increases), due to the decrease of the electromagnetic blockage effect (the thickness of the blocking structure above the corresponding lower UHF antenna decreases) caused by the main fuselage and the nose against the radiation of the lower UHF antenna towards the hemisphere above the main fuselage and the nose. In addition to this, in the region where $0^\circ < \theta < 90^\circ$ and $270^\circ < \theta < 360^\circ$, many sidelobes having lower directivity values are observed for all directivity patterns.
- As it is shown in Figures 3-23 to 3-30, in the region where $90^\circ < \theta < 180^\circ$, all 3D directivity patterns resemble the 3D radiation pattern of a monopole antenna above infinite ground plane, since the main fuselage and the nose function as a finite size ground plane. Besides, as the location of the lower UHF antenna changes from the first (antenna #7) to the fourth location (antenna #12) one by one, since the electrical distance between the lower UHF antenna and the back side of the main fuselage increases and the electrical distance between this antenna and the tip of the nose decreases, the amount of power directed towards the region indicated with the dashed

circles in Figures 3-24, 3-26, 3-28 and 3-30 increases and the amount of power directed towards the region indicated with the dashed circles in Figures 3-23, 3-25, 3-27 and 3-29 decreases. On the other hand, as the location of the lower UHF antenna changes from the first (antenna #7) to the fourth location (antenna #12) one by one, in the region where $0^\circ < \theta < 90^\circ$, directivity values of the 3D radiation pattern increase (the amount of power directed towards the hemisphere above the main fuselage and the nose increases) and the number of sidelobes decreases, due to the decrease of the electromagnetic blockage effect (the thickness of the blocking structure above the corresponding lower UHF antenna decreases) caused by the main fuselage and the nose against the radiation of the lower UHF antenna towards the hemisphere above the main fuselage and the nose. Also, as the location of the lower UHF antenna changes from the first (antenna #7) to the fourth location (antenna #12) one by one, since the electrical distance between the lower UHF antenna and the back side of the main fuselage increases and the electrical distance between this antenna and the tip of the nose decreases, the difference between the amount of power directed towards the region where $0^\circ < \theta < 90^\circ$ and $180^\circ < \Phi < 360^\circ$ and the amount of power directed towards the region where $0^\circ < \theta < 90^\circ$ and $0^\circ < \Phi < 180^\circ$ increases.

3.3. Analysis of Antennas on the Main Fuselage, Nose and Wings

As a result of the electromagnetic analysis of the lower and upper UHF antennas mounted on the main fuselage, the nose and the wings of the simplified F-4 model, the electromagnetic coupling levels between the lower and upper UHF antennas and the far field radiation patterns of the lower UHF antenna are obtained for four different locations of the lower UHF antenna, shown in Figures 3-31, 3-32, 3-33 and 3-34 as antennas #7, #10, #11 and #12, respectively.

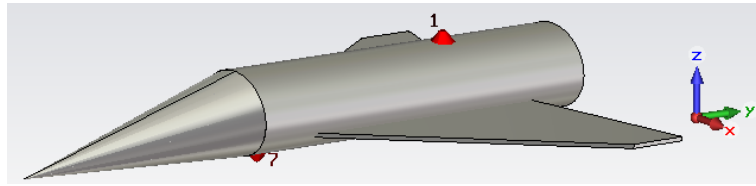


Figure 3-31 The Lower (#7) and Upper (#1) UHF Antennas on the Main Fuselage, the Nose and the Wings

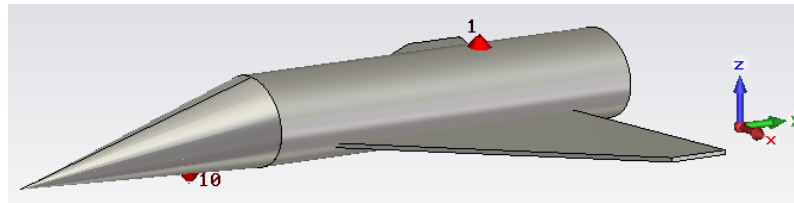


Figure 3-32 The Lower (#10) and Upper (#1) UHF Antennas on the Main Fuselage, the Nose and the Wings

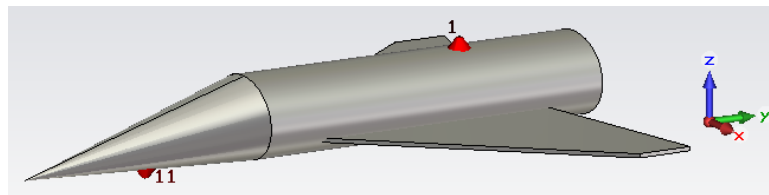


Figure 3-33 The Lower (#11) and Upper (#1) UHF Antennas on the Main Fuselage, the Nose and the Wings

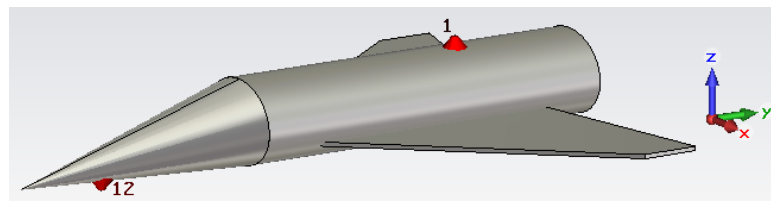


Figure 3-34 The Lower (#12) and Upper (#1) UHF Antennas on the Main Fuselage, the Nose and the Wings

The plots of the electromagnetic coupling levels ($S_{1,7}$, $S_{1,10}$, $S_{1,11}$ and $S_{1,12}$) between the lower and upper UHF antennas, obtained for four different locations of the lower UHF antenna, over 225 – 400 MHz frequency band are given in Figure 3-35.

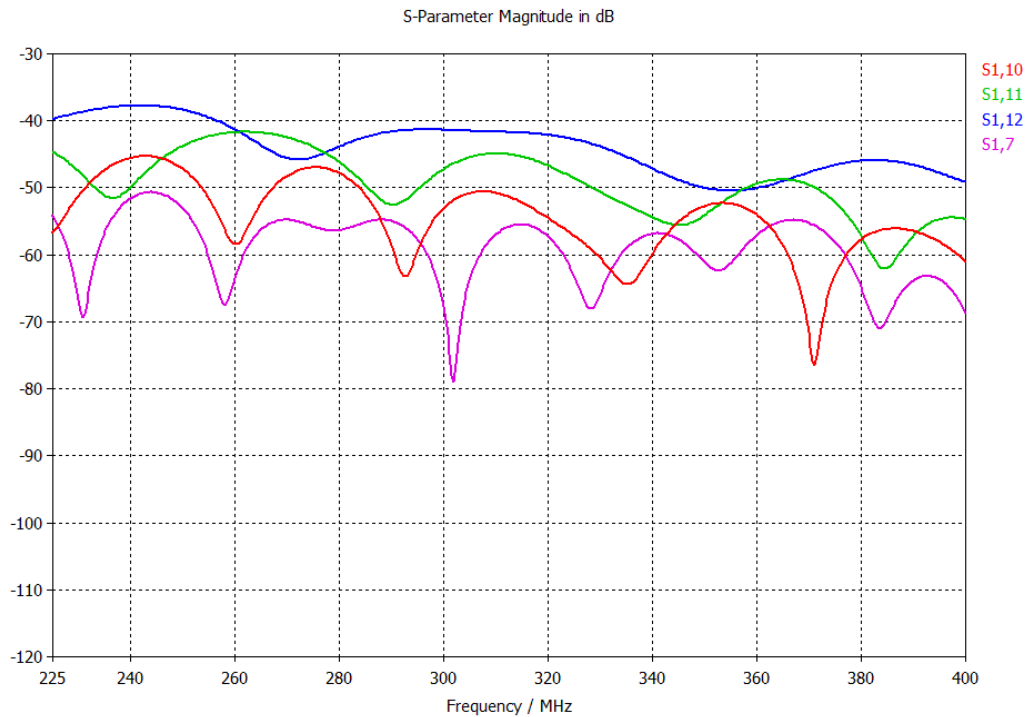


Figure 3-35 Coupling Levels – $S_{1,7}$, $S_{1,10}$, $S_{1,11}$ and $S_{1,12}$

The mean values of the electromagnetic coupling levels ($S_{1,7}$, $S_{1,10}$, $S_{1,11}$ and $S_{1,12}$) over 225 – 400 MHz frequency band are calculated as:

- The mean value of $S_{1,7}$: -59.22 dB
- The mean value of $S_{1,10}$: -54.58 dB
- The mean value of $S_{1,11}$: -49.36 dB
- The mean value of $S_{1,12}$: -43.94 dB

In consequence of the observation of Figure 3-35 and the mean values of the electromagnetic coupling levels, it can be concluded that:

- As the location of the lower UHF antenna changes from the first (antenna #7) to the fourth location (antenna #12) one by one, the mean value of the electromagnetic coupling levels between the lower and upper UHF antennas increases gradually due to the following factors:
 - a. The effectiveness of the electromagnetic blockage caused by the main fuselage, the nose and the wings against the radiation of the lower and upper UHF antennas towards each other decreases and the amount of power directed towards the hemisphere above the main fuselage, the nose and the wings increases. Because the thickness of the blocking structure above the corresponding lower UHF antenna decreases gradually and the electrical distance between the lower UHF antenna and the wings increases.
 - b. The angle between the x-y plane, which the gains of the lower and upper UHF antennas above infinite ground plane are maximum ($\theta = 90^\circ$ plane), and the distance vector between the antennas decreases gradually.
 - c. Although the physical distance between the lower and upper UHF antennas increases, the mean value of the electromagnetic coupling levels between the antennas increases due to the fact that the effects of the electromagnetic blockage caused by the main fuselage, the nose and the wings and the angle between $\theta = 90^\circ$ plane and the distance vector between the antennas are much more dominant than the effect of the physical distance between the antennas.
- When the lower UHF antenna is at the first location (antenna #7), the mean value of the electromagnetic coupling levels between the lower and upper UHF antennas is minimum among the corresponding results of four different locations, since the electromagnetic blockage caused by the main fuselage, the nose and the wings is most effective and the angle between

$\theta = 90^\circ$ plane and the distance vector between the antennas is maximum in this case.

- When the lower UHF antenna is at the fourth location (antenna #12), the mean value of the electromagnetic coupling levels between the lower and upper UHF antennas is maximum among the corresponding results of four different locations, since the electromagnetic blockage caused by the main fuselage, the nose and the wings is least effective and the angle between $\theta = 90^\circ$ plane and the distance vector between the antennas is minimum in this case.

The far field radiation patterns of the lower UHF antenna, which are obtained for four different locations of the lower UHF antenna, are given in Figures 3-36 to 3-46.

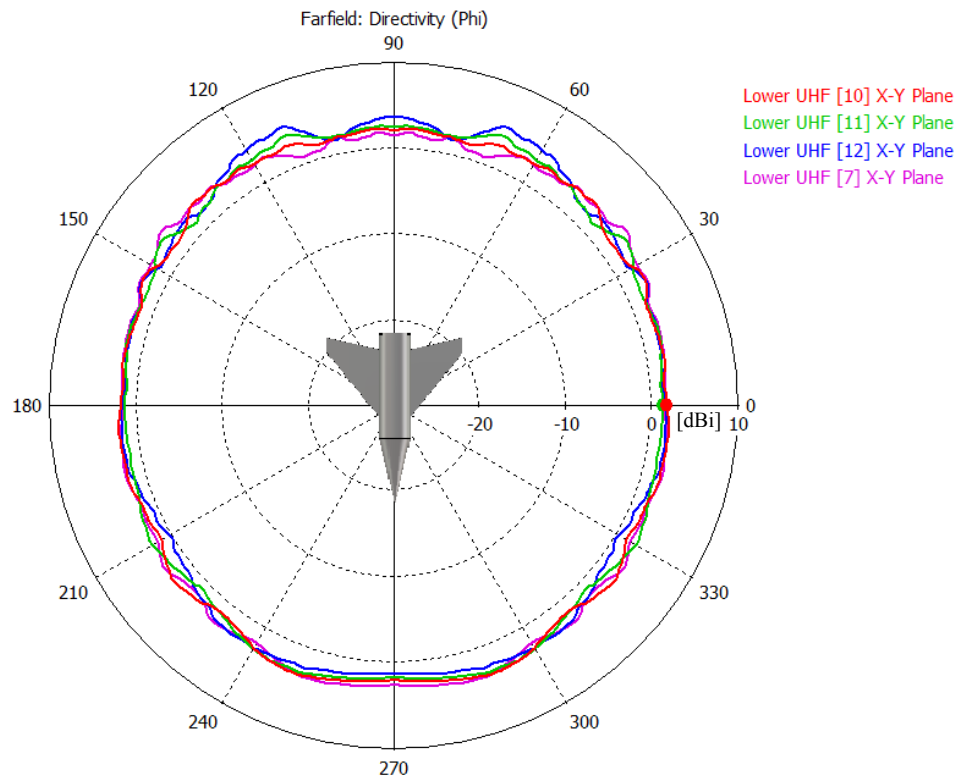


Figure 3-36 Polar Radiation Patterns of the Lower UHF Antenna in x-y Plane

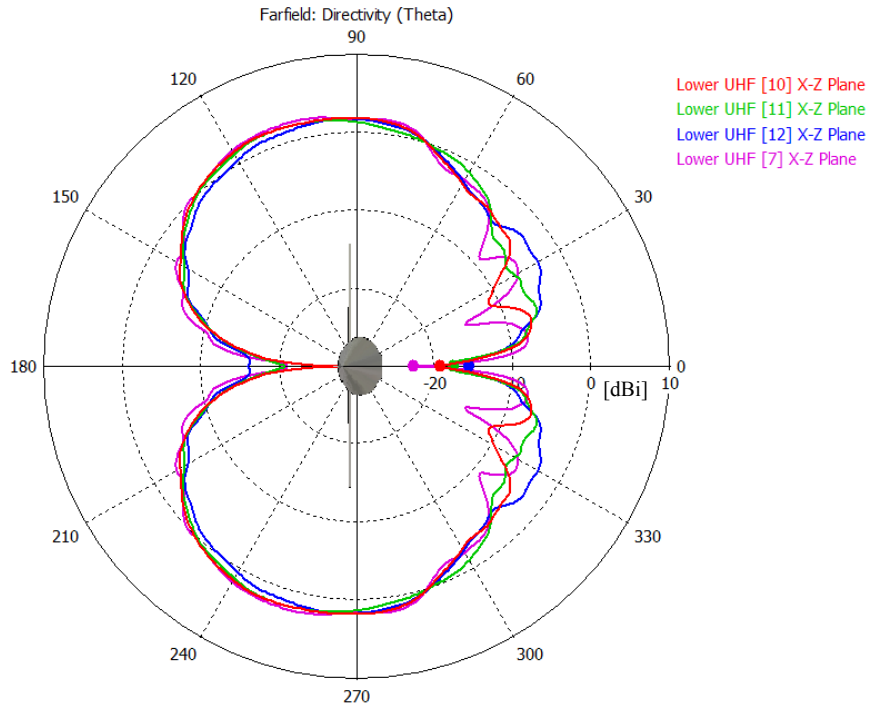


Figure 3-37 Polar Radiation Patterns of the Lower UHF Antenna in x-z Plane

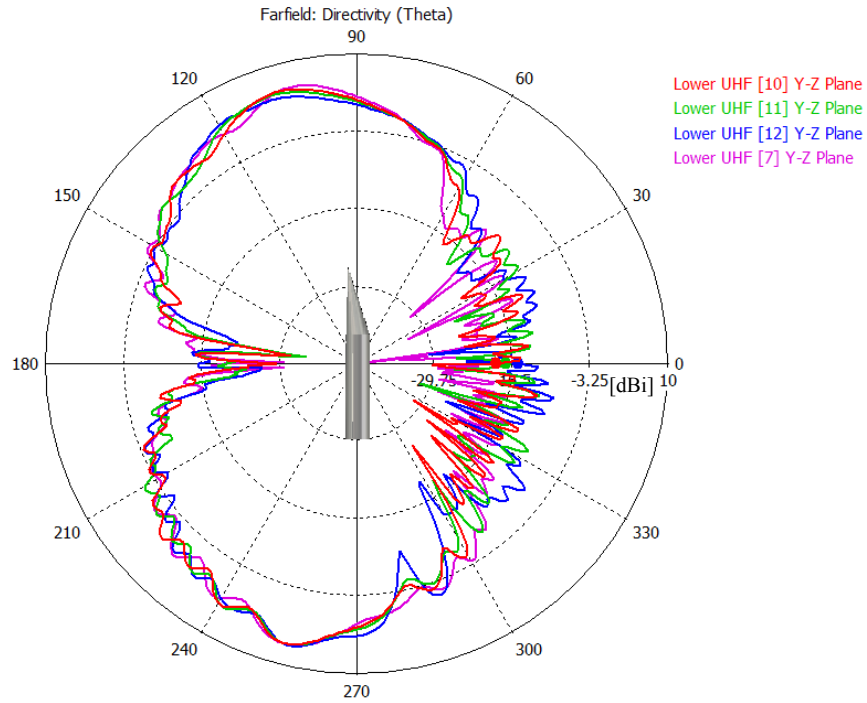


Figure 3-38 Polar Radiation Patterns of the Lower UHF Antenna in y-z Plane

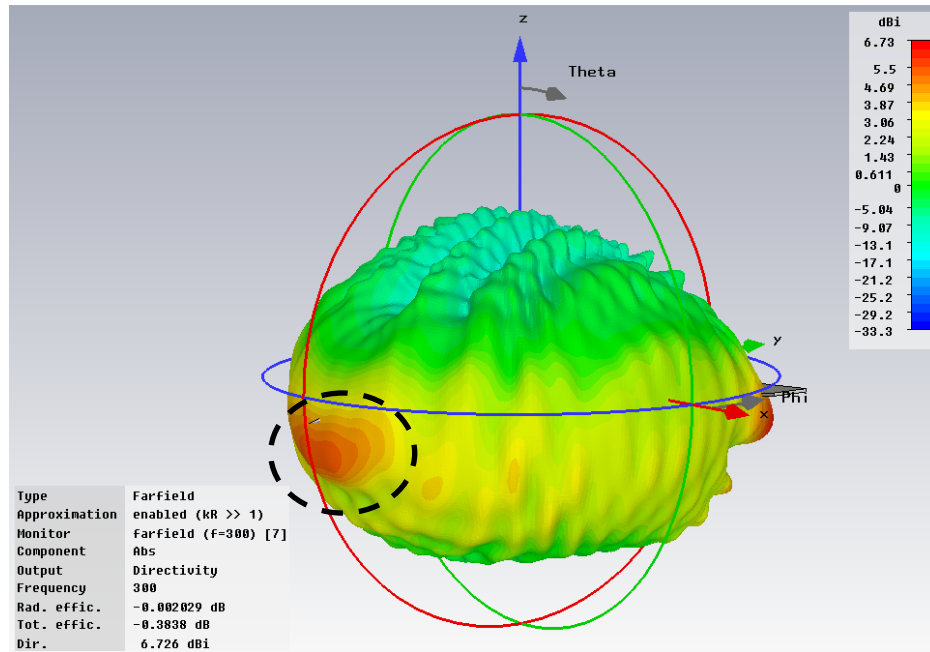


Figure 3-39 3D Radiation Pattern of the Lower UHF Antenna (#7)
 – 1st Angle of View

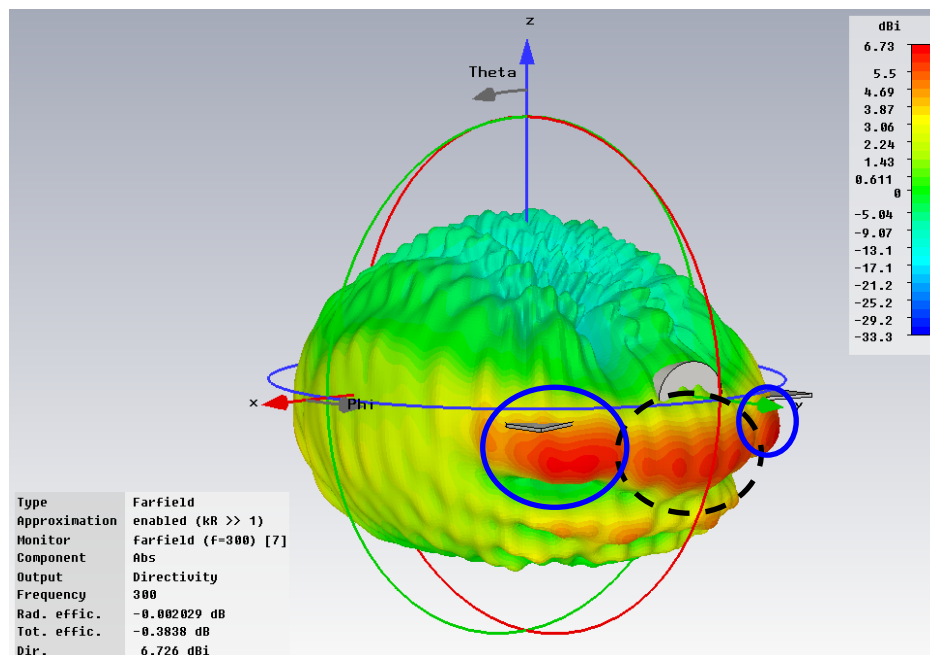


Figure 3-40 3D Radiation Pattern of the Lower UHF Antenna (#7)
 – 2nd Angle of View

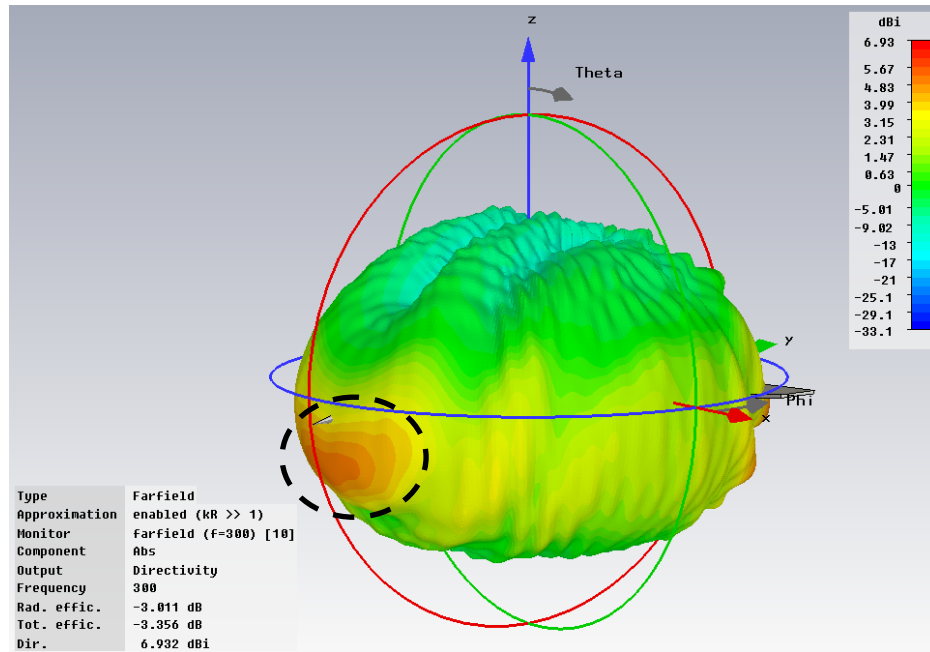


Figure 3-41 3D Radiation Pattern of the Lower UHF Antenna (#10)
 – 1st Angle of View

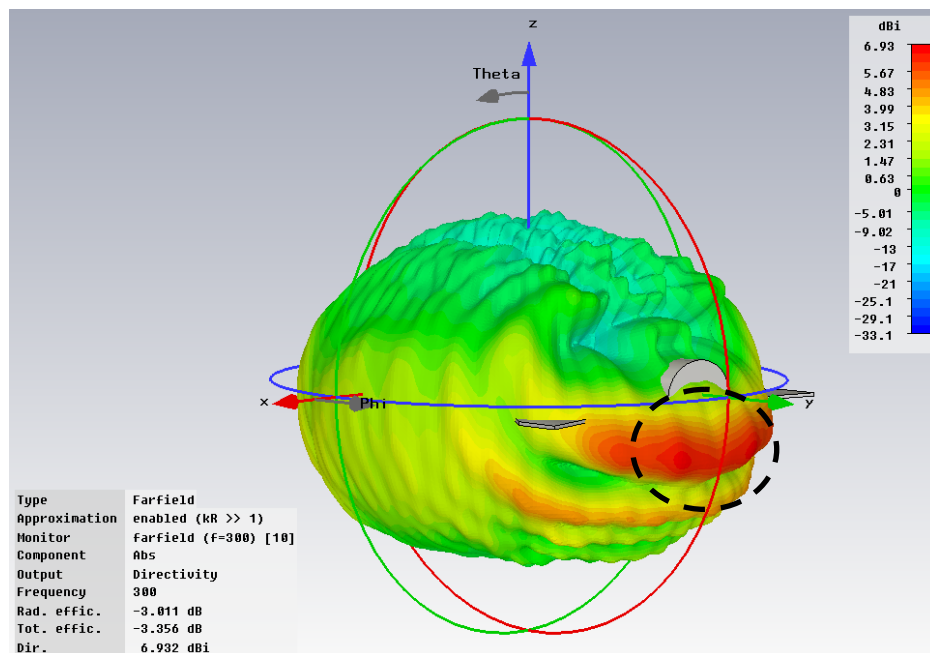


Figure 3-42 3D Radiation Pattern of the Lower UHF Antenna (#10)
 – 2nd Angle of View

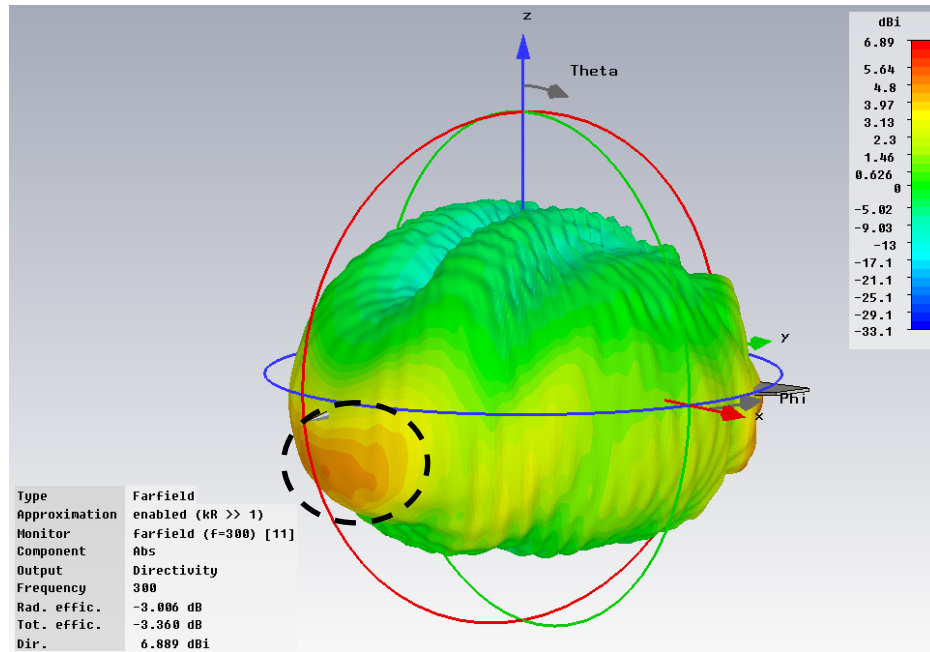


Figure 3-43 3D Radiation Pattern of the Lower UHF Antenna (#11)
 - 1st Angle of View

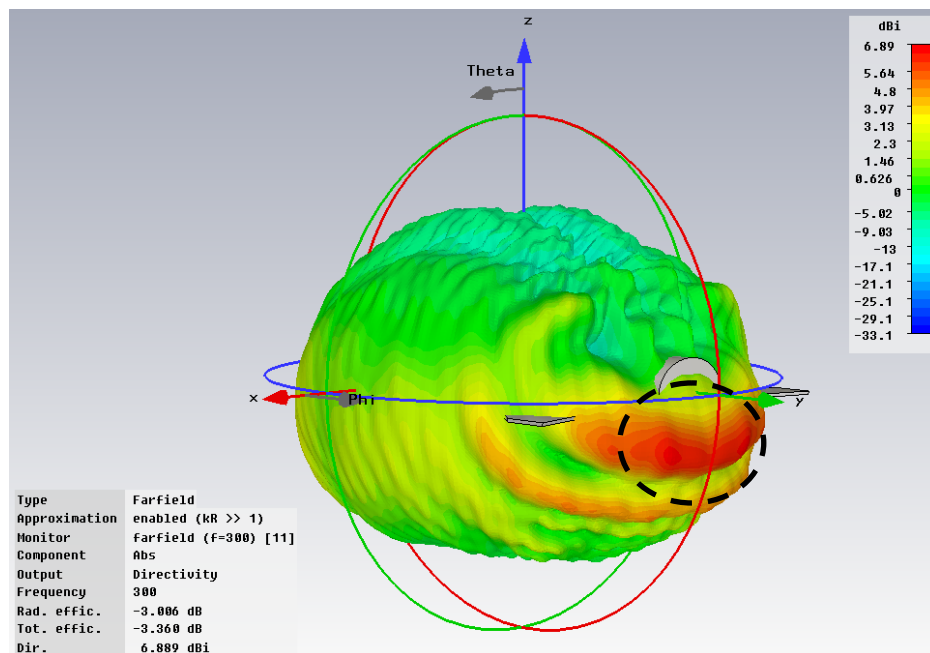


Figure 3-44 3D Radiation Pattern of the Lower UHF Antenna (#11)
 - 2nd Angle of View

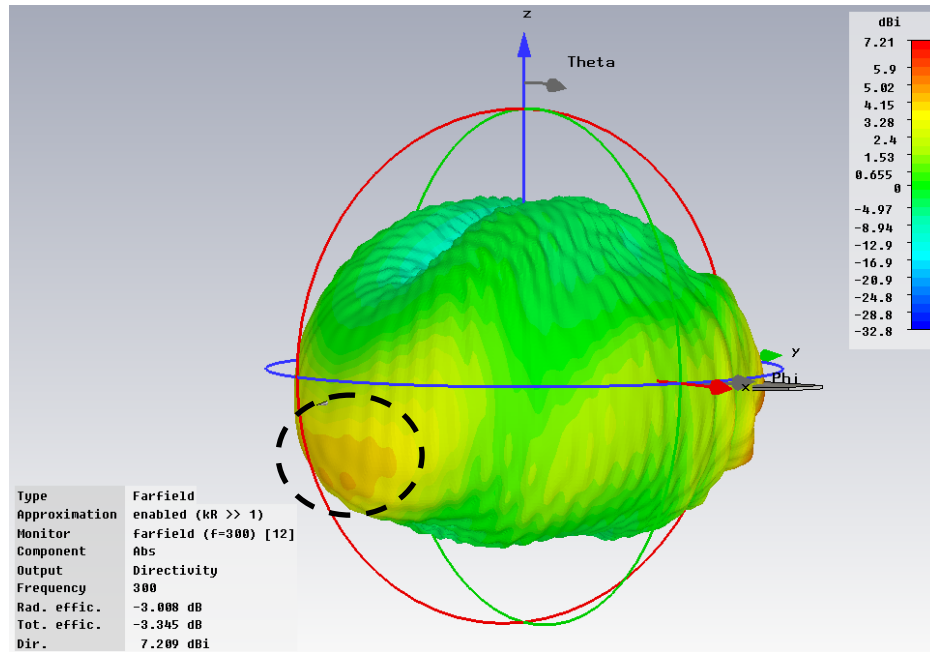


Figure 3-45 3D Radiation Pattern of the Lower UHF Antenna (#12)
 – 1st Angle of View

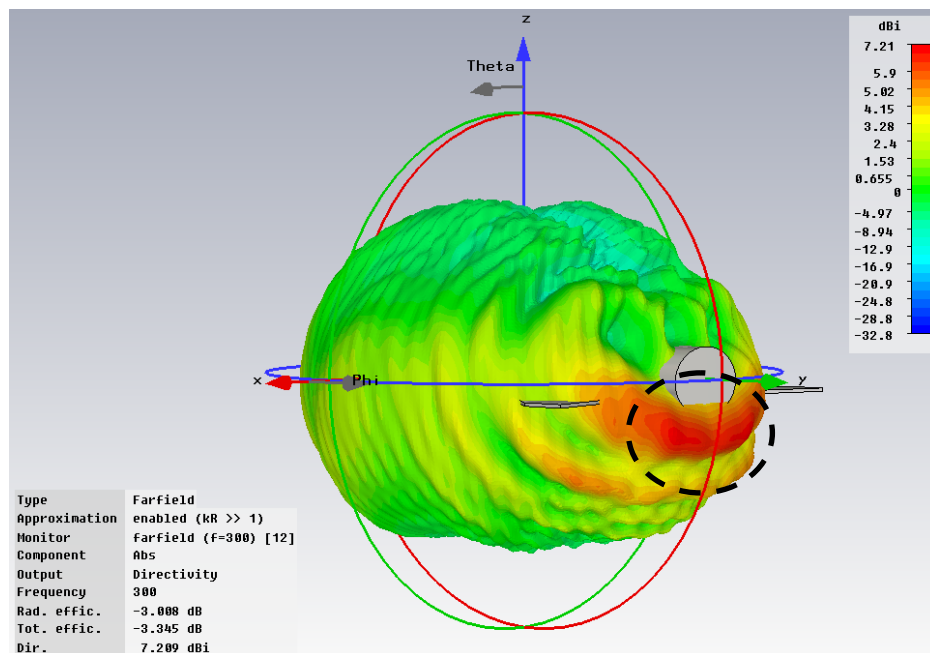


Figure 3-46 3D Radiation Pattern of the Lower UHF Antenna (#12)
 – 2nd Angle of View

In consequence of the observation of the 3D radiation patterns and the polar radiation patterns of the lower UHF antenna in x-y, x-z and y-z planes, which are obtained for four different locations of the lower UHF antenna, it can be concluded that:

- As it is shown in Figure 3-36, all directivity patterns in x-y plane are almost omnidirectional like the azimuth plane pattern of a monopole antenna above infinite ground plane, since the main fuselage, the nose and the wings function as a finite size ground plane. Besides, as the location of the lower UHF antenna changes from the first (antenna #7) to the fourth location (antenna #12) one by one, since the electrical distance between the lower UHF antenna and the back side of the main fuselage increases and the electrical distance between this antenna and the tip of the nose decreases, the amount of power directed towards the back of the main fuselage (the region where $60^\circ < \Phi < 120^\circ$) increases and the amount of power directed towards the front of the nose (the region where $240^\circ < \Phi < 300^\circ$) decreases.
- As it is shown in Figure 3-37, in the region where $90^\circ < \theta < 270^\circ$, all directivity patterns in x-z plane resemble the elevation plane pattern of a monopole antenna above infinite ground plane, since the main fuselage, the nose and the wings function as a finite size ground plane. On the other hand, as the location of the lower UHF antenna changes from the first (antenna #7) to the fourth location (antenna #12) one by one, in the region where $0^\circ < \theta < 90^\circ$ and $270^\circ < \theta < 360^\circ$, directivity values of the polar radiation pattern increase (the amount of power directed towards the hemisphere above the main fuselage, the nose and the wings increases) and the number of sidelobes decreases, due to the decrease of the electromagnetic blockage effect (the thickness of the blocking structure above the corresponding lower UHF antenna decreases and the electrical distance between the lower UHF antenna and the wings increases) caused by the main fuselage, the nose and the wings against the radiation of the

lower UHF antenna towards the hemisphere above the main fuselage, the nose and the wings.

- As it is shown in Figure 3-38, in the region where $90^\circ < \theta < 270^\circ$, all directivity patterns in y-z plane resemble the elevation plane pattern of a monopole antenna above infinite ground plane, since the main fuselage, the nose and the wings function as a finite size ground plane. Besides, as the location of the lower UHF antenna changes from the first (antenna #7) to the fourth location (antenna #12) one by one, since the electrical distance between the lower UHF antenna and the back side of the main fuselage increases and the electrical distance between this antenna and the tip of the nose decreases, the amount of power directed towards the region where $255^\circ < \theta < 270^\circ$ increases and the amount of power directed towards the region where $90^\circ < \theta < 105^\circ$ decreases. On the other hand, as the location of the lower UHF antenna changes from the first (antenna #7) to the fourth location (antenna #12) one by one, in the region where $0^\circ < \theta < 90^\circ$ and $270^\circ < \theta < 360^\circ$, directivity values of the polar radiation pattern increase (the amount of power directed towards the hemisphere above the main fuselage, the nose and the wings increases), due to the decrease of the electromagnetic blockage effect (the thickness of the blocking structure above the corresponding lower UHF antenna decreases and the electrical distance between the lower UHF antenna and the wings increases) caused by the main fuselage, the nose and the wings against the radiation of the lower UHF antenna towards the hemisphere above the main fuselage, the nose and the wings. In addition to this, in the region where $0^\circ < \theta < 90^\circ$ and $270^\circ < \theta < 360^\circ$, many sidelobes having lower directivity values are observed for all directivity patterns.
- As it is shown in Figures 3-39 to 3-46, in the region where $90^\circ < \theta < 180^\circ$, all 3D directivity patterns resemble the 3D radiation pattern of a monopole antenna above infinite ground plane, since the main fuselage, the nose and the wings function as a finite size ground plane. Besides, as the location of the lower UHF antenna changes from the first (antenna #7) to the fourth

location (antenna #12) one by one, since the electrical distance between the lower UHF antenna and the back side of the main fuselage increases and the electrical distance between this antenna and the tip of the nose decreases, the amount of power directed towards the region indicated with the dashed circles in Figures 3-40, 3-42, 3-44 and 3-46 increases and the amount of power directed towards the region indicated with the dashed circles in Figures 3-39, 3-41, 3-43 and 3-45 decreases. In addition to this, when the lower UHF antenna is at the first location (antenna #7), since the lower UHF antenna is very close to the wings, more power is directed towards the regions indicated with the blue circles in Figure 3-40 compared to the power directed towards the same regions in the 3D radiation patterns obtained for the other three different locations. On the other hand, as the location of the lower UHF antenna changes from the first (antenna #7) to the fourth location (antenna #12) one by one, in the region where $0^\circ < \theta < 90^\circ$, directivity values of the 3D radiation pattern increase (the amount of power directed towards the hemisphere above the main fuselage, the nose and the wings increases) and the number of sidelobes decreases, due to the decrease of the electromagnetic blockage effect (the thickness of the blocking structure above the corresponding lower UHF antenna decreases and the electrical distance between the lower UHF antenna and the wings increases) caused by the main fuselage, the nose and the wings against the radiation of the lower UHF antenna towards the hemisphere above the main fuselage, the nose and the wings. Also, as the location of the lower UHF antenna changes from the first (antenna #7) to the fourth location (antenna #12) one by one, since the electrical distance between the lower UHF antenna and the back side of the main fuselage increases and the electrical distance between this antenna and the tip of the nose decreases, the difference between the amount of power directed towards the region where $0^\circ < \theta < 90^\circ$ and $180^\circ < \Phi < 360^\circ$ and the amount of power directed towards the region where $0^\circ < \theta < 90^\circ$ and $0^\circ < \Phi < 180^\circ$ increases.

3.4. Analysis of Antennas on the Simplified F-4 Aircraft

As a result of the electromagnetic analysis of the lower and upper UHF antennas mounted on the simplified F-4 aircraft, the electromagnetic coupling levels between the lower and upper UHF antennas and the far field radiation patterns of the lower UHF antenna are obtained for four different locations of the lower UHF antenna, shown in Figures 3-47, 3-48, 3-49 and 3-50 as antennas #7, #10, #11 and #12, respectively.

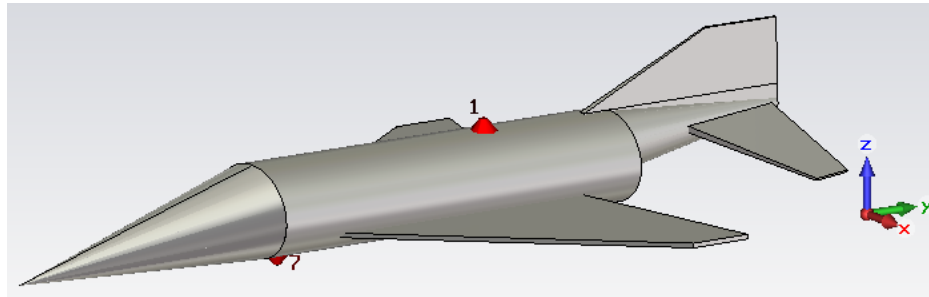


Figure 3-47 The Lower (#7) and Upper (#1) UHF Antennas on the Simplified F-4 Aircraft

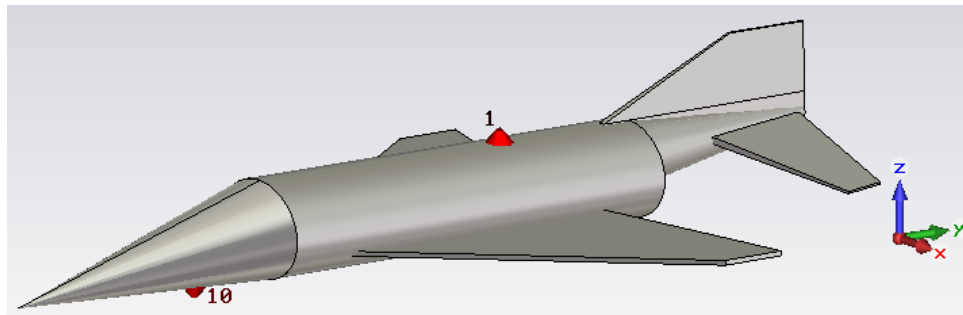


Figure 3-48 The Lower (#10) and Upper (#1) UHF Antennas on the Simplified F-4 Aircraft

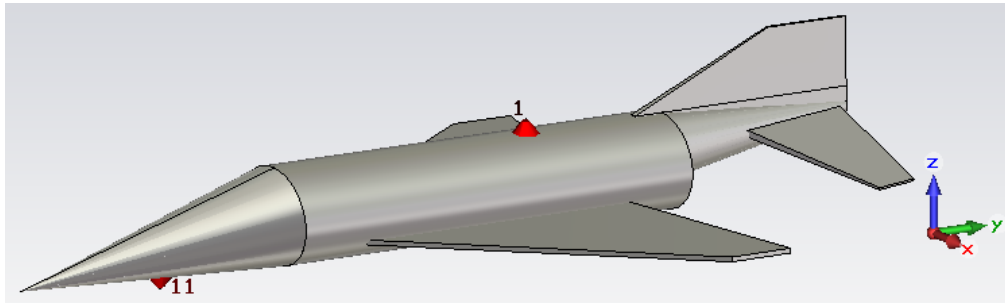


Figure 3-49 The Lower (#11) and Upper (#1) UHF Antennas on the Simplified F-4 Aircraft

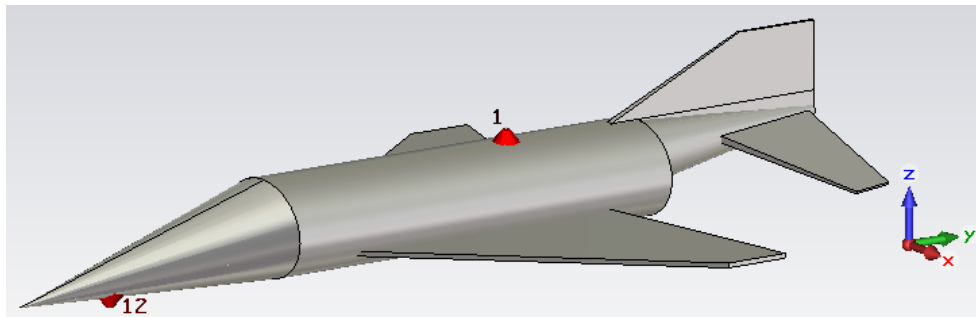


Figure 3-50 The Lower (#12) and Upper (#1) UHF Antennas on the Simplified F-4 Aircraft

The plots of the electromagnetic coupling levels ($S_{1,7}$, $S_{1,10}$, $S_{1,11}$ and $S_{1,12}$) between the lower and upper UHF antennas, obtained for four different locations of the lower UHF antenna, over 225 – 400 MHz frequency band are given in Figure 3-51. The mean values of the electromagnetic coupling levels ($S_{1,7}$, $S_{1,10}$, $S_{1,11}$ and $S_{1,12}$) over 225 – 400 MHz frequency band are calculated as:

- The mean value of $S_{1,7}$: -59.66 dB
- The mean value of $S_{1,10}$: -54.8 dB
- The mean value of $S_{1,11}$: -50.16 dB
- The mean value of $S_{1,12}$: -44.61 dB

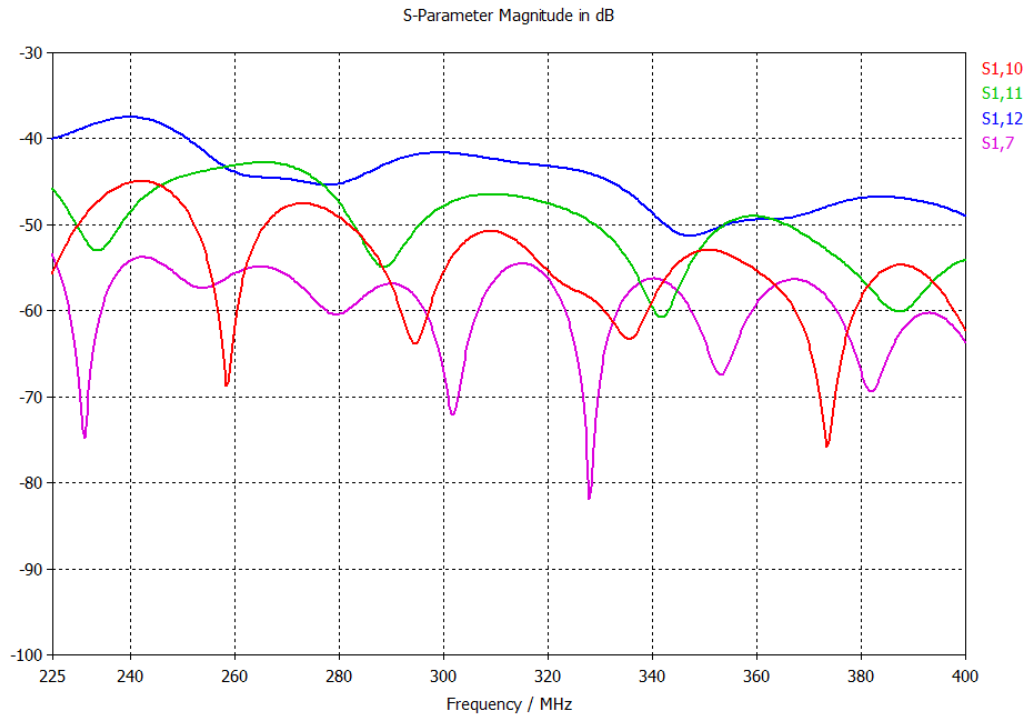


Figure 3-51 Coupling Levels – $S_{1,7}$, $S_{1,10}$, $S_{1,11}$ and $S_{1,12}$

In consequence of the observation of Figure 3-51 and the mean values of the electromagnetic coupling levels, it can be concluded that:

- As the location of the lower UHF antenna changes from the first (antenna #7) to the fourth location (antenna #12) one by one, the mean value of the electromagnetic coupling levels between the lower and upper UHF antennas increases gradually due to the following factors:
 - a. The effectiveness of the electromagnetic blockage caused by the simplified F-4 aircraft against the radiation of the lower and upper UHF antennas towards each other decreases and the amount of power directed towards the hemisphere above the aircraft increases. Because the thickness of the blocking structure above the corresponding lower UHF antenna decreases gradually and the

electrical distance between the lower UHF antenna and the wings increases.

- b. The angle between the x-y plane, which the gains of the lower and upper UHF antennas above infinite ground plane are maximum ($\theta = 90^\circ$ plane), and the distance vector between the antennas decreases gradually.
 - c. Although the physical distance between the lower and upper UHF antennas increases, the mean value of the electromagnetic coupling levels between the antennas increases due to the fact that the effects of the electromagnetic blockage caused by the simplified F-4 aircraft and the angle between $\theta = 90^\circ$ plane and the distance vector between the antennas are much more dominant than the effect of the physical distance between the antennas.
- When the lower UHF antenna is at the first location (antenna #7), the mean value of the electromagnetic coupling levels between the lower and upper UHF antennas is minimum among the corresponding results of four different locations, since the electromagnetic blockage caused by the simplified F-4 aircraft is most effective and the angle between $\theta = 90^\circ$ plane and the distance vector between the antennas is maximum in this case.
 - When the lower UHF antenna is at the fourth location (antenna #12), the mean value of the electromagnetic coupling levels between the lower and upper UHF antennas is maximum among the corresponding results of four different locations, since the electromagnetic blockage caused by the simplified F-4 aircraft is least effective and the angle between $\theta = 90^\circ$ plane and the distance vector between the antennas is minimum in this case.

The far field radiation patterns of the lower UHF antenna, which are obtained for four different locations of the lower UHF antenna, are given in Figures 3-52 to 3-62.

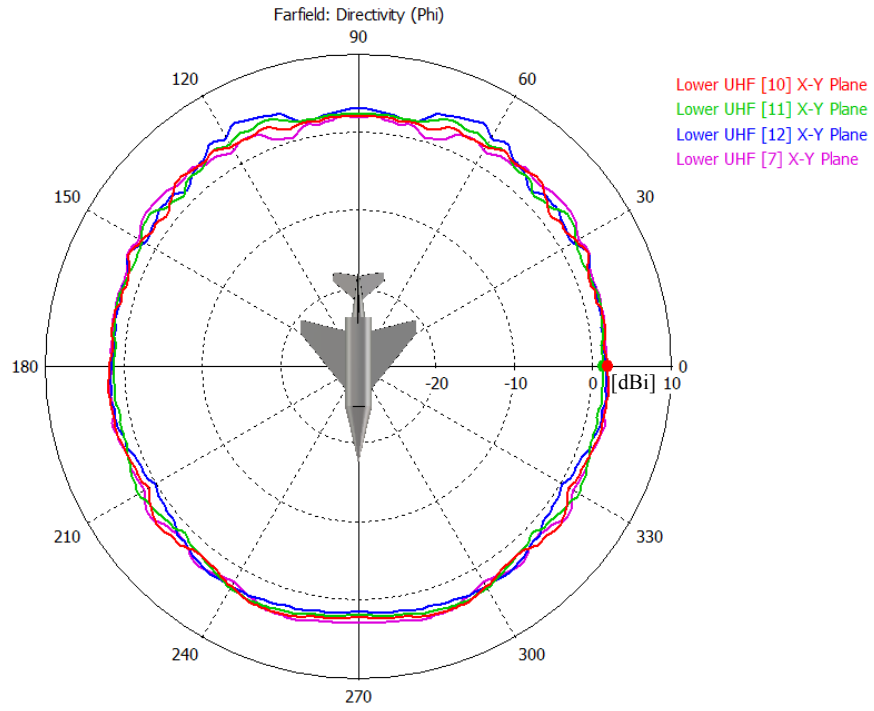


Figure 3-52 Polar Radiation Patterns of the Lower UHF Antenna in x-y Plane

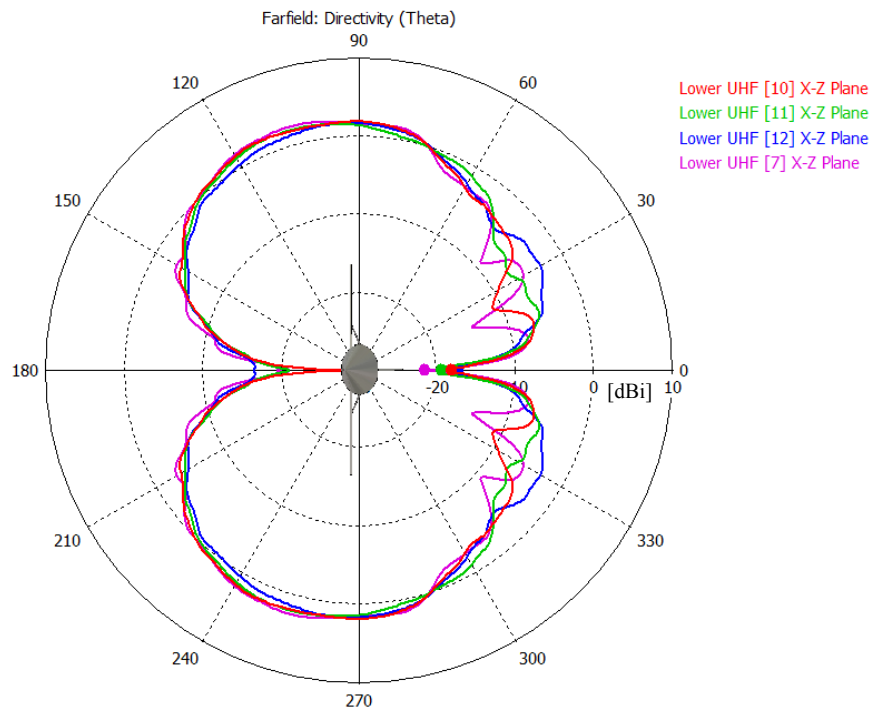


Figure 3-53 Polar Radiation Patterns of the Lower UHF Antenna in x-z Plane

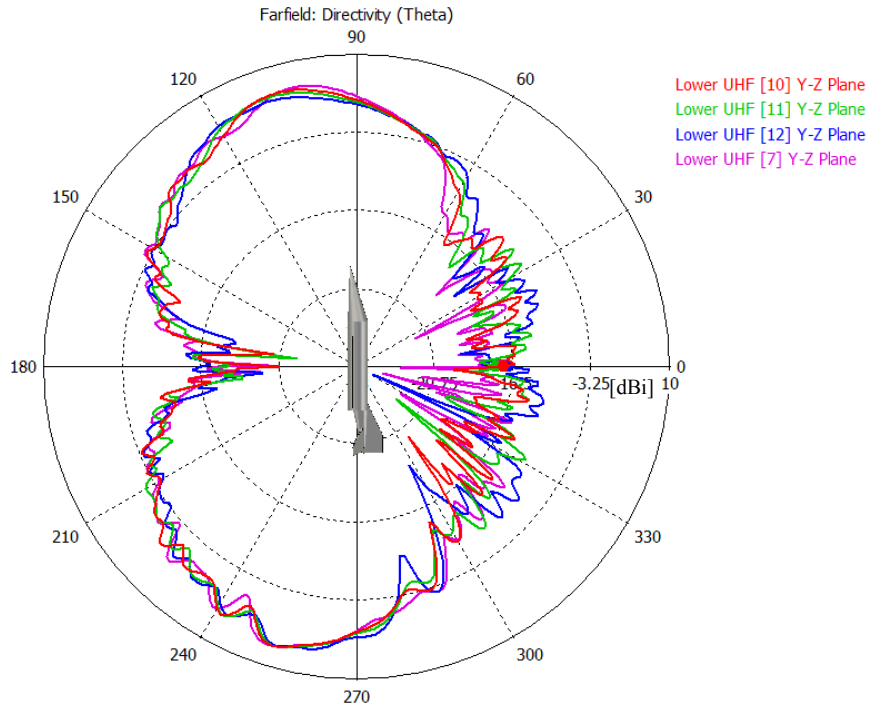


Figure 3-54 Polar Radiation Patterns of the Lower UHF Antenna in y-z Plane

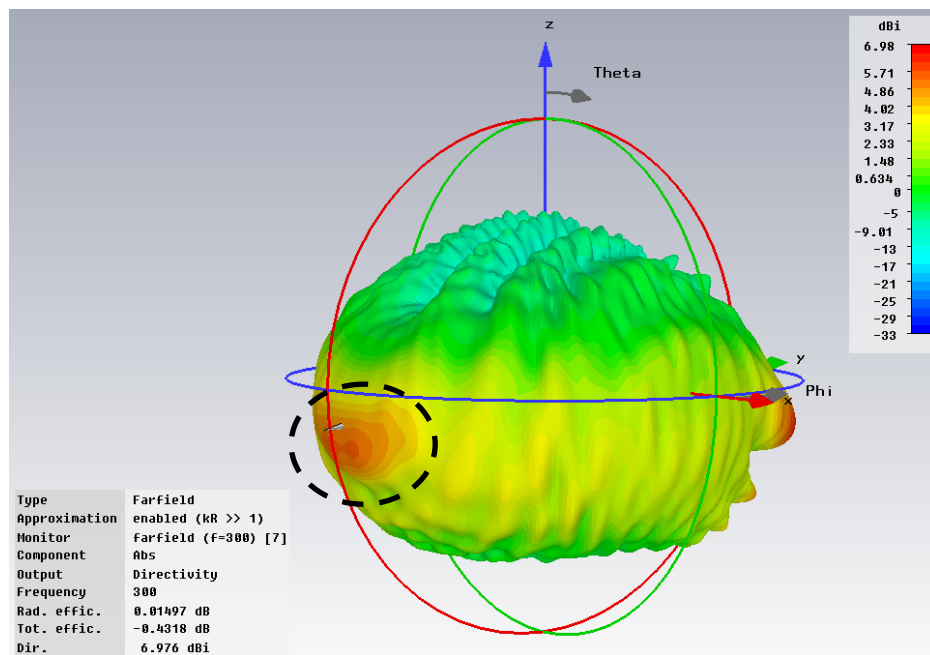


Figure 3-55 3D Radiation Pattern of the Lower UHF Antenna (#7)
- 1st Angle of View

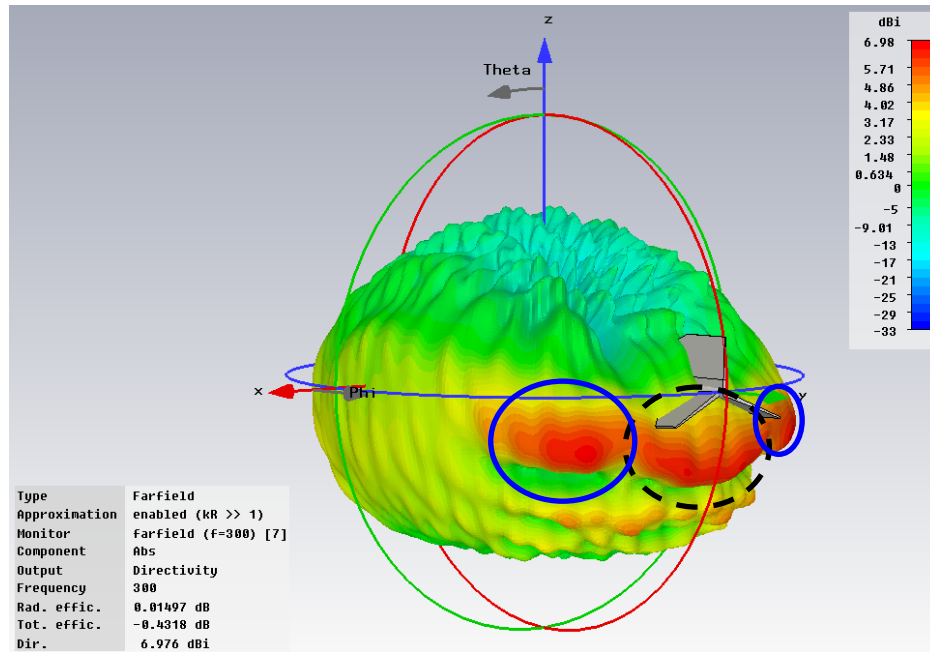


Figure 3-56 3D Radiation Pattern of the Lower UHF Antenna (#7)
 – 2nd Angle of View

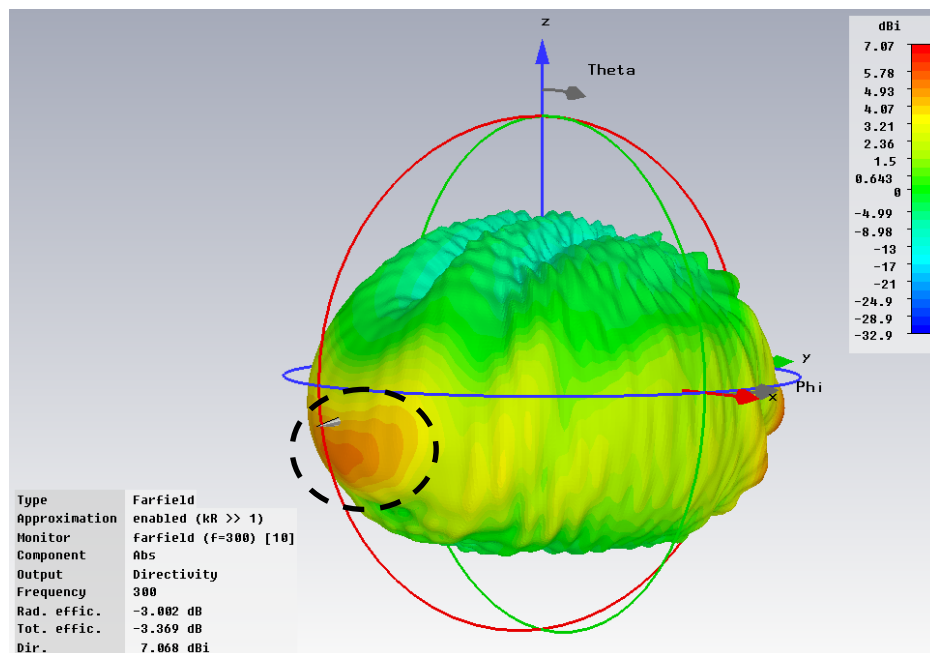


Figure 3-57 3D Radiation Pattern of the Lower UHF Antenna (#10)
 – 1st Angle of View

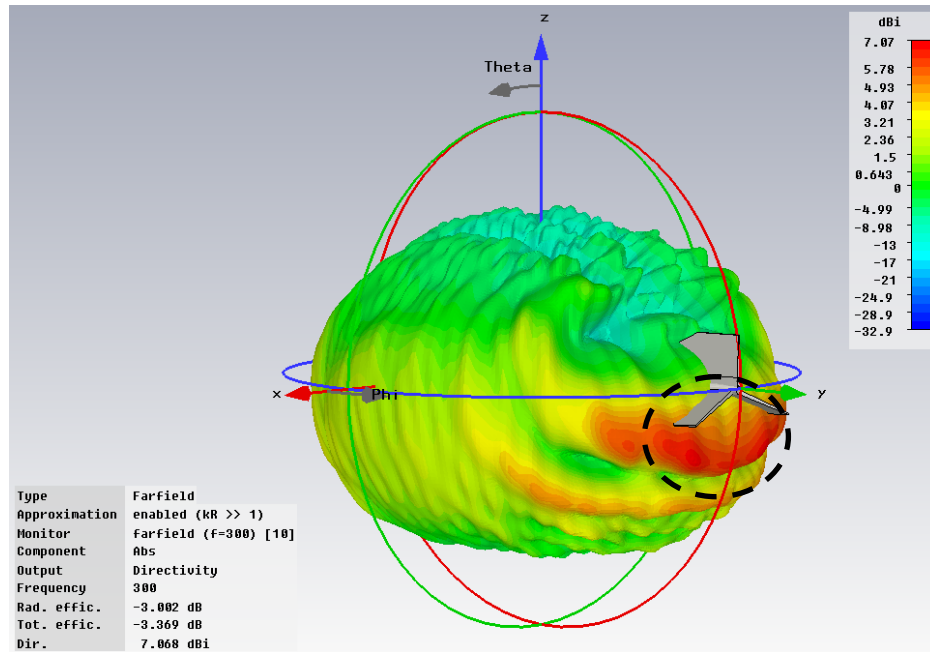


Figure 3-58 3D Radiation Pattern of the Lower UHF Antenna (#10)
 – 2nd Angle of View

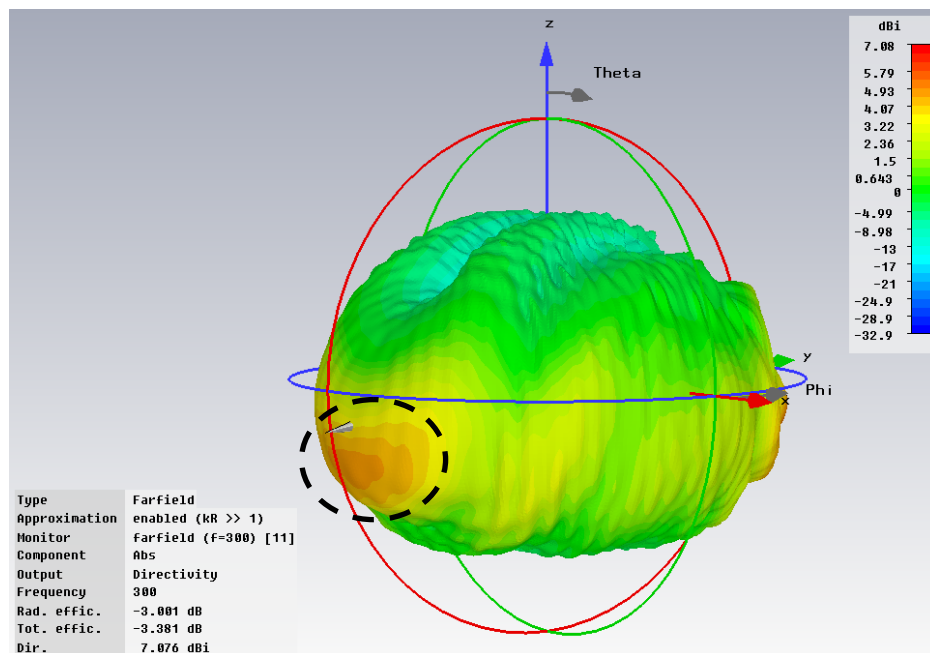


Figure 3-59 3D Radiation Pattern of the Lower UHF Antenna (#11)
 – 1st Angle of View

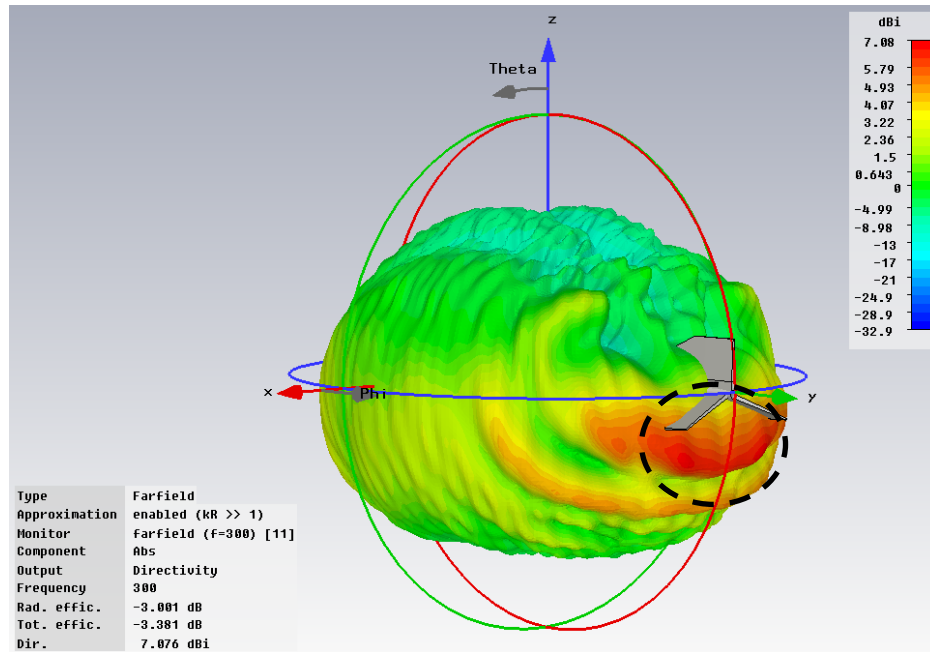


Figure 3-60 3D Radiation Pattern of the Lower UHF Antenna (#11)
 – 2nd Angle of View

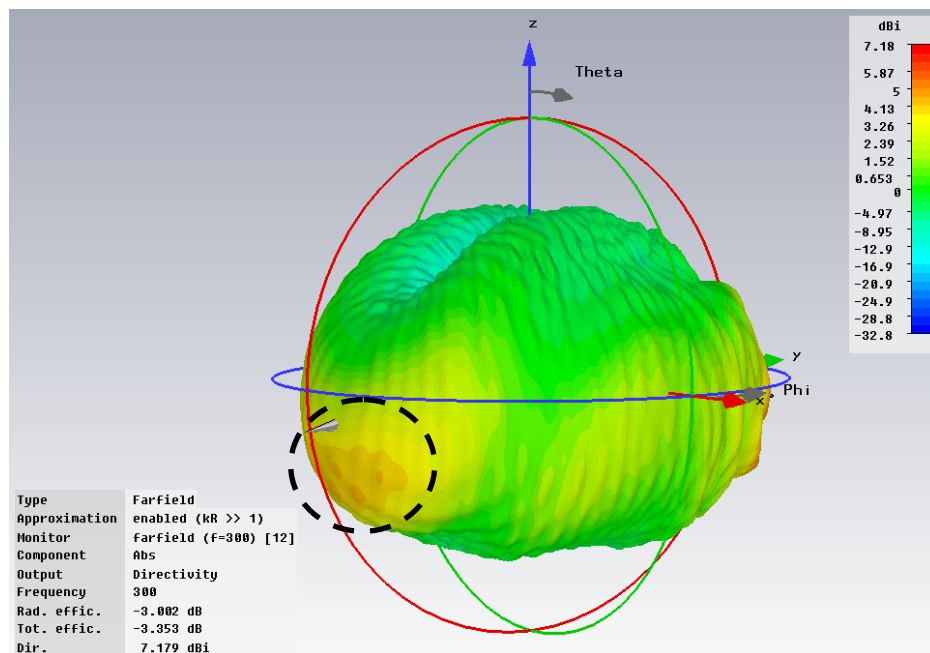


Figure 3-61 3D Radiation Pattern of the Lower UHF Antenna (#12)
 – 1st Angle of View

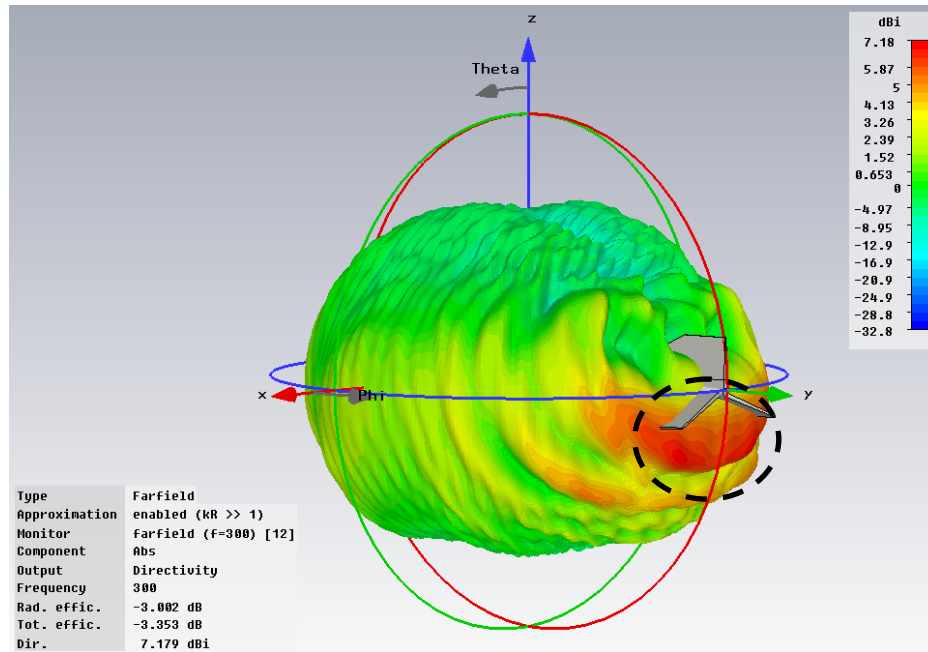


Figure 3-62 3D Radiation Pattern of the Lower UHF Antenna (#12)
– 2nd Angle of View

In consequence of the observation of the 3D radiation patterns and the polar radiation patterns of the lower UHF antenna in x-y, x-z and y-z planes, which are obtained for four different locations of the lower UHF antenna, it can be concluded that:

- As it is shown in Figure 3-52, all directivity patterns in x-y plane are almost omnidirectional like the azimuth plane pattern of a monopole antenna above infinite ground plane, since the simplified F-4 aircraft functions as a finite size ground plane. Besides, as the location of the lower UHF antenna changes from the first (antenna #7) to the fourth location (antenna #12) one by one, since the electrical distance between the lower UHF antenna and the back side of the aircraft increases and the electrical distance between this antenna and the tip of the nose decreases, the amount of power directed towards the back of the aircraft (the region where

$60^\circ < \Phi < 120^\circ$) increases and the amount of power directed towards the front of the nose (the region where $240^\circ < \Phi < 300^\circ$) decreases.

- As it is shown in Figure 3-53, in the region where $90^\circ < \theta < 270^\circ$, all directivity patterns in x-z plane resemble the elevation plane pattern of a monopole antenna above infinite ground plane, since the simplified F-4 aircraft functions as a finite size ground plane. On the other hand, as the location of the lower UHF antenna changes from the first (antenna #7) to the fourth location (antenna #12) one by one, in the region where $0^\circ < \theta < 90^\circ$ and $270^\circ < \theta < 360^\circ$, directivity values of the polar radiation pattern increase (the amount of power directed towards the hemisphere above the aircraft increases) and the number of sidelobes decreases, due to the decrease of the electromagnetic blockage effect (the thickness of the blocking structure above the corresponding lower UHF antenna decreases and the electrical distance between the lower UHF antenna and the wings increases) caused by the aircraft against the radiation of the lower UHF antenna towards the hemisphere above the aircraft.
- As it is shown in Figure 3-54, in the region where $90^\circ < \theta < 270^\circ$, all directivity patterns in y-z plane resemble the elevation plane pattern of a monopole antenna above infinite ground plane, since the simplified F-4 aircraft functions as a finite size ground plane. Besides, as the location of the lower UHF antenna changes from the first (antenna #7) to the fourth location (antenna #12) one by one, since the electrical distance between the lower UHF antenna and the back side of the aircraft increases and the electrical distance between this antenna and the tip of the nose decreases, the amount of power directed towards the region where $255^\circ < \theta < 270^\circ$ increases and the amount of power directed towards the region where $90^\circ < \theta < 105^\circ$ decreases. On the other hand, as the location of the lower UHF antenna changes from the first (antenna #7) to the fourth location (antenna #12) one by one, in the region where $0^\circ < \theta < 90^\circ$ and $270^\circ < \theta < 360^\circ$, directivity values of the polar radiation pattern increase (the amount of power directed towards the hemisphere above the aircraft

increases), due to the decrease of the electromagnetic blockage effect (the thickness of the blocking structure above the corresponding lower UHF antenna decreases and the electrical distance between the lower UHF antenna and the wings increases) caused by the aircraft against the radiation of the lower UHF antenna towards the hemisphere above the aircraft. In addition to this, in the region where $0^\circ < \theta < 90^\circ$ and $270^\circ < \theta < 360^\circ$, many sidelobes having lower directivity values are observed for all directivity patterns.

- As it is shown in Figures 3-55 to 3-62, in the region where $90^\circ < \theta < 180^\circ$, all 3D directivity patterns resemble the 3D radiation pattern of a monopole antenna above infinite ground plane, since the simplified F-4 aircraft functions as a finite size ground plane. Besides, as the location of the lower UHF antenna changes from the first (antenna #7) to the fourth location (antenna #12) one by one, since the electrical distance between the lower UHF antenna and the back side of the aircraft increases and the electrical distance between this antenna and the tip of the nose decreases, the amount of power directed towards the region indicated with the dashed circles in Figures 3-56, 3-58, 3-60 and 3-62 increases and the amount of power directed towards the region indicated with the dashed circles in Figures 3-55, 3-57, 3-59 and 3-61 decreases. In addition to this, when the lower UHF antenna is at the first location (antenna #7), since the lower UHF antenna is very close to the wings, more power is directed towards the regions indicated with the blue circles in Figure 3-56 compared to the power directed towards the same regions in the 3D radiation patterns obtained for the other three different locations. On the other hand, as the location of the lower UHF antenna changes from the first (antenna #7) to the fourth location (antenna #12) one by one, in the region where $0^\circ < \theta < 90^\circ$, directivity values of the 3D radiation pattern increase (the amount of power directed towards the hemisphere above the aircraft increases) and the number of sidelobes decreases, due to the decrease of the electromagnetic blockage effect (the thickness of the blocking structure

above the corresponding lower UHF antenna decreases and the electrical distance between the lower UHF antenna and the wings increases) caused by the aircraft against the radiation of the lower UHF antenna towards the hemisphere above the aircraft. Also, as the location of the lower UHF antenna changes from the first (antenna #7) to the fourth location (antenna #12) one by one, since the electrical distance between the lower UHF antenna and the back side of the aircraft increases and the electrical distance between this antenna and the tip of the nose decreases, the difference between the amount of power directed towards the region where $0^\circ < \theta < 90^\circ$ and $180^\circ < \Phi < 360^\circ$ and the amount of power directed towards the region where $0^\circ < \theta < 90^\circ$ and $0^\circ < \Phi < 180^\circ$ increases.

3.5. Analysis of Antennas on the Original F-4 Aircraft

As a result of the electromagnetic analysis of the lower and upper UHF antennas mounted on the original F-4 aircraft, the electromagnetic coupling levels between the lower and upper UHF antennas are obtained for four different locations of the lower UHF antenna, shown in Figures 3-63, 3-64, 3-65 and 3-66 as antennas #7, #10, #11 and #12, respectively.

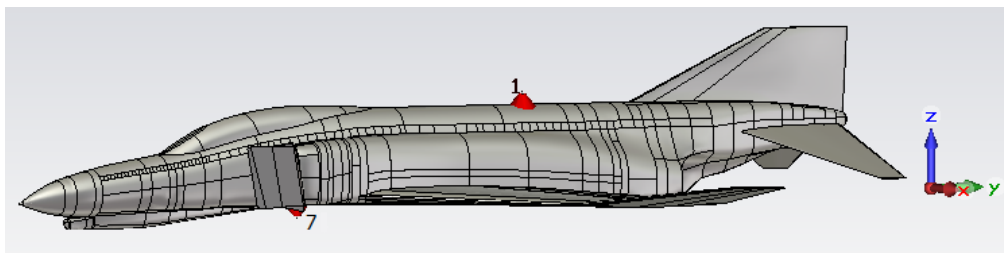


Figure 3-63 The Lower (#7) and Upper (#1) UHF Antennas on the Original F-4 Aircraft

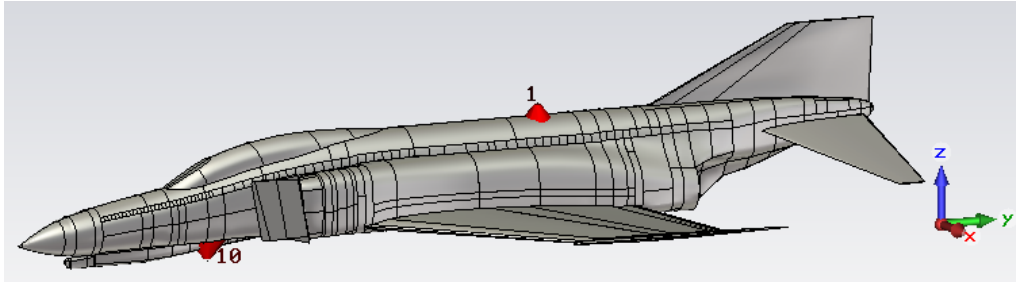


Figure 3-64 The Lower (#10) and Upper (#1) UHF Antennas on the Original F-4 Aircraft

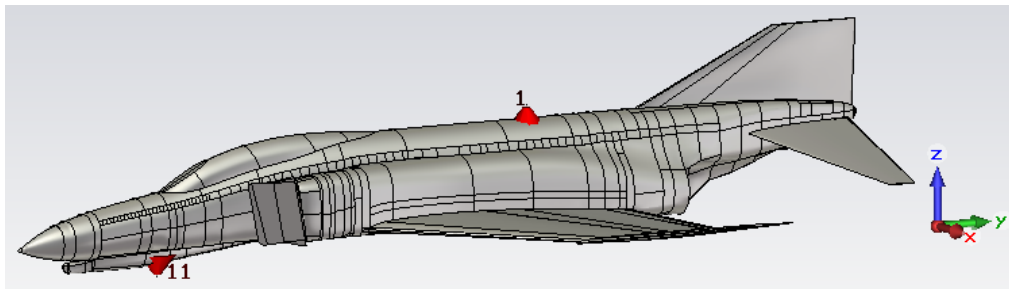


Figure 3-65 The Lower (#11) and Upper (#1) UHF Antennas on the Original F-4 Aircraft

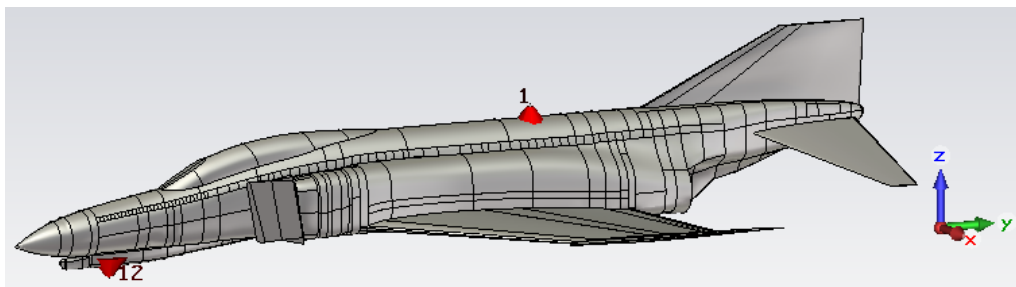


Figure 3-66 The Lower (#12) and Upper (#1) UHF Antennas on the Original F-4 Aircraft

The plots of the electromagnetic coupling levels ($S_{1,7}$, $S_{1,10}$, $S_{1,11}$ and $S_{1,12}$) between the lower and upper UHF antennas, obtained for four different locations of the lower UHF antenna, over 225 – 400 MHz frequency band are given in Figure 3-67.

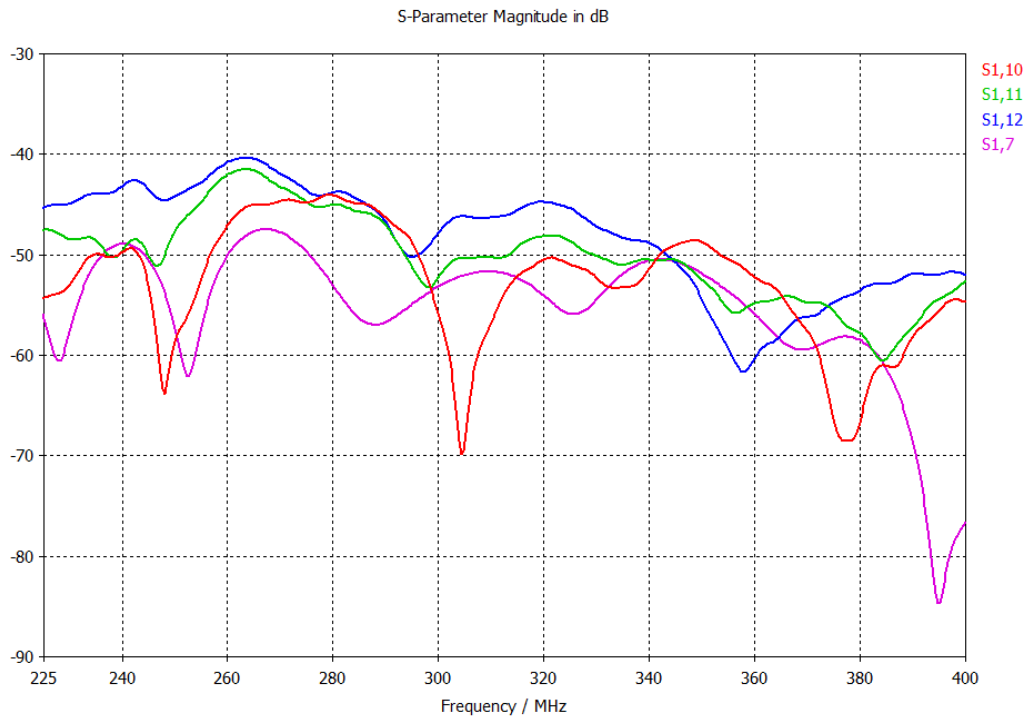


Figure 3-67 Coupling Levels – $S_{1,7}$, $S_{1,10}$, $S_{1,11}$ and $S_{1,12}$

The mean values of the electromagnetic coupling levels ($S_{1,7}$, $S_{1,10}$, $S_{1,11}$ and $S_{1,12}$) over 225 – 400 MHz frequency band are calculated as:

- The mean value of $S_{1,7}$: -55.53 dB
- The mean value of $S_{1,10}$: -52.8 dB
- The mean value of $S_{1,11}$: -50.25 dB
- The mean value of $S_{1,12}$: -48.23 dB

In consequence of the observation of Figure 3-67 and the mean values of the electromagnetic coupling levels, it can be concluded that:

- As the location of the lower UHF antenna changes from the first (antenna #7) to the fourth location (antenna #12) one by one, the mean value of the electromagnetic coupling levels between the lower and upper UHF antennas increases gradually due to the following factors:
 - a. The effectiveness of the electromagnetic blockage caused by the original F-4 aircraft against the radiation of the lower and upper UHF antennas towards each other decreases and the amount of power directed towards the hemisphere above the aircraft increases. Because the thickness of the blocking structure above the corresponding lower UHF antenna decreases gradually and the electrical distance between the lower UHF antenna and the wings increases.
 - b. The angle between the x-y plane, which the gains of the lower and upper UHF antennas above infinite ground plane are maximum ($\theta = 90^\circ$ plane), and the distance vector between the antennas decreases gradually.
 - c. Although the physical distance between the lower and upper UHF antennas increases, the mean value of the electromagnetic coupling levels between the antennas increases due to the fact that the effects of the electromagnetic blockage caused by the original F-4 aircraft and the angle between $\theta = 90^\circ$ plane and the distance vector between the antennas are much more dominant than the effect of the physical distance between the antennas.
- When the lower UHF antenna is at the first location (antenna #7), the mean value of the electromagnetic coupling levels between the lower and upper UHF antennas is minimum among the corresponding results of four different locations, since the electromagnetic blockage caused by the

original F-4 aircraft is most effective and the angle between $\theta = 90^\circ$ plane and the distance vector between the antennas is maximum in this case.

- When the lower UHF antenna is at the fourth location (antenna #12), the mean value of the electromagnetic coupling levels between the lower and upper UHF antennas is maximum among the corresponding results of four different locations, since the electromagnetic blockage caused by the original F-4 aircraft is least effective and the angle between $\theta = 90^\circ$ plane and the distance vector between the antennas is minimum in this case.

It is observed that there is a good agreement between the electromagnetic coupling levels obtained in the analysis performed on the simplified F-4 aircraft and the electromagnetic coupling levels obtained in the analysis performed on the original F-4 aircraft. However, there is a little difference between these two sets of results due to the fact that the geometrical structure of the original F-4 aircraft is much more complex than that of the simplified F-4 aircraft and the geometrical structure of the original F-4 aircraft includes many geometrical details which affect the radiation characteristics of the lower and upper UHF antennas.

Consequently, according to the electromagnetic coupling levels between the lower and upper UHF antennas obtained in the analysis performed on the simplified F-4 aircraft and the original F-4 aircraft, the first location (antenna #7) is determined as the optimal location for the lower UHF antenna among these four different locations. In addition to this, at this optimal location whether the far field radiation pattern of the lower UHF antenna has sufficient directivity values in the region where the antenna has to operate efficiently is investigated. Within this context, the 3D far field radiation pattern (shown in Figures 3-68 and 3-69) of the lower UHF antenna at this optimal location, in the region where $90^\circ \leq \theta \leq 120^\circ$ (the region where the lower UHF antenna has to operate efficiently so that the operational performance of the antenna shall not be degraded), is compared with the 3D far field radiation pattern (shown in Figure 3-70) of the lower UHF antenna

above infinite ground plane, in the region where $60^\circ \leq \theta \leq 90^\circ$, in the way of the following criteria:

- At least 90 % of the directivity values of the 3D far field radiation pattern of the lower UHF antenna at the optimal location, in the region where $90^\circ \leq \theta \leq 120^\circ$, shall be greater than those of the lower UHF antenna above infinite ground plane, in the region where $60^\circ \leq \theta \leq 90^\circ$, minus 10 dB.
- At least 70 % of the directivity values of the 3D far field radiation pattern of the lower UHF antenna at the optimal location, in the region where $90^\circ \leq \theta \leq 120^\circ$, shall be greater than those of the lower UHF antenna above infinite ground plane, in the region where $60^\circ \leq \theta \leq 90^\circ$, minus 6 dB.

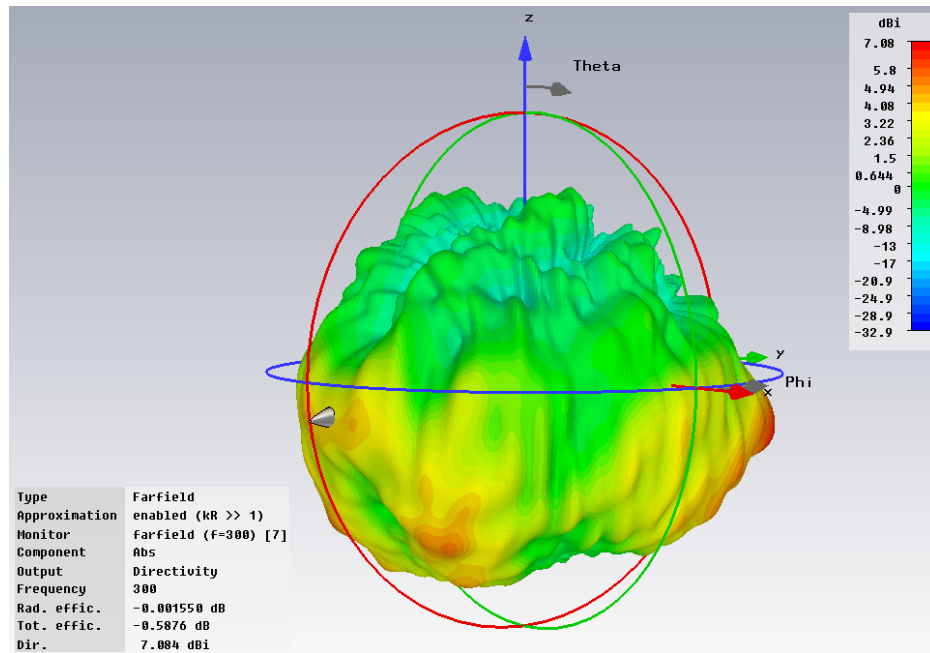


Figure 3-68 3D Radiation Pattern of the Lower UHF Antenna (#7)

– 1st Angle of View

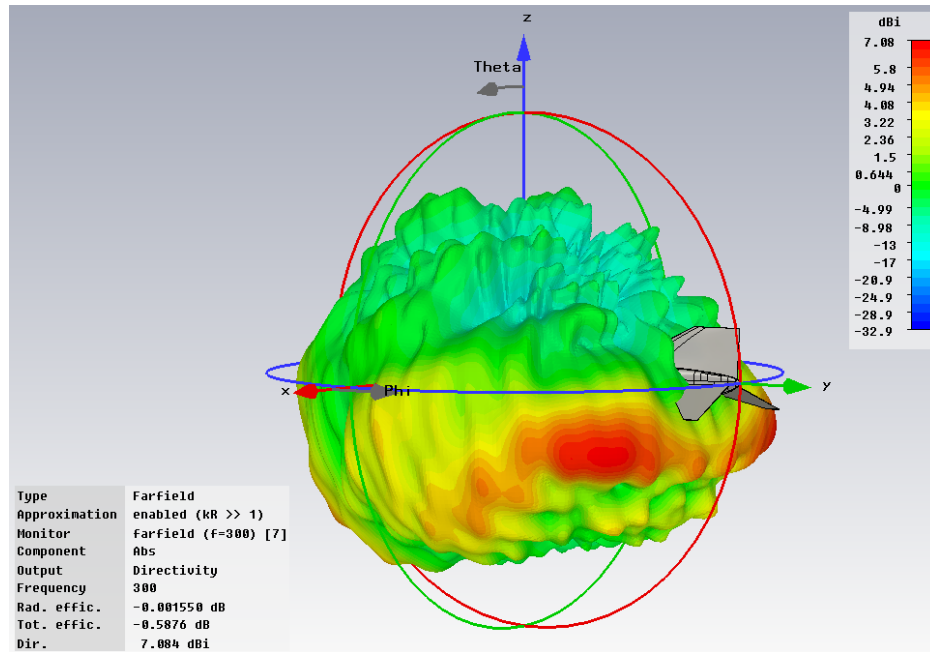


Figure 3-69 3D Radiation Pattern of the Lower UHF Antenna (#7)
 – 2nd Angle of View

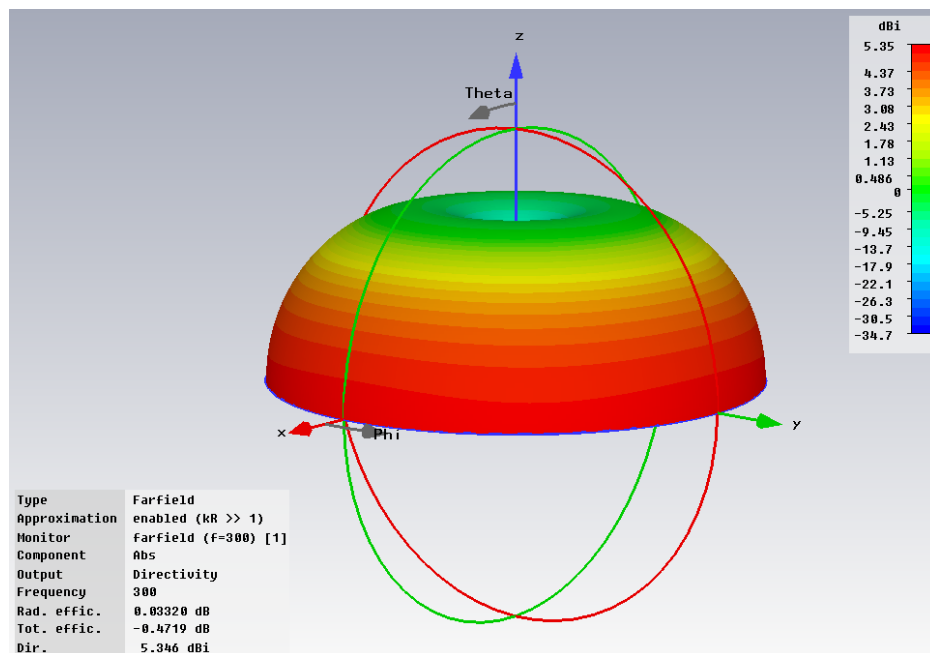


Figure 3-70 3D Radiation Pattern of the Lower UHF Antenna above Infinite
 Ground Plane

In consequence of the comparison done between the 3D far field radiation pattern of the lower UHF antenna at this optimal location, in the region where $90^\circ \leq \theta \leq 120^\circ$, and that of the lower UHF antenna above infinite ground plane, in the region where $60^\circ \leq \theta \leq 90^\circ$, it can be concluded that:

- 100 % of the directivity values of the 3D far field radiation pattern of the lower UHF antenna at the optimal location, in the region where $90^\circ \leq \theta \leq 120^\circ$, are greater than those of the lower UHF antenna above infinite ground plane, in the region where $60^\circ \leq \theta \leq 90^\circ$, minus 10 dB.
- 96.7 % of the directivity values of the 3D far field radiation pattern of the lower UHF antenna at the optimal location, in the region where $90^\circ \leq \theta \leq 120^\circ$, are greater than those of the lower UHF antenna above infinite ground plane, in the region where $60^\circ \leq \theta \leq 90^\circ$, minus 6 dB.

Finally, according to these results, the far field radiation pattern of the lower UHF antenna at the optimal location (antenna #7) has sufficient directivity values in the region where the antenna has to operate efficiently.

CHAPTER 4

ANALYSIS OF ANTENNAS MOUNTED ON WARSHIP

In this chapter, electromagnetic analysis of antennas mounted on the warship, shown in Figure 4-1, performed for improving the operational performance of antennas by arranging their placements on the platform is explained.

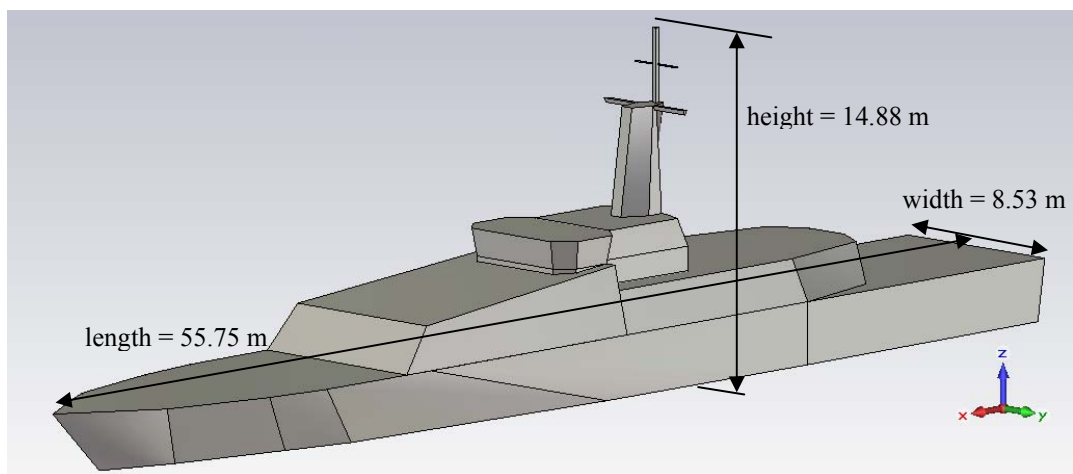


Figure 4-1 The Warship on which Analysis of Antennas Performed

In the scope of this study, electromagnetic analysis of the communication antennas, listed in Table 4-1, mounted on the warship is performed by using the

transient solver of CST MWS[®], in order to determine the optimal locations of these antennas for the operational performance of these antennas to be optimum. For HF antennas, eleven different placement plans shown in Figures 4-2 to 4-12; for VHF and V/UHF antennas, four different placement plans shown in Figures 4-27 to 4-30 are specified on the warship by taking into account the physical and operational constraints of the warship. Antenna numbers seen in Table 4-1 indicate the numbers of discrete ports used for feeding these antennas modeled in the simulations.

Table 4-1 Properties of the Communication Antennas Mounted on the Warship

| Antenna No | Antenna Name | Antenna Type | Antenna Length (m) | Frequency Band (MHz) |
|-------------------|---------------------|---------------------|---------------------------|-----------------------------|
| 1 | HF 1 | Monopole | 10 | 1.5 – 30 |
| 2 | HF 2 | Monopole | 8 | 1.5 – 30 |
| 3 | V/UHF 1 | Coaxial Dipole | 0.91 | 118 – 170 225 – 400 |
| 4 | V/UHF 2 | Coaxial Dipole | 0.91 | 118 – 170 225 – 400 |
| 5 | VHF 1 | Linear Dipole | 0.83 | 148 – 164 |
| 6 | VHF 2 | Linear Dipole | 0.83 | 148 – 164 |

According to operational frequency bands of the communication antennas listed in Table 4-1, the interaction matrix of these antennas, shown in Table 4-2, is prepared. In this interaction matrix, probable in-band interference between HF, VHF and V/UHF communication antennas is indicated. There is a possibility of in-band interference between the antennas whose operational frequency bands coincide with each other.

Table 4-2 The Interaction Matrix of HF, VHF and V/UHF Antennas

| Victim Source | HF 1 | HF 2 | V/UHF 1 | V/UHF 2 | VHF 1 | VHF 2 |
|--------------------------------|------|------|---------|---------|-------|-------|
| HF 1 | | + | - | - | - | - |
| HF 2 | + | | - | - | - | - |
| V/UHF 1 | - | - | | + | + | + |
| V/UHF 2 | - | - | + | | + | + |
| VHF 1 | - | - | + | + | | + |
| VHF 2 | - | - | + | + | + | |

+: In-band interference is probable

- : No in-band interference

The optimal placement plan for these communication antennas is determined among these eleven different placement plans for HF antennas, and these four different placement plans for VHF and V/UHF antennas, depending on the following two criteria ensuring the operational performance of these communication antennas to be optimum:

1. Decreasing the electromagnetic coupling between the antennas between which there is a possibility of in-band interference (Table 4-2) as much as possible.
2. The far field radiation pattern of each antenna shall have sufficient directivity values in the region where the antenna has to operate efficiently.

Within the scope of the analysis of HF, VHF and V/UHF antennas mounted on the warship, the electromagnetic coupling levels between the antennas between which there is a possibility of in-band interference (Table 4-2), are obtained for different placement plans. The electromagnetic coupling levels between HF antennas are

obtained for these eleven different placement plans. On the other hand, the electromagnetic coupling levels between VHF and V/UHF antennas are obtained for these four different placement plans. For each probable in-band interference (Table 4-2), the mean values of the electromagnetic coupling levels between the related antennas obtained for different placement plans are calculated over their operational frequency bands coinciding with each other. These mean values obtained for different placement plans are compared with each other. Thus for each probable in-band interference, the placement plan, that the electromagnetic coupling between the related antennas is minimal, is determined.

Basically, since decreasing the electromagnetic coupling between the antennas between which there is a possibility of in-band interference as much as possible is the primary criterion for determining the optimal placement plan for these communication antennas;

1. The placement plan, that the mean value of the electromagnetic coupling levels between HF antennas is minimal, is determined as the optimal placement plan for HF antennas among these eleven different placement plans.
2. The placement plan, that the sum of the mean values of the electromagnetic coupling levels between VHF and V/UHF antennas is minimal, is determined as the optimal placement plan for VHF and V/UHF antennas among these four different placement plans.

In this way, the optimal placement plan for HF, VHF and V/UHF antennas is composed of these two optimal placement plans determined above. In addition to this, when these communication antennas are mounted on the warship in accordance with this optimal placement plan, whether the far field radiation patterns of each antenna at particular frequencies have sufficient directivity values in the region where the antenna has to operate efficiently is investigated.

For modeling the structures in the simulations of the electromagnetic analysis of the communication antennas mounted on the warship, the following steps are applied:

- The lengths of HF, VHF and V/UHF antennas are specified in accordance with the lengths indicated in Table 4-1.
- The calculation domains including the structures modeled in the simulations and electromagnetic properties of the materials surrounding the structures are specified.
 - a. The sizes and the boundaries of the calculation domains are determined by setting the boundary conditions as open (absorbing) boundary conditions operating like free space [10], since the structures modeled involve antennas radiating into free space.
 - b. The materials surrounding the structures within the calculation domains are specified as free space (electrical conductivity, $\sigma = 0$; relative permittivity and permeability, $\epsilon_r = \mu_r = 1$).
- The sea is modeled as a conducting wall having a conductivity of 5 S/m (typical conductivity of sea water).
- The materials of HF, VHF, V/UHF antennas and the warship are specified as PEC.
- HF antennas are excited with discrete ports having impedances of 50 Ω . On the other hand, VHF and V/UHF antennas are excited with discrete ports having impedances of 75 Ω .

4.1. Analysis of HF Antennas

As a result of the electromagnetic analysis of HF antennas mounted on the warship, the electromagnetic coupling levels between HF antennas are obtained for eleven different placement plans shown in Figures 4-2 to 4-12.

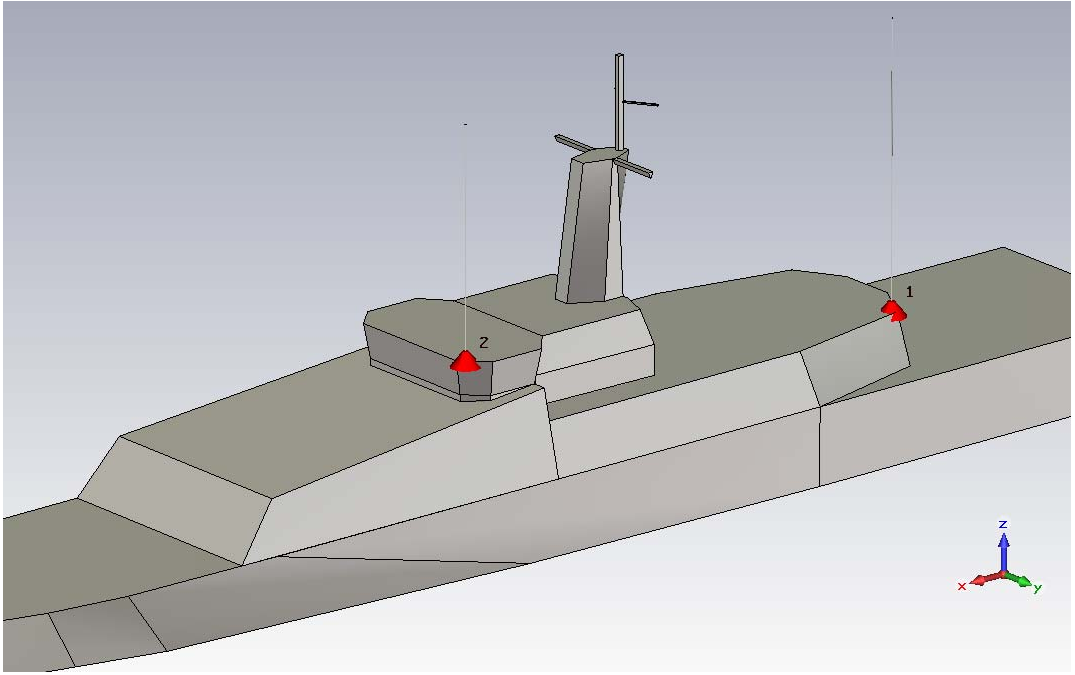


Figure 4-2 Placement Plan 1 for HF Antennas

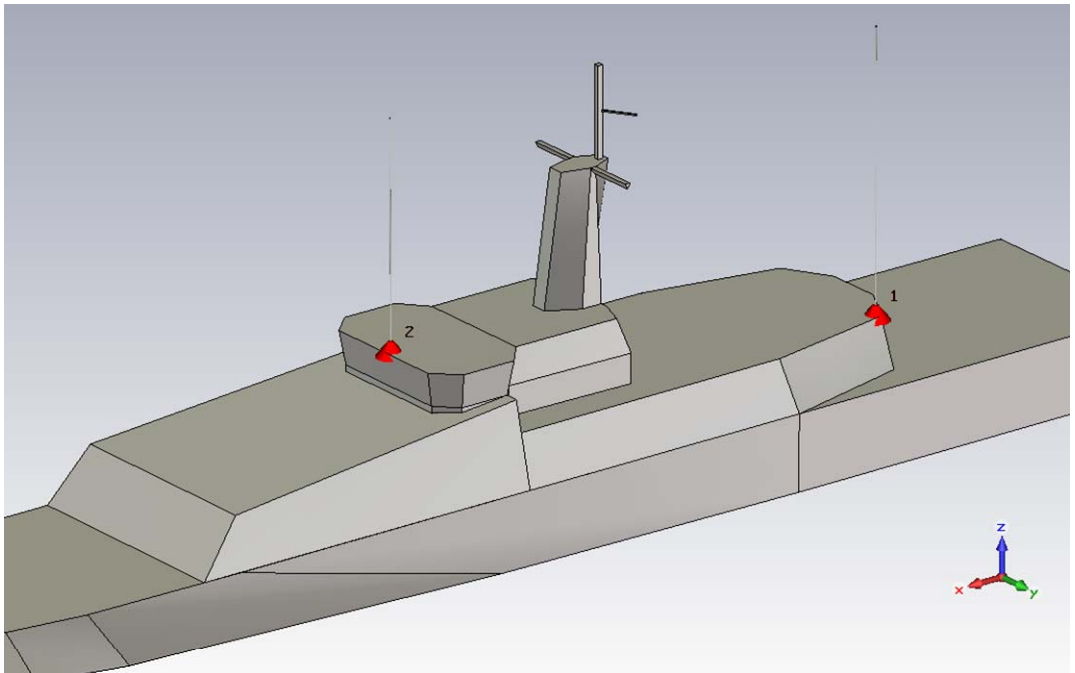


Figure 4-3 Placement Plan 2 for HF Antennas

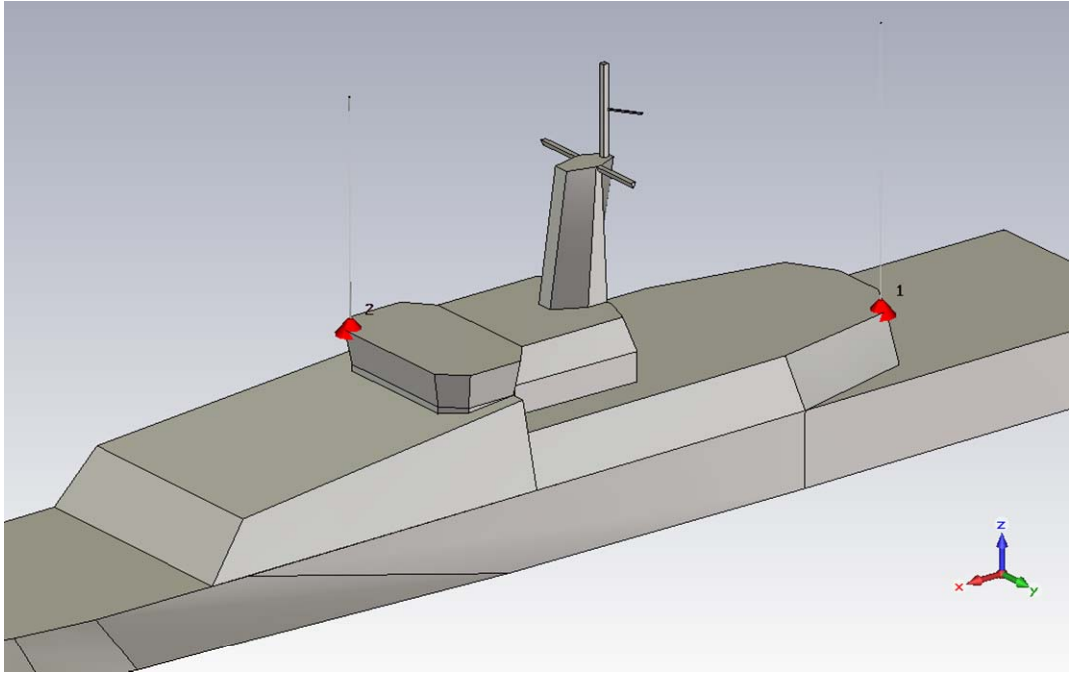


Figure 4-4 Placement Plan 3 for HF Antennas

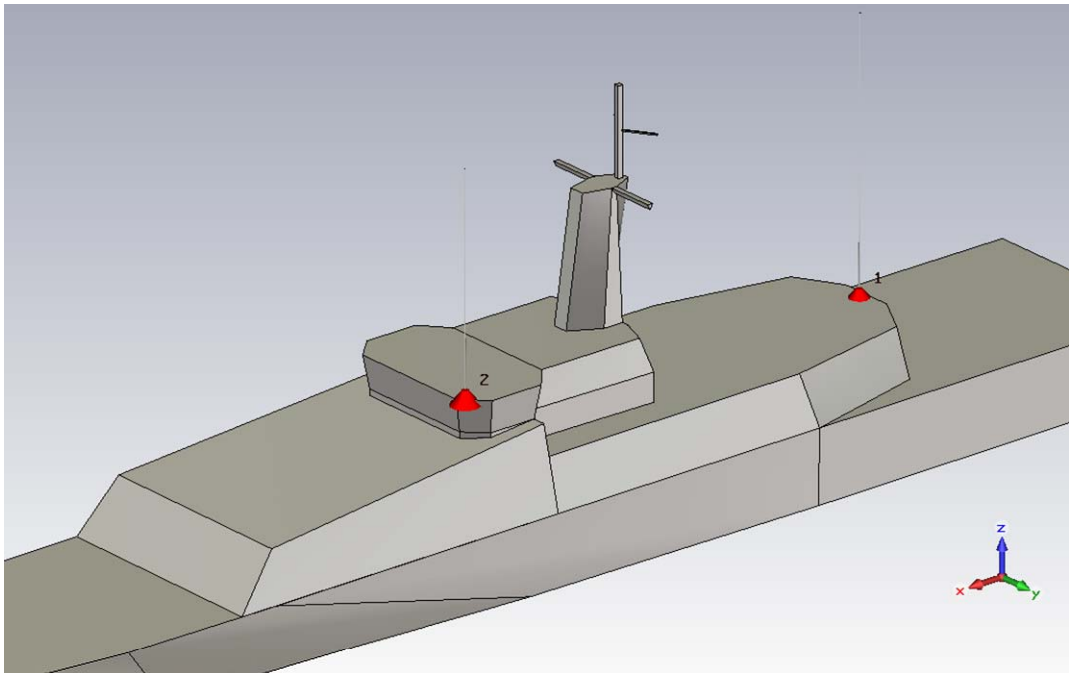


Figure 4-5 Placement Plan 4 for HF Antennas

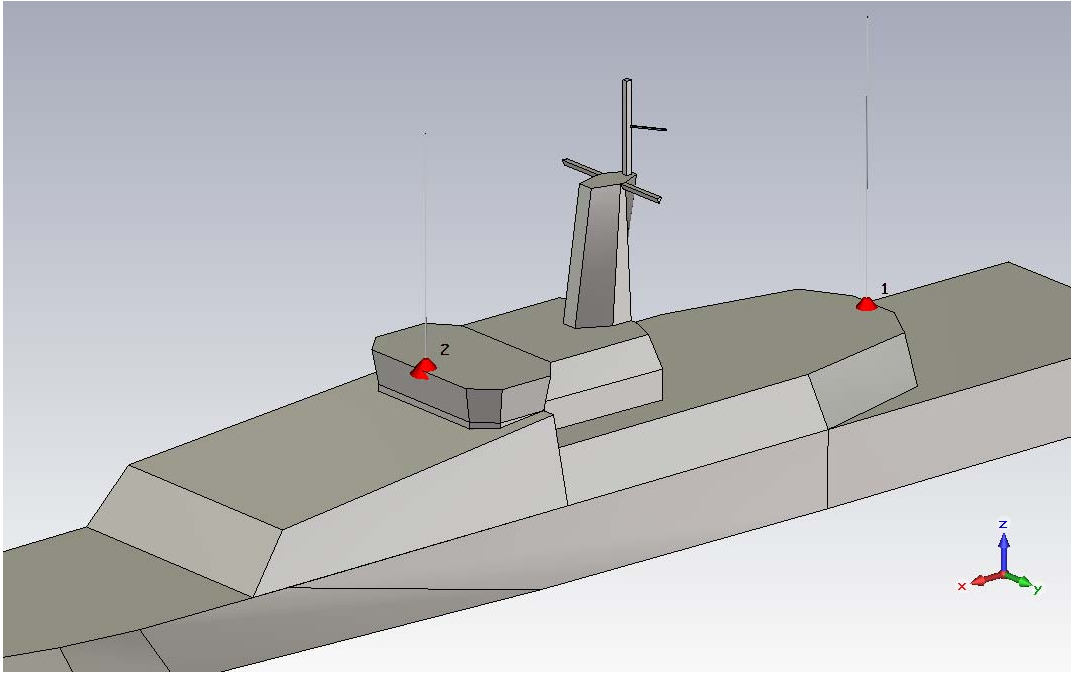


Figure 4-6 Placement Plan 5 for HF Antennas

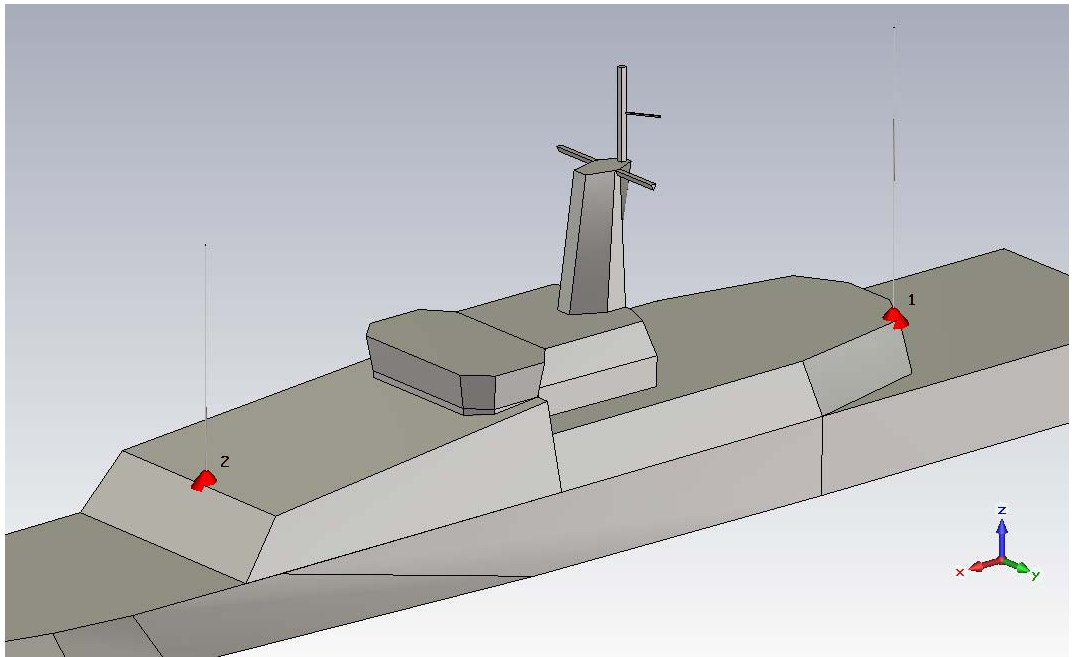


Figure 4-7 Placement Plan 6 for HF Antennas

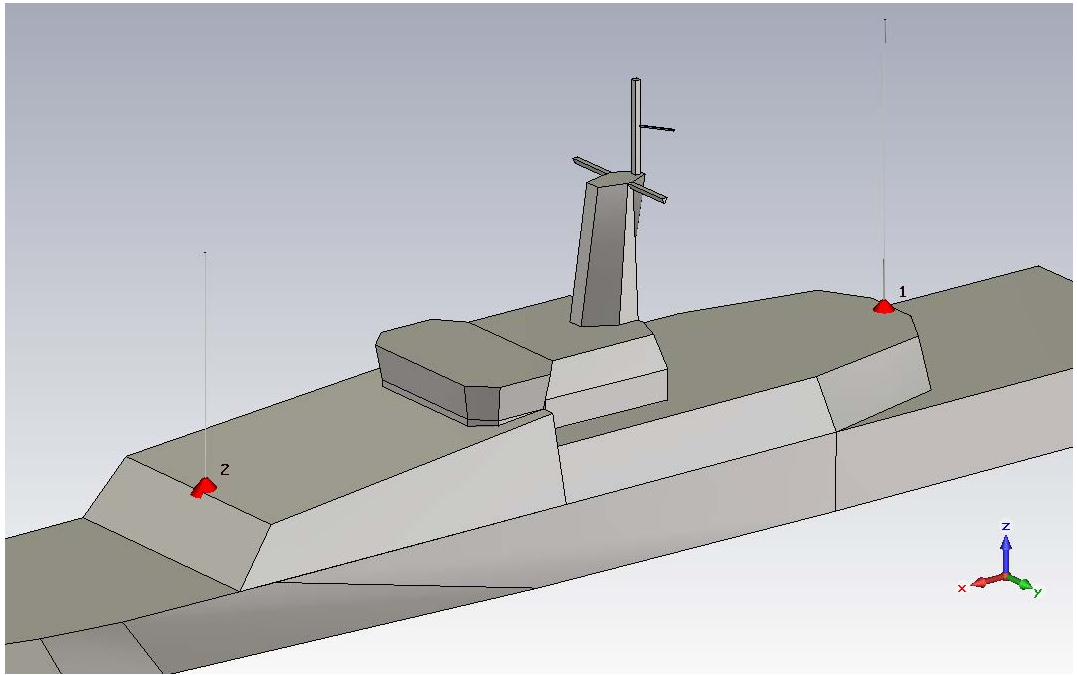


Figure 4-8 Placement Plan 7 for HF Antennas

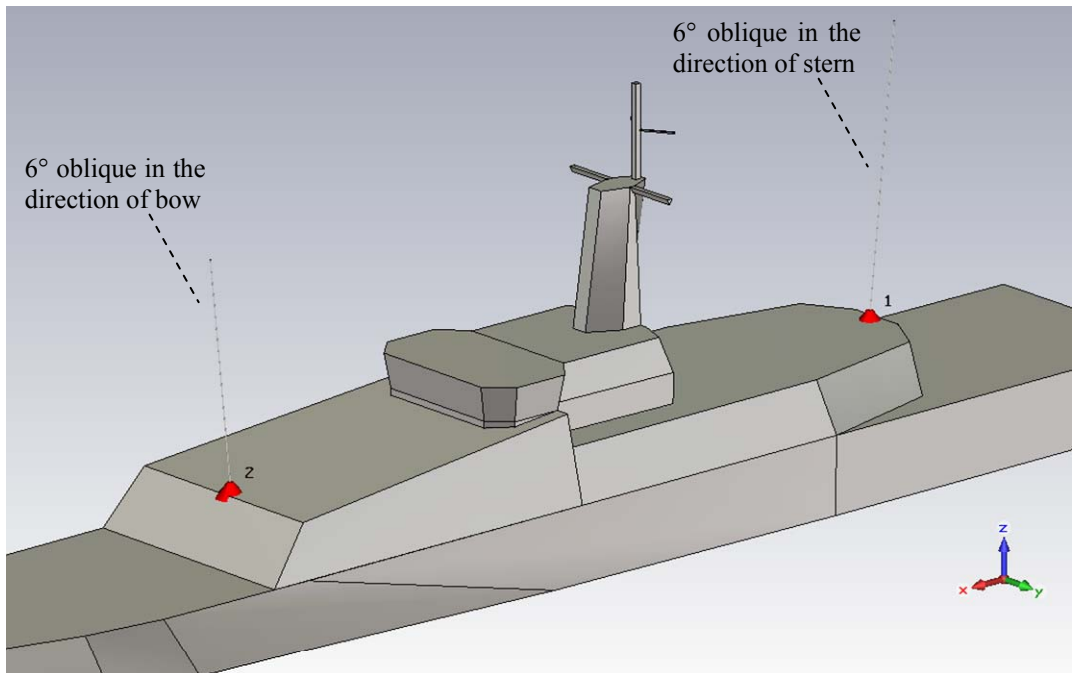


Figure 4-9 Placement Plan 8 for HF Antennas

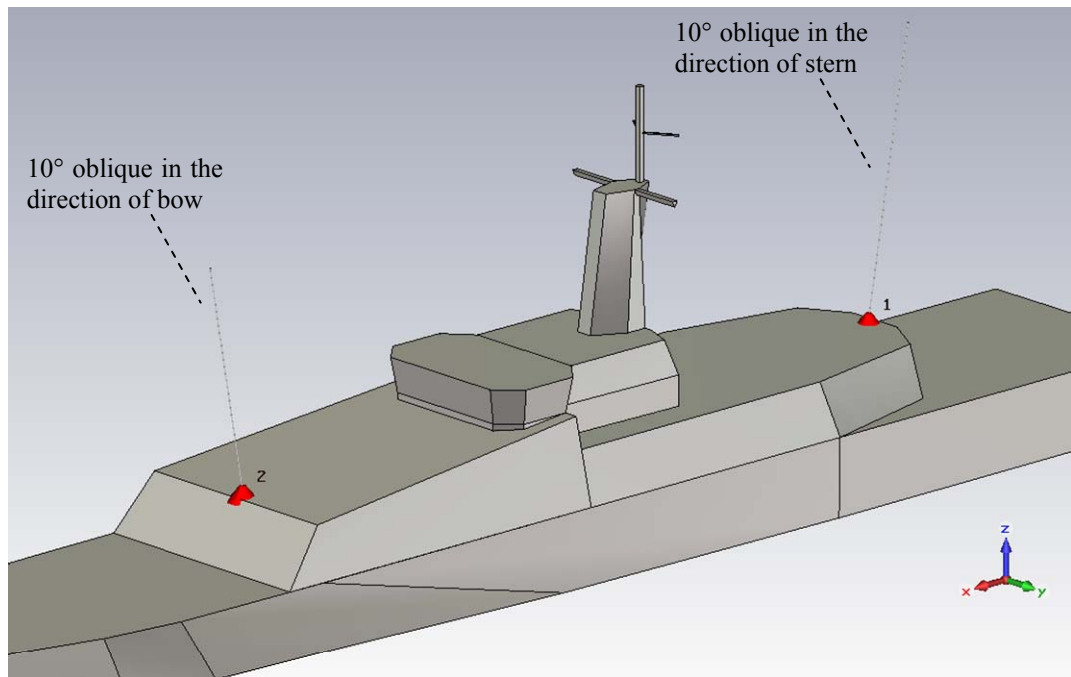


Figure 4-10 Placement Plan 9 for HF Antennas

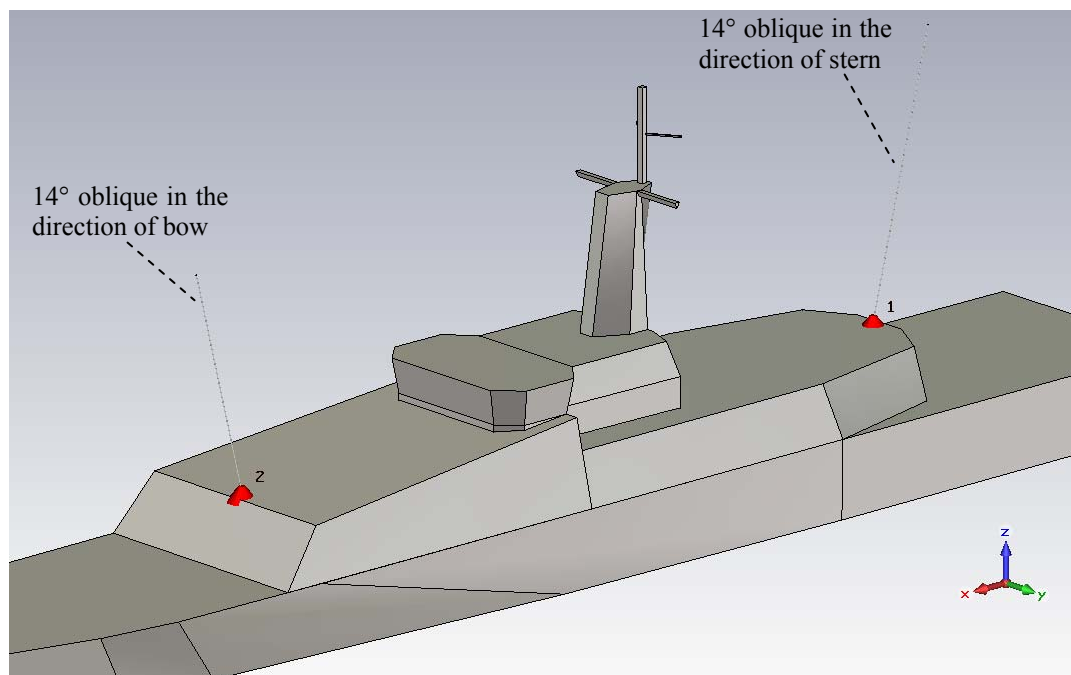


Figure 4-11 Placement Plan 10 for HF Antennas

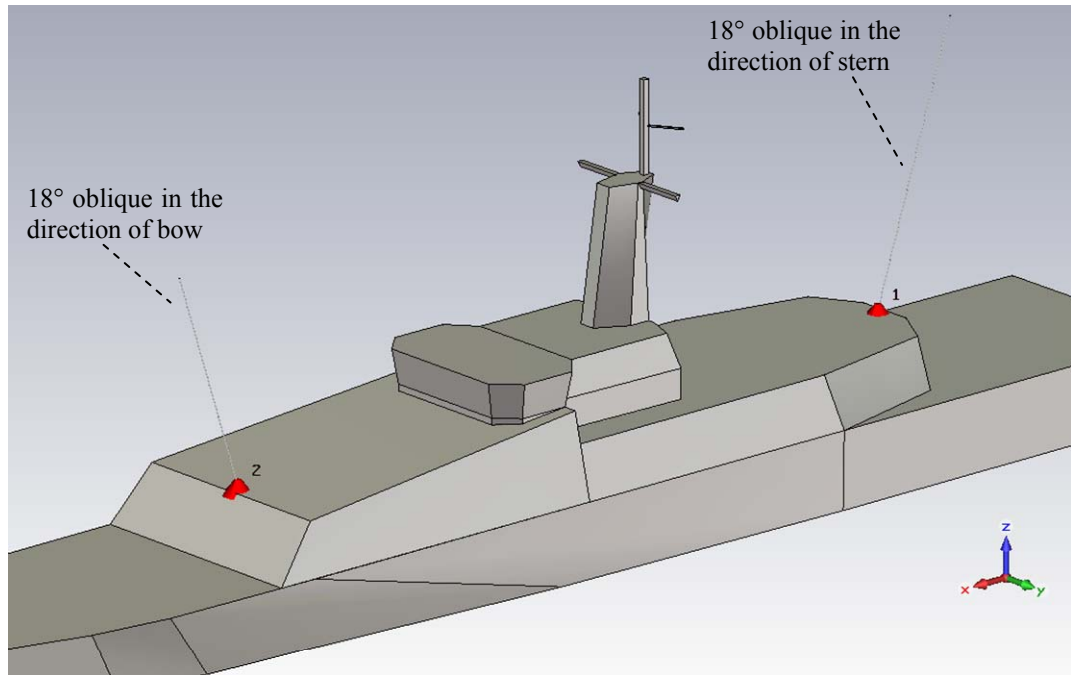


Figure 4-12 Placement Plan 11 for HF Antennas

In the analysis performed for the first seven placement plans, how the electromagnetic coupling between HF antennas changes due to the variation of the locations of these antennas is examined. The plots of the electromagnetic coupling levels ($S_{2,1}$) between HF antennas, obtained for the first seven placement plans, over 1.5 – 30 MHz frequency band are given in Figure 4-13. The mean values of the electromagnetic coupling levels over 1.5 – 30 MHz frequency band are calculated for the first seven placement plans and given in Table 4-3. As it is seen in Table 4-3, when HF antennas are mounted on the warship in accordance with placement plan 7, the mean value of the electromagnetic coupling levels is minimal among the corresponding results of the first seven placement plans.

Moreover, in order to observe how the electromagnetic coupling between HF antennas changes due to the variation of the polarization mismatch between these antennas, the electromagnetic analysis is carried out for four more placement plans shown in Figures 4-9 to 4-12. In these four placement plans, whereas HF 1 antenna

is slanted in the direction of the stern of the warship, HF 2 antenna is slanted in the direction of the bow at four different angles. Besides, in these four plans, the locations of HF antennas are identical to the locations of these antennas in placement plan 7.

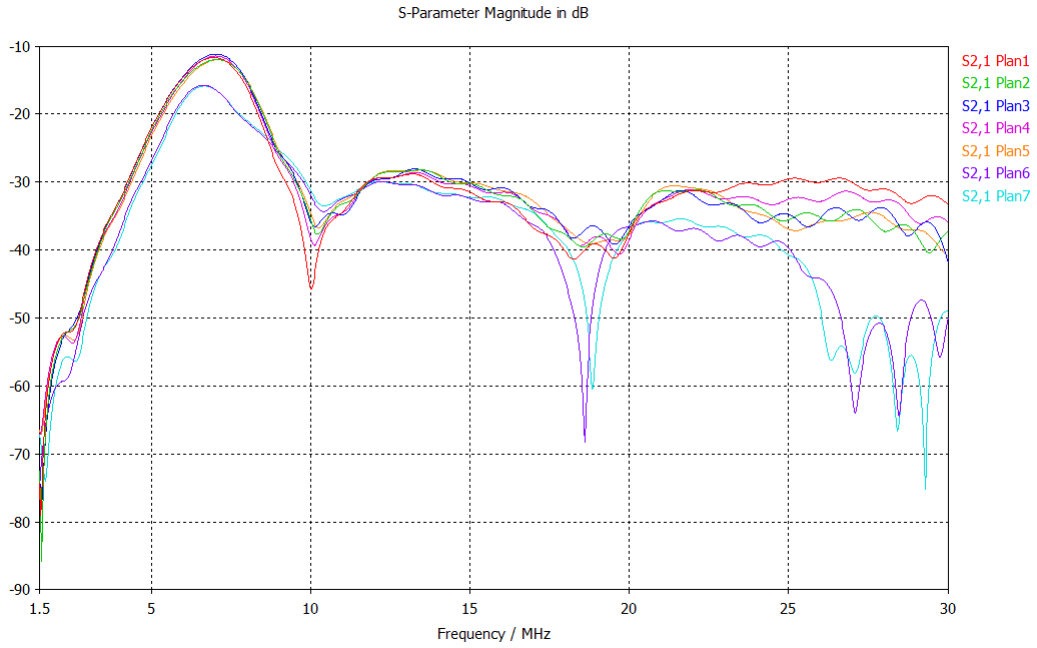


Figure 4-13 Coupling Levels for the First Seven Placement Plans

Table 4-3 Mean Values of Coupling Levels for the First Seven Plans

| Placement Plan of HF Antennas | Mean of $S_{2,1}$ (dB) |
|-------------------------------|------------------------|
| Plan 1 | -31.79 |
| Plan 2 | -32.36 |
| Plan 3 | -32.18 |
| Plan 4 | -31.87 |
| Plan 5 | -32.26 |
| Plan 6 | -37.5 |
| Plan 7 | -37.67 |

The plots of the electromagnetic coupling levels, obtained for the last four placement plans, over 1.5 – 30 MHz frequency band are given in Figure 4-14. The mean values of the electromagnetic coupling levels over 1.5 – 30 MHz frequency band are calculated for the last four placement plans and given in Table 4-4.

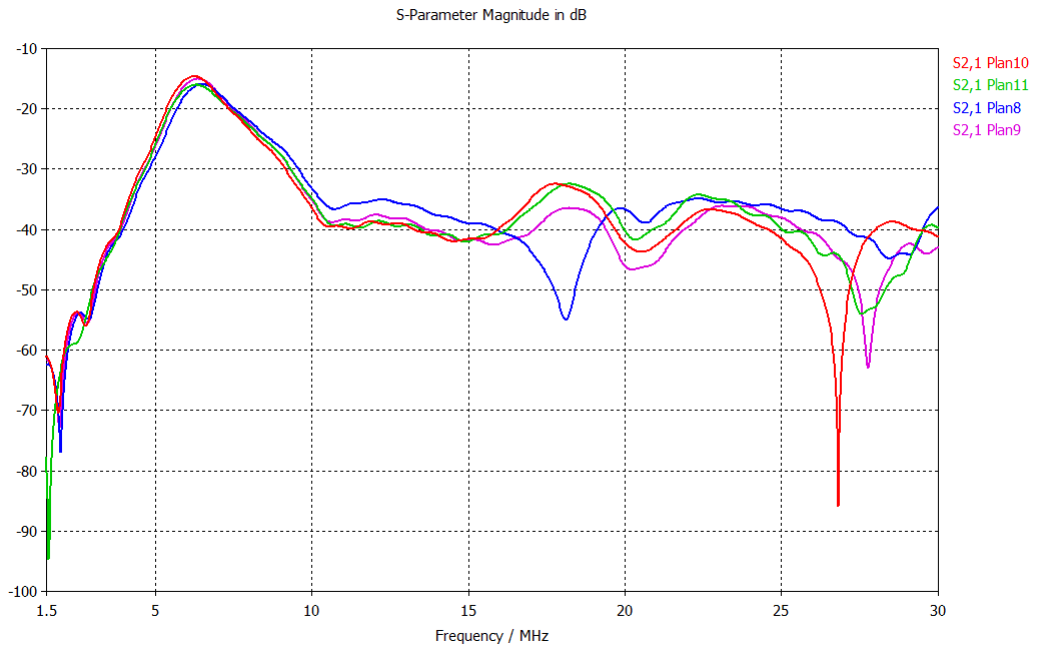


Figure 4-14 Coupling Levels for the Last Four Placement Plans

Table 4-4 Mean Values of Coupling Levels for the Last Four Plans

| Placement Plan of HF Antennas | Mean of $S_{2,1}$ (dB) |
|-------------------------------|------------------------|
| Plan 8 | -37.24 |
| Plan 9 | -38.51 |
| Plan 10 | -38.02 |
| Plan 11 | -37.94 |

In consequence of the observation of the mean values of the electromagnetic coupling levels between HF antennas, it can be concluded that:

- As it is seen in Table 4-3, there is not a major difference between the mean values obtained for the first five placement plans. Also, there is a slight difference between the mean values of placement plans 6 and 7. On the other hand, there is a major difference of approximately 5 – 6 dB between the mean values of the first five plans and those of plans 6 and 7. This difference arises from the following factors:
 - a. The physical distances between HF antennas in plans 6 and 7 are approximately 1.5 times greater than those in the first five plans.
 - b. In plans 6 and 7, there is more electromagnetic blockage caused by the bridge of the warship against the radiation of HF antennas towards each other.
- As it is seen in Table 4-4, there is a slight difference between the mean values of the last four plans. Also, there is a slight difference between the mean values of the last four plans and that of plan 7.
- It is observed that the electromagnetic coupling between HF antennas changes slightly due to the polarization mismatch between these antennas.
- The mean value of the electromagnetic coupling levels obtained for placement plan 9 is minimal among the corresponding results of these eleven placement plans.

Consequently, since the mean value of the electromagnetic coupling levels between HF antennas obtained for placement plan 9 is minimal, placement plan 9 is determined as the optimal placement plan for HF antennas among these eleven different placement plans. In addition to this, for this optimal placement plan, whether the far field radiation patterns of each HF antenna at particular frequencies have sufficient directivity values in the region where the antenna has to operate efficiently is investigated. Within this context, 3D far field radiation patterns (at 6,

18 and 30 MHz shown in Figures 4-15 to 4-20) of each HF antenna on the warship are compared with 3D far field radiation patterns (shown in Figures 4-21 to 4-26) of the related HF antenna above infinite ground plane, in the region where $10^\circ \leq \theta \leq 90^\circ$ (the region where each HF antenna has to operate efficiently so that the operational performance of the antenna shall not be degraded), in the way of the following two criteria:

1. At least 90 % of the directivity values of 3D far field radiation patterns of each HF antenna on the warship shall be greater than those of the related HF antenna above infinite ground plane minus 10 dB, in the region where $10^\circ \leq \theta \leq 90^\circ$.
2. At least 70 % of the directivity values of 3D far field radiation patterns of each HF antenna on the warship shall be greater than those of the related HF antenna above infinite ground plane minus 6 dB, in the region where $10^\circ \leq \theta \leq 90^\circ$.

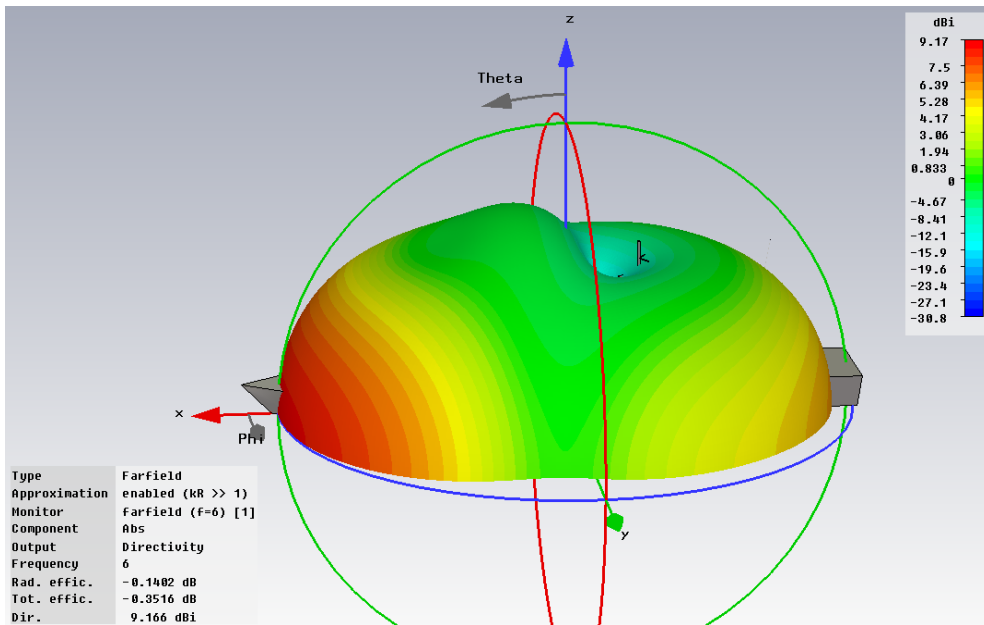


Figure 4-15 3D Radiation Pattern of HF 1 Antenna at 6 MHz – Plan 9

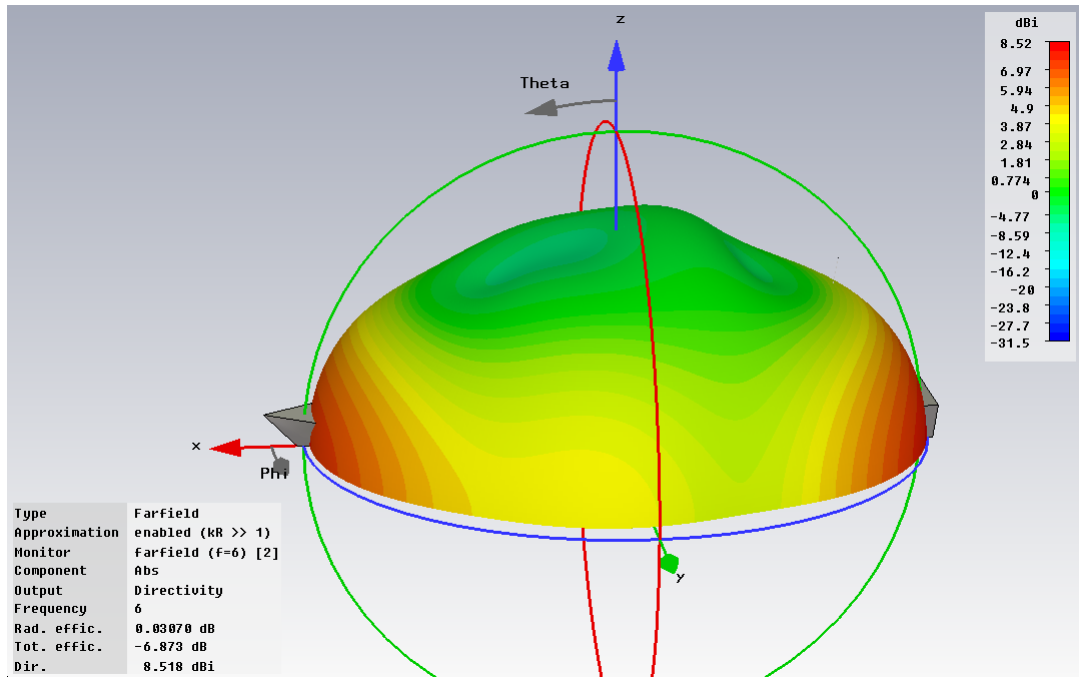


Figure 4-16 3D Radiation Pattern of HF 2 Antenna at 6 MHz – Plan 9

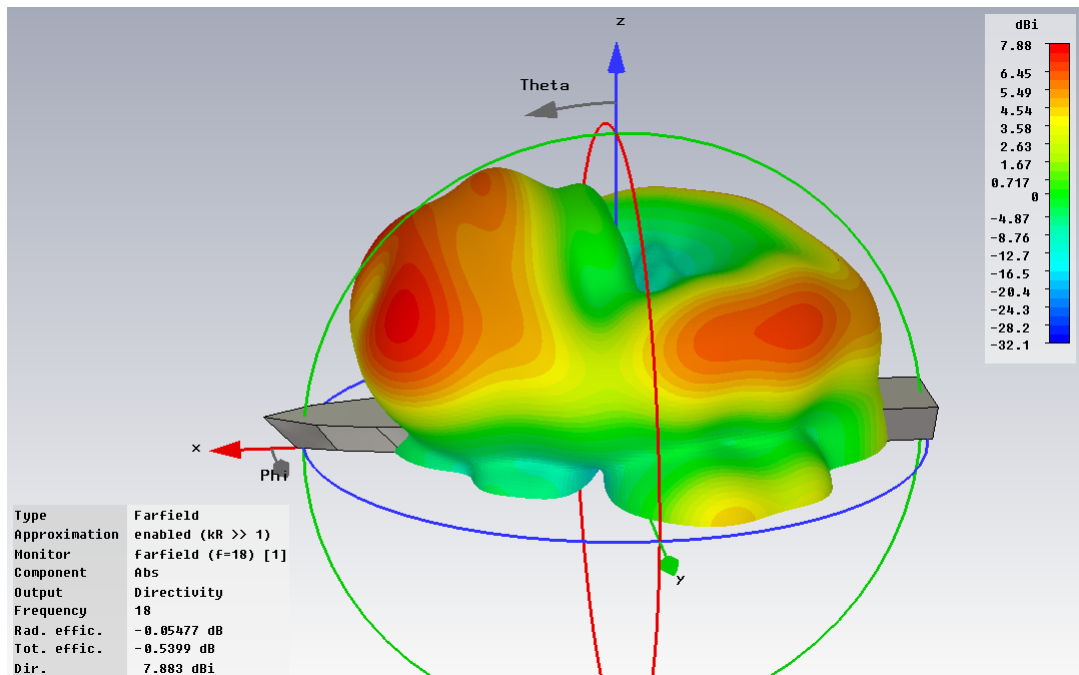


Figure 4-17 3D Radiation Pattern of HF 1 Antenna at 18 MHz – Plan 9

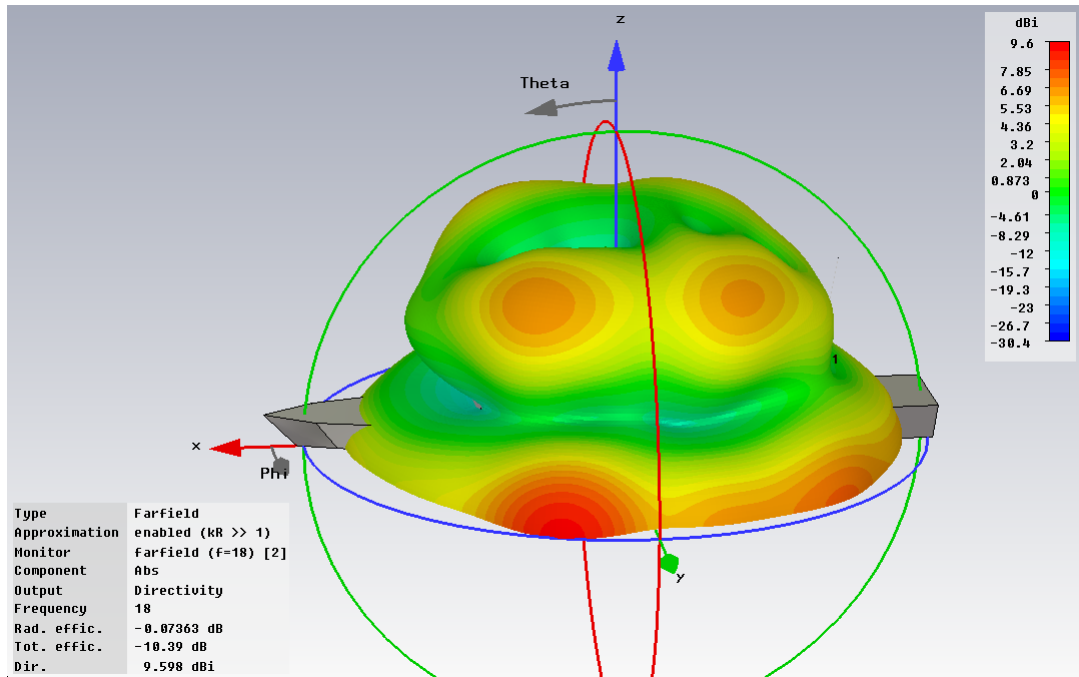


Figure 4-18 3D Radiation Pattern of HF 2 Antenna at 18 MHz – Plan 9

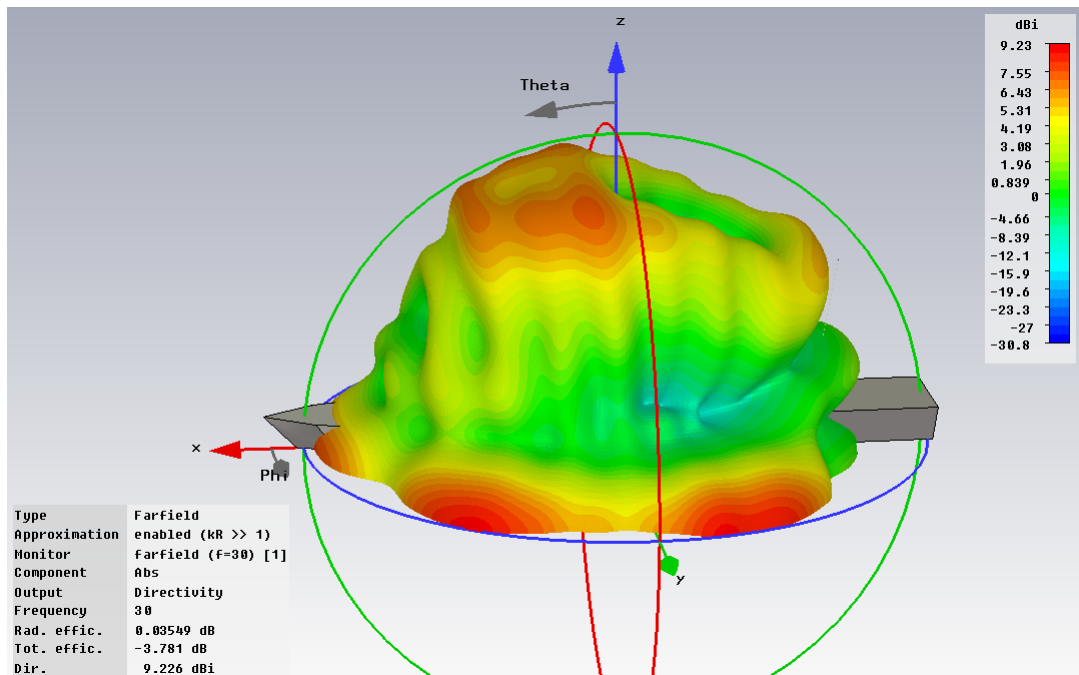


Figure 4-19 3D Radiation Pattern of HF 1 Antenna at 30 MHz – Plan 9

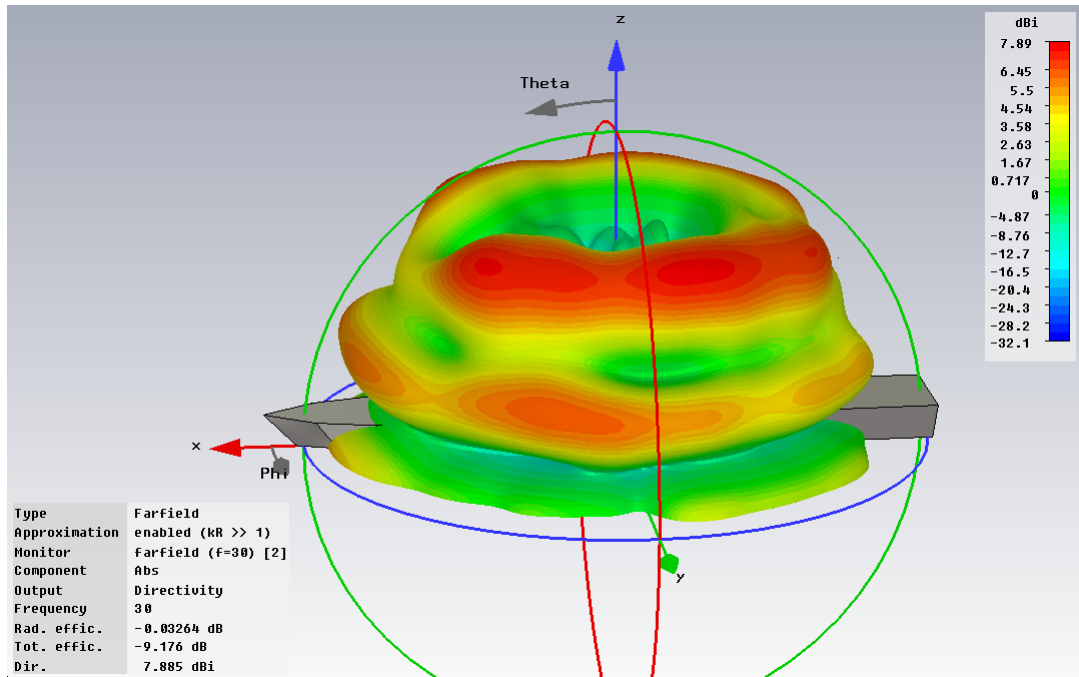


Figure 4-20 3D Radiation Pattern of HF 2 Antenna at 30 MHz – Plan 9

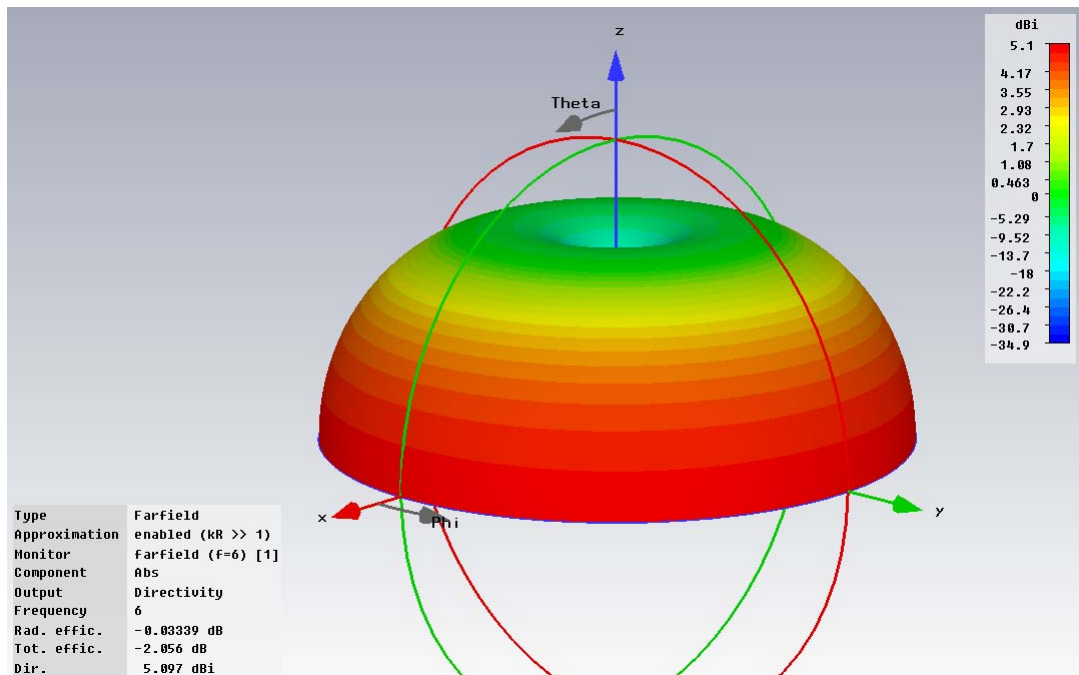


Figure 4-21 3D Radiation Pattern of HF 1 Antenna at 6 MHz – Above Infinite Ground Plane

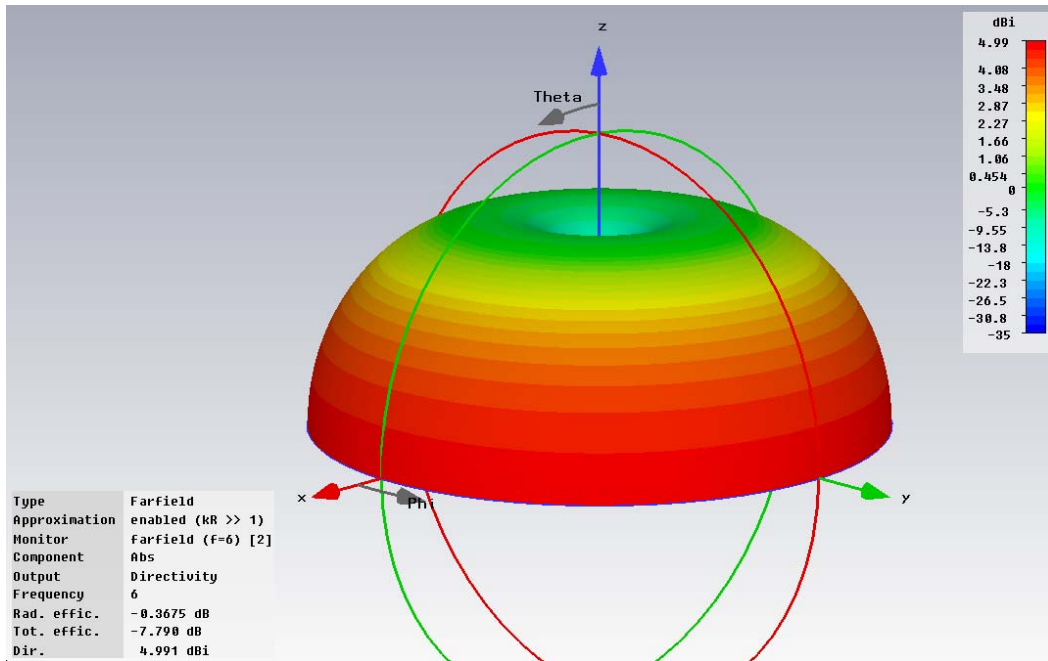


Figure 4-22 3D Radiation Pattern of HF 2 Antenna at 6 MHz – Above Infinite Ground Plane

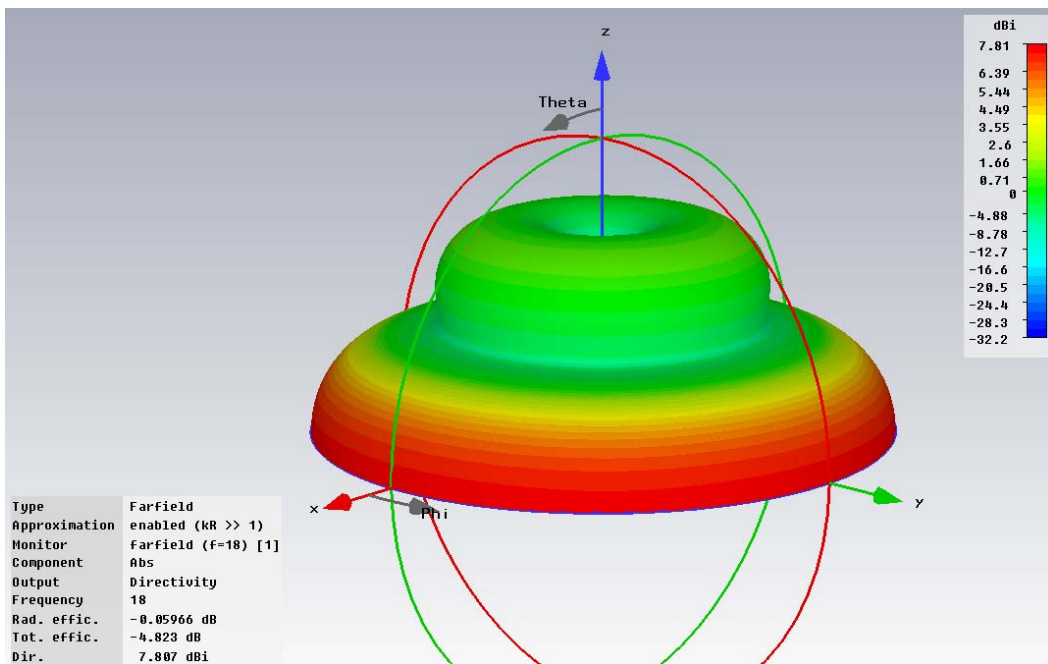


Figure 4-23 3D Radiation Pattern of HF 1 Antenna at 18 MHz – Above Infinite Ground Plane

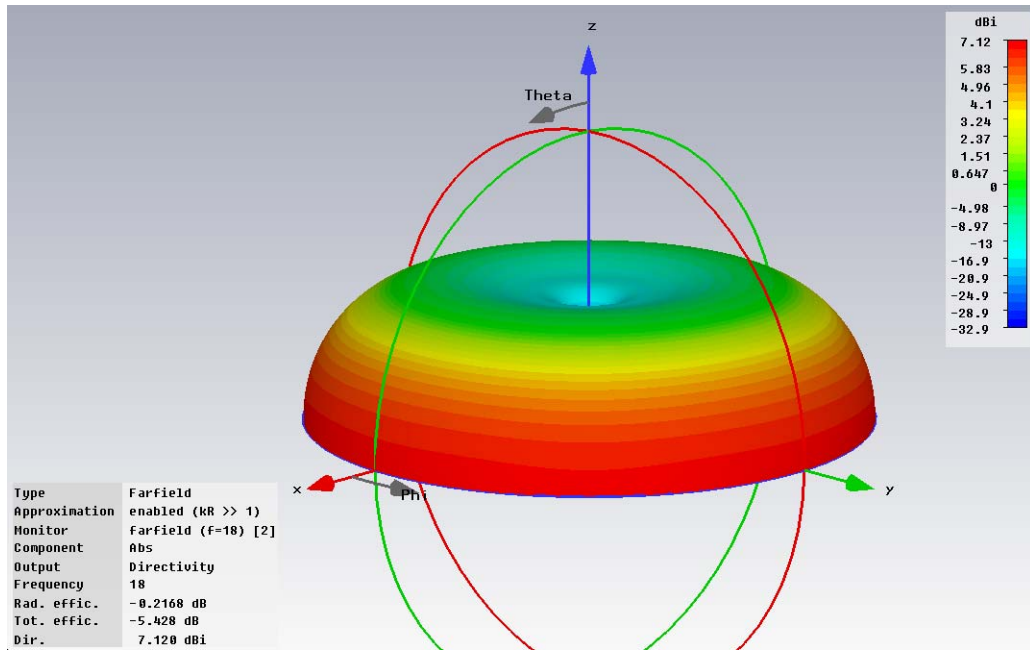


Figure 4-24 3D Radiation Pattern of HF 2 Antenna at 18 MHz – Above Infinite Ground Plane

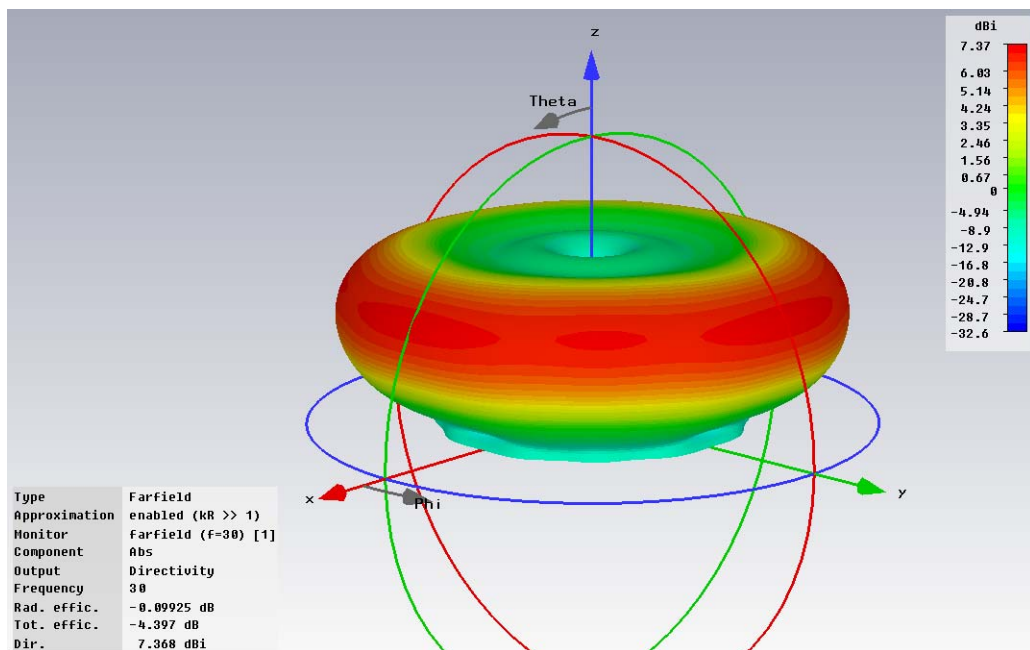


Figure 4-25 3D Radiation Pattern of HF 1 Antenna at 30 MHz – Above Infinite Ground Plane

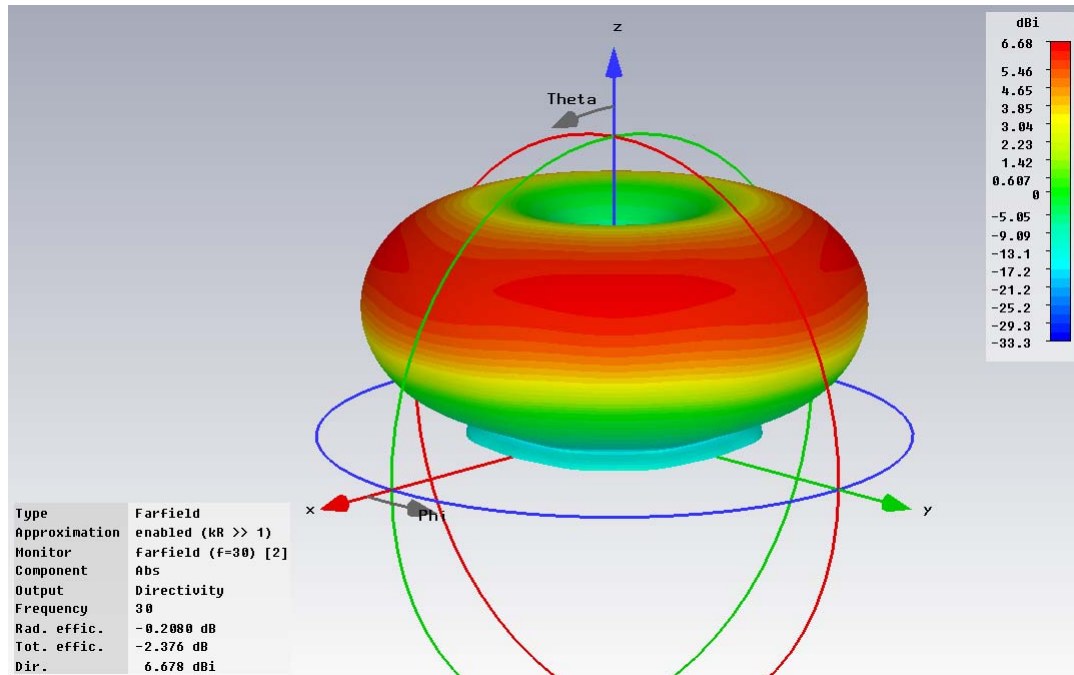


Figure 4-26 3D Radiation Pattern of HF 2 Antenna at 30 MHz – Above Infinite Ground Plane

Since the warship and HF antennas in placement plan 9 are symmetrical with respect to x-z plane, 3D far field radiation patterns of HF antennas on the warship are symmetrical with respect to x-z plane. Therefore, each of these patterns is given for only one angle of view.

In consequence of the comparison done between 3D far field radiation patterns of HF antennas at their optimal locations (Plan 9) and those of HF antennas above infinite ground plane, in the region where $10^\circ \leq \theta \leq 90^\circ$, the results of percentage of coverage of HF antennas are obtained and given in Table 4-5.

Finally, according to these results, the far field radiation patterns of HF antennas at their optimal locations have sufficient directivity values in the region where these antennas have to operate efficiently.

Table 4-5 Results of Percentage of Coverage of HF Antennas for Plan 9

| Antenna Name | Frequency (MHz) | Results of Percentage of Coverage of HF Antennas for Plan 9 | |
|--------------|-----------------|---|--|
| | | Comparison for 1 st Criterion | Comparison for 2 nd Criterion |
| HF 1 | 6 | 99.7 % | 96.3 % |
| | 18 | 92.3 % | 78.7 % |
| | 30 | 93.5 % | 85 % |
| HF 2 | 6 | 100 % | 100 % |
| | 18 | 97 % | 89.7 % |
| | 30 | 99.5 % | 96.3 % |

4.2. Analysis of VHF and V/UHF Antennas

As a result of the electromagnetic analysis of VHF and V/UHF antennas mounted on the warship, the electromagnetic coupling levels between these antennas are obtained for four different placement plans shown in Figures 4-27 to 4-30.

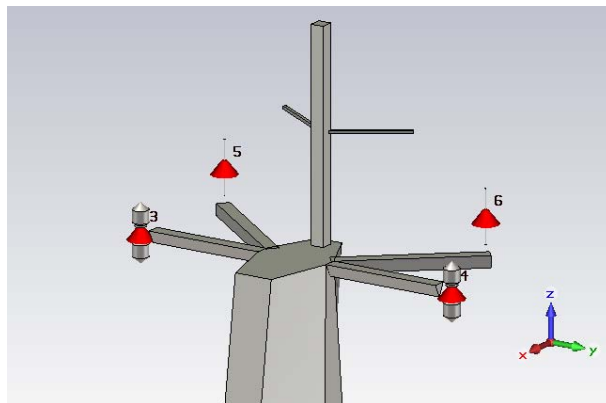


Figure 4-27 Placement Plan 1 for VHF and V/UHF Antennas

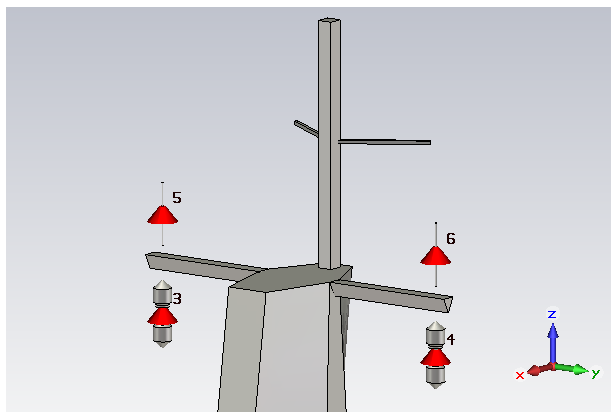


Figure 4-28 Placement Plan 2 for VHF and V/UHF Antennas

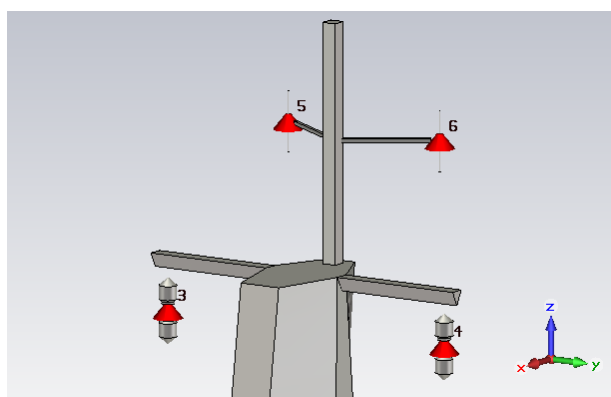


Figure 4-29 Placement Plan 3 for VHF and V/UHF Antennas

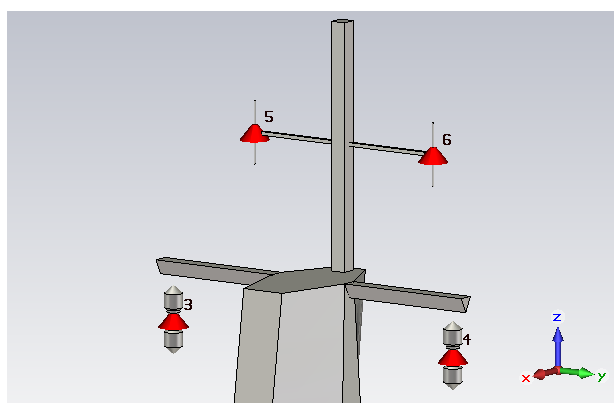


Figure 4-30 Placement Plan 4 for VHF and V/UHF Antennas

4.2.1. Coupling between V/UHF 1 and V/UHF 2 Antennas

The plots of the electromagnetic coupling levels ($S_{4,3}$) between V/UHF 1 and V/UHF 2 antennas, obtained for four different placement plans, over 118 – 400 MHz frequency band are given in Figure 4-31. The mean values of the electromagnetic coupling levels over 118 – 170 MHz and 225 – 400 MHz frequency bands (Table 4-1) are calculated for four placement plans and given in Table 4-6.

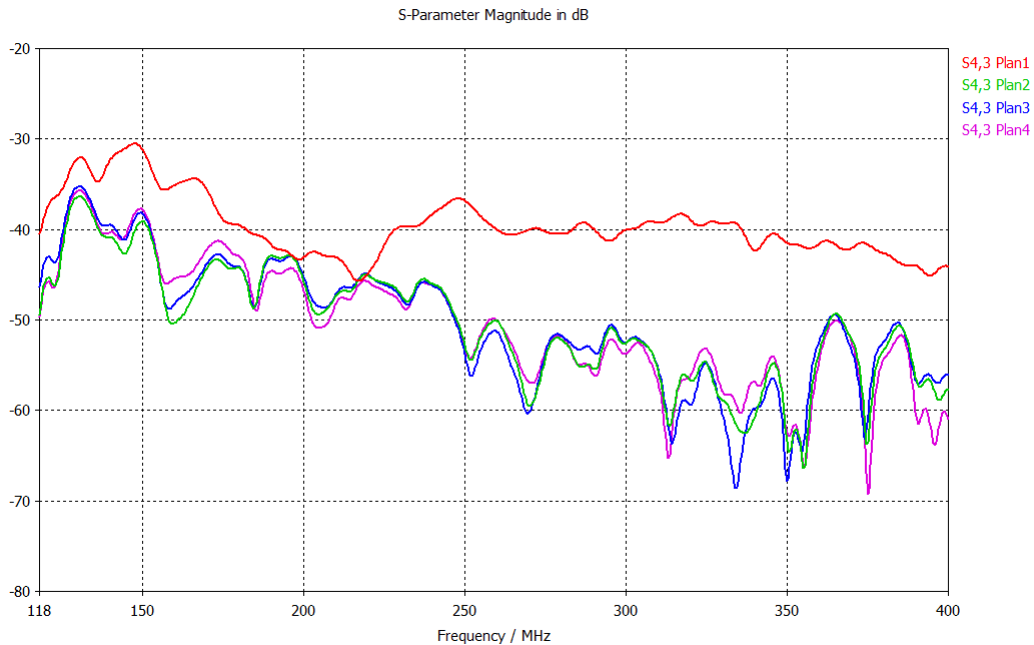


Figure 4-31 Coupling Levels between V/UHF 1 and V/UHF 2 Antennas

4.2.2. Coupling between V/UHF 1 and VHF 1 Antennas

The plots of the electromagnetic coupling levels ($S_{5,3}$) between V/UHF 1 and VHF 1 antennas, obtained for four different placement plans, over 148 – 164 MHz

frequency band are given in Figure 4-32. The mean values of the electromagnetic coupling levels over 148 – 164 MHz frequency band (Table 4-1) are calculated for four placement plans and given in Table 4-6.

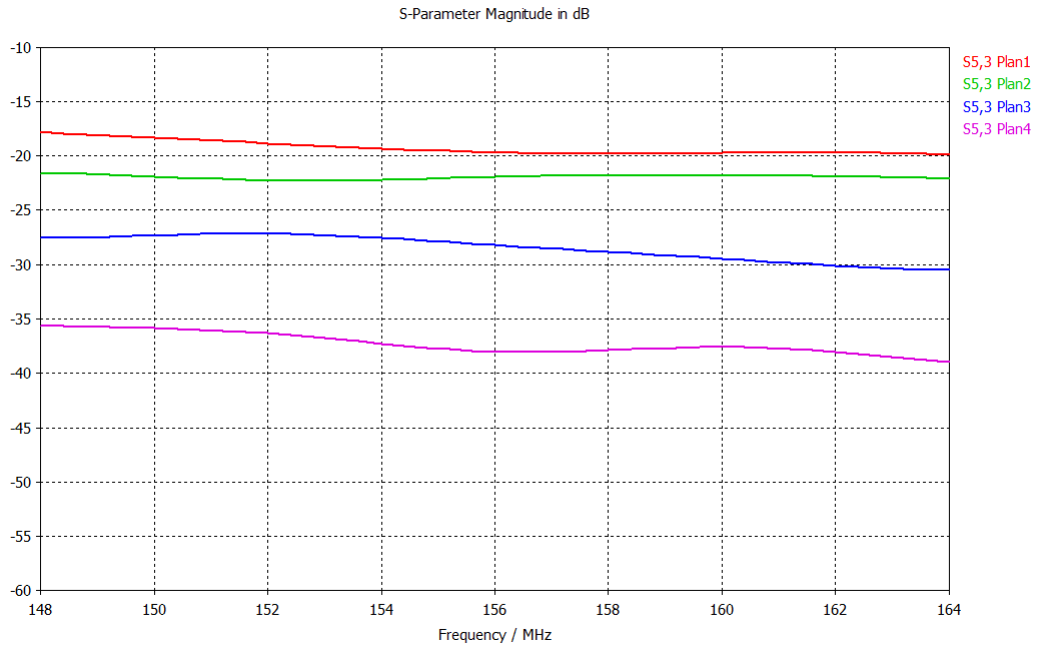


Figure 4-32 Coupling Levels between V/UHF 1 and VHF 1 Antennas

4.2.3. Coupling between V/UHF 1 and VHF 2 Antennas

The plots of the electromagnetic coupling levels ($S_{6,3}$) between V/UHF 1 and VHF 2 antennas, obtained for four different placement plans, over 148 – 164 MHz frequency band are given in Figure 4-33. The mean values of the electromagnetic coupling levels over 148 – 164 MHz frequency band (Table 4-1) are calculated for four placement plans and given in Table 4-6.

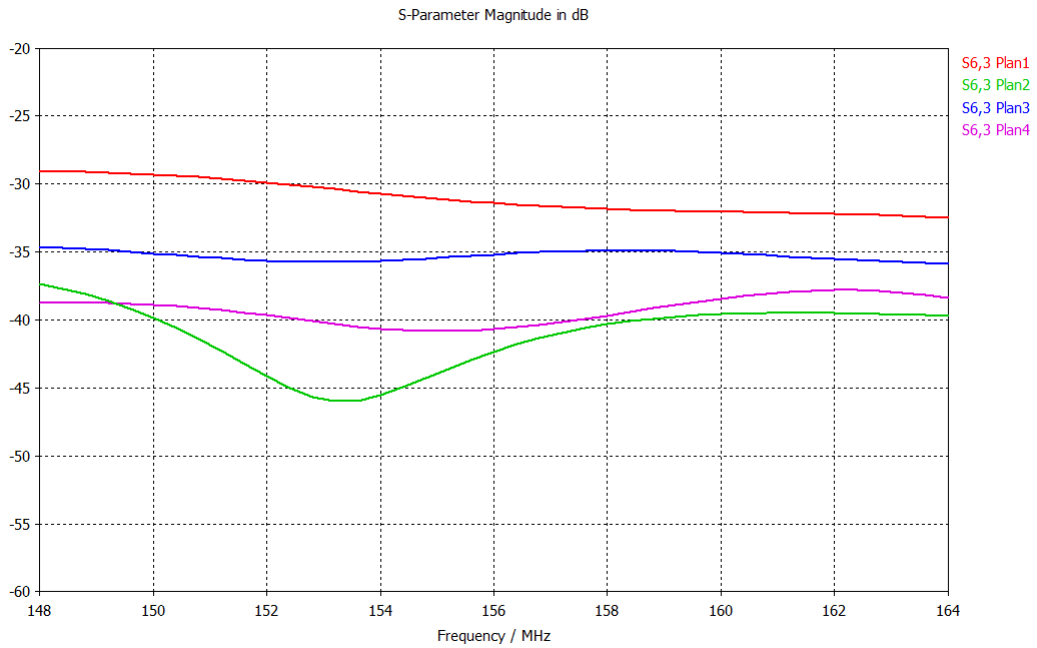


Figure 4-33 Coupling Levels between V/UHF 1 and VHF 2 Antennas

4.2.4. Coupling between V/UHF 2 and VHF 1 Antennas

The plots of the electromagnetic coupling levels ($S_{5,4}$) between V/UHF 2 and VHF 1 antennas, obtained for four different placement plans, over 148 – 164 MHz frequency band are given in Figure 4-34. The mean values of the electromagnetic coupling levels over 148 – 164 MHz frequency band (Table 4-1) are calculated for four placement plans and given in Table 4-6.

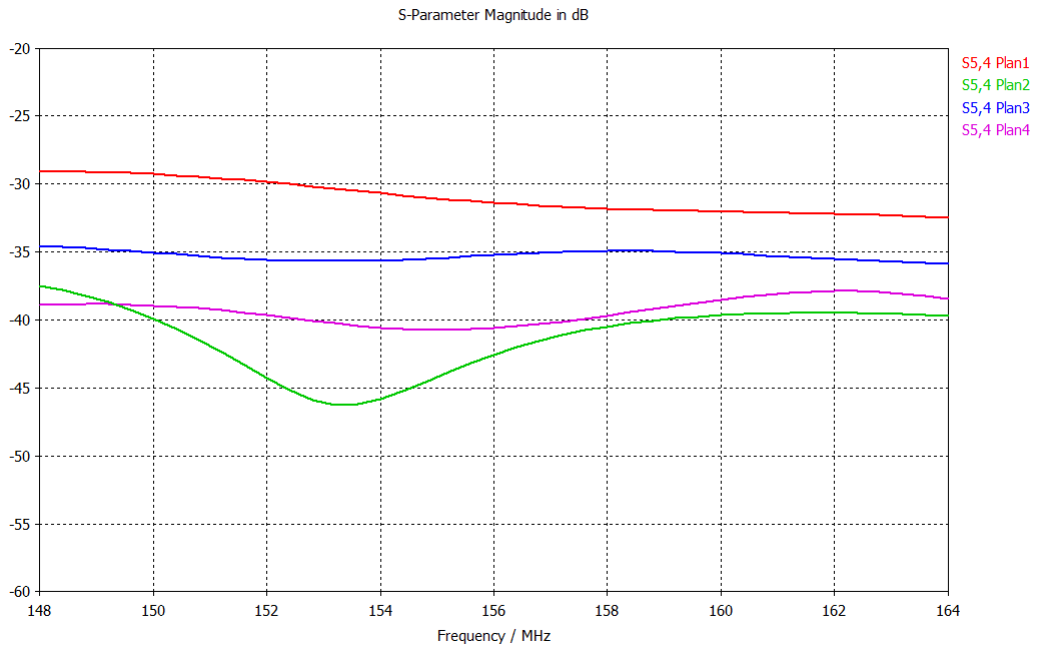


Figure 4-34 Coupling Levels between V/UHF 2 and VHF 1 Antennas

4.2.5. Coupling between V/UHF 2 and VHF 2 Antennas

The plots of the electromagnetic coupling levels ($S_{6,4}$) between V/UHF 2 and VHF 2 antennas, obtained for four different placement plans, over 148 – 164 MHz frequency band are given in Figure 4-35. The mean values of the electromagnetic coupling levels over 148 – 164 MHz frequency band (Table 4-1) are calculated for four placement plans and given in Table 4-6.

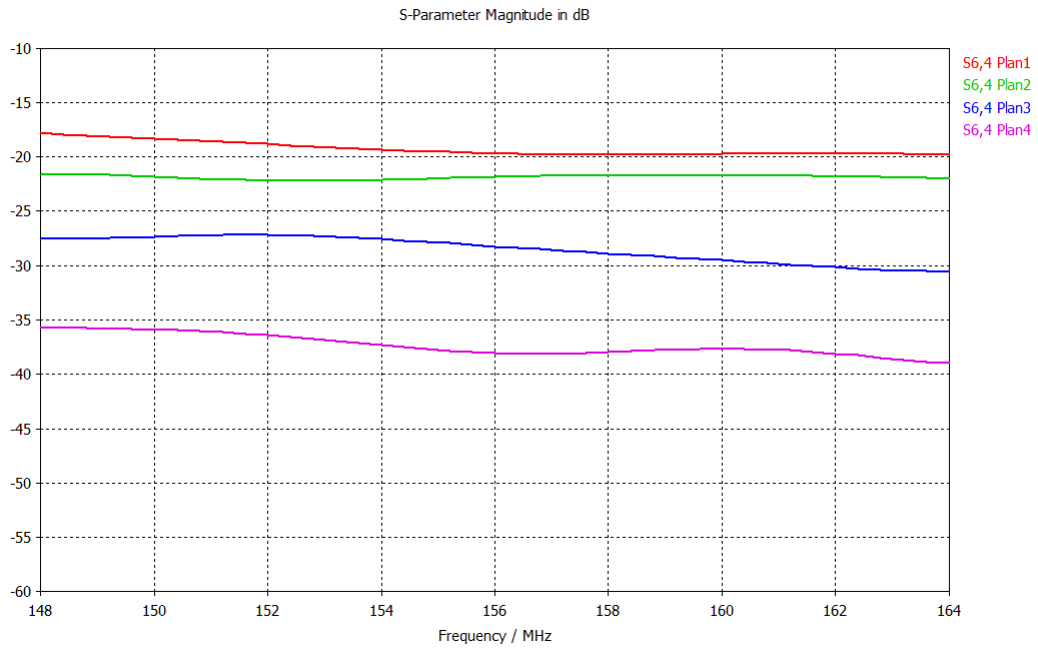


Figure 4-35 Coupling Levels between V/UHF 2 and VHF 2 Antennas

4.2.6. Coupling between VHF 1 and VHF 2 Antennas

The plots of the electromagnetic coupling levels ($S_{6,5}$) between VHF 1 and VHF 2 antennas, obtained for four different placement plans, over 148 – 164 MHz frequency band are given in Figure 4-36. The mean values of the electromagnetic coupling levels over 148 – 164 MHz frequency band (Table 4-1) are calculated for four placement plans and given in Table 4-6.

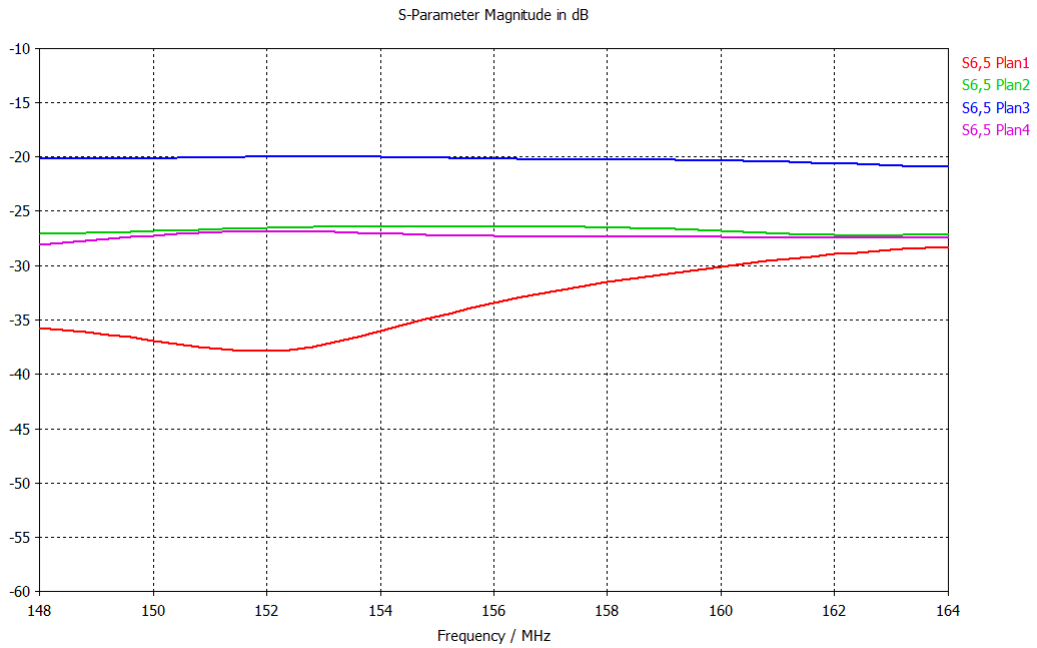


Figure 4-36 Coupling Levels between VHF 1 and VHF 2 Antennas

4.2.7. The Optimal Placement Plan for VHF and V/UHF Antennas

The mean values of the electromagnetic coupling levels between VHF and V/UHF antennas, obtained for four different placement plans, are given in Table 4-6. In consequence of the observation of these mean values, it can be concluded that:

- For the mean values of the coupling levels between V/UHF 1 and V/UHF 2 antennas, it can be concluded that:
 - a. Since the electromagnetic blockage caused by the mainmast of the warship against the radiation of V/UHF antennas towards each other in plans 2, 3 and 4 is quite more than that in plan 1, the mean values of plans 2, 3 and 4 are quite less than that of plan 1.
 - b. The mean values of plans 2, 3, and 4 are almost the same as expected.

- For the mean values of the coupling levels between V/UHF 1 and VHF 1 antennas, it can be concluded that:
 - a. Although the physical distance between these antennas in plan 1 is quite more than that in plan 2, the mean value of plan 2 is less than that of plan 1. Because the angle between the x-y plane, which the gains of these antennas above infinite ground plane are maximum ($\theta = 90^\circ$ plane), and the distance vector between these antennas in plan 2 is much more than that in plan 1. Also, there exists electromagnetic blockage caused by the main yard (at the starboard) of the warship against the radiation of these antennas towards each other in plan 2.
 - b. The angle between $\theta = 90^\circ$ plane and the distance vector between these antennas in plan 3 is less than that in plan 2. On the other hand, the physical distance between these antennas in plan 3 is quite more than that in plan 2. Therefore, the mean value of plan 3 is quite less than that of plan 2.
 - c. The physical distance between these antennas in plan 4 is a bit less than that in plan 3. On the other hand, the angle between $\theta = 90^\circ$ plane and the distance vector between these antennas in plan 4 is more than that in plan 3. Therefore, the mean value of plan 4 is quite less than that of plan 3.
- For the mean values of the coupling levels between V/UHF 1 and VHF 2 antennas, it can be concluded that:
 - a. Although the physical distance between these antennas in plan 1 is more than that in plan 3, the mean value of plan 3 is less than that of plan 1. Because the angle between $\theta = 90^\circ$ plane and the distance vector between these antennas in plan 3 is quite more than that in plan 1.
 - b. The physical distance between these antennas in plan 4 is a bit less than that in plan 3. On the other hand, the angle between $\theta = 90^\circ$ plane and the distance vector between these antennas in plan 4 is

- more than that in plan 3. Therefore, the mean value of plan 4 is less than that of plan 3.
- c. The mean value of plan 2 is less than that of plan 4. Because there exists electromagnetic blockage caused by the main yard and the mainmast against the radiation of these antennas towards each other in plan 2. Also, the physical distance between these antennas in plan 2 is a bit more than that in plan 4.
- For the mean values of the coupling levels between V/UHF 2 and VHF 1 antennas, it can be concluded that:
 - a. Although the physical distance between these antennas in plan 1 is more than that in plan 3, the mean value of plan 3 is less than that of plan 1. Because the angle between $\theta = 90^\circ$ plane and the distance vector between these antennas in plan 3 is quite more than that in plan 1.
 - b. The physical distance between these antennas in plan 4 is a bit less than that in plan 3. On the other hand, the angle between $\theta = 90^\circ$ plane and the distance vector between these antennas in plan 4 is more than that in plan 3. Therefore, the mean value of plan 4 is less than that of plan 3.
 - c. The mean value of plan 2 is less than that of plan 4. Because there exists electromagnetic blockage caused by the main yard and the mainmast against the radiation of these antennas towards each other in plan 2. Also, the physical distance between these antennas in plan 2 is a bit more than that in plan 4.
 - For the mean values of the coupling levels between V/UHF 2 and VHF 2 antennas, it can be concluded that:
 - a. Although the physical distance between these antennas in plan 1 is quite more than that in plan 2, the mean value of plan 2 is less than that of plan 1. Because the angle between $\theta = 90^\circ$ plane and the distance vector between these antennas in plan 2 is much more than that in plan 1. Also, there exists electromagnetic blockage caused

- by the main yard (at the portside) against the radiation of these antennas towards each other in plan 2.
- b. The angle between $\theta = 90^\circ$ plane and the distance vector between these antennas in plan 3 is less than that in plan 2. On the other hand, the physical distance between these antennas in plan 3 is quite more than that in plan 2. Therefore, the mean value of plan 3 is quite less than that of plan 2.
 - c. The physical distance between these antennas in plan 4 is a bit less than that in plan 3. On the other hand, the angle between $\theta = 90^\circ$ plane and the distance vector between these antennas in plan 4 is more than that in plan 3. Therefore, the mean value of plan 4 is quite less than that of plan 3.
- For the mean values of the coupling levels between VHF 1 and VHF 2 antennas, it can be concluded that:
 - a. Although the physical distance between these antennas in plan 2 is slightly more than that in plan 1, the mean value of plan 1 is quite less than that of plan 2. Because there are reflected fields from top surfaces of the main yard and the mainmast, generated by the incident fields from these antennas, which increase the coupling between these antennas in plan 2.
 - b. Since the physical distance between these antennas in plan 3 is quite less than that in plan 2, the mean value of plan 3 is quite more than that of plan 2.
 - c. The mean value of plan 4 is quite less than that of plan 3. Because there exists electromagnetic blockage caused by the topmast of the warship against the radiation of these antennas towards each other in plan 4. Also, the physical distance between these antennas in plan 4 is more than that in plan 3.
 - d. Although the physical distance between these antennas in plan 2 is more than that in plan 4, the mean value of plan 4 is slightly less than that of plan 2. Because there exists electromagnetic blockage

caused by the topmast against the radiation of these antennas towards each other in plan 4. Also, there are reflected fields from top surfaces of the main yard and the mainmast, generated by the incident fields from these antennas, which increase the coupling between these antennas in plan 2.

Table 4-6 Mean Values of Coupling Levels for Four Placement Plans

| Placement Plan of VHF and V/UHF Antennas | Mean Values of Coupling Levels (dB) | | | | | | Sum of Mean Values |
|--|-------------------------------------|-----------------|-----------------|-----------------|-----------------|---------------|--------------------|
| | V/UHF 1 – V/UHF 2 | V/UHF 1 – VHF 1 | V/UHF 1 – VHF 2 | V/UHF 2 – VHF 1 | V/UHF 2 – VHF 2 | VHF 1 – VHF 2 | |
| Plan 1 | -39.01 | -19.28 | -31.01 | -30.98 | -19.27 | -33.33 | -172.88 |
| Plan 2 | -51.73 | -21.95 | -41.18 | -41.3 | -21.86 | -26.73 | -204.75 |
| Plan 3 | -51.69 | -28.47 | -35.28 | -35.28 | -28.51 | -20.26 | -199.49 |
| Plan 4 | -51.63 | -37.27 | -39.27 | -39.28 | -37.34 | -27.3 | -232.09 |

Consequently, since the sum of the mean values of the electromagnetic coupling levels obtained for placement plan 4 is minimal, placement plan 4 is determined as the optimal placement plan for VHF and V/UHF antennas among these four different placement plans. In addition to this, for this optimal placement plan, whether the far field radiation patterns of each antenna at particular frequencies have sufficient directivity values in the region where the antenna has to operate efficiently is investigated. Within this context;

- 3D far field radiation patterns (at 150 and 300 MHz shown in Figures 4-37 to 4-40) of V/UHF 1 antenna on the warship are compared with 3D far field radiation patterns (shown in Figures 4-41 and 4-42) of V/UHF 1 antenna above infinite ground plane (the vertical distance between V/UHF 1 antenna and ground plane is the same as the vertical distance between this antenna and the sea in plan 4), in the region where $60^\circ \leq \theta \leq 90^\circ$ and $180^\circ \leq \Phi \leq 360^\circ$ (the region where V/UHF 1 antenna has to operate efficiently so that the operational performance of this antenna shall not be degraded), in the way of the following two criteria:
 1. At least 90 % of the directivity values of 3D far field radiation patterns of V/UHF 1 antenna on the warship shall be greater than those of V/UHF 1 antenna above infinite ground plane minus 10 dB, in the region where $60^\circ \leq \theta \leq 90^\circ$ and $180^\circ \leq \Phi \leq 360^\circ$.
 2. At least 70 % of the directivity values of 3D far field radiation patterns of V/UHF 1 antenna on the warship shall be greater than those of V/UHF 1 antenna above infinite ground plane minus 6 dB, in the region where $60^\circ \leq \theta \leq 90^\circ$ and $180^\circ \leq \Phi \leq 360^\circ$.
- The 3D far field radiation pattern (at 150 MHz shown in Figures 4-43 and 4-44) of VHF 1 antenna on the warship is compared with the 3D far field radiation pattern (shown in Figure 4-45) of VHF 1 antenna above infinite ground plane (the vertical distance between VHF 1 antenna and ground plane is the same as the vertical distance between this antenna and the sea in plan 4), in the region where $60^\circ \leq \theta \leq 90^\circ$ and $180^\circ \leq \Phi \leq 360^\circ$ (the region where VHF 1 antenna has to operate efficiently so that the operational performance of this antenna shall not be degraded), in the way of the following two criteria:
 1. At least 90 % of the directivity values of the 3D far field radiation pattern of VHF 1 antenna on the warship shall be greater than those of VHF 1 antenna above infinite ground plane minus 10 dB, in the region where $60^\circ \leq \theta \leq 90^\circ$ and $180^\circ \leq \Phi \leq 360^\circ$.

- At least 70 % of the directivity values of the 3D far field radiation pattern of VHF 1 antenna on the warship shall be greater than those of VHF 1 antenna above infinite ground plane minus 6 dB, in the region where $60^\circ \leq \theta \leq 90^\circ$ and $180^\circ \leq \Phi \leq 360^\circ$.

The locations of V/UHF 1 and V/UHF 2 antennas are symmetrical with respect to x-z plane in plan 4. Also, the locations of VHF 1 and VHF 2 antennas are symmetrical with respect to x-z plane. Therefore, far field radiation patterns of V/UHF 2 and VHF 2 antennas are symmetric (with respect to x-z plane) of those of V/UHF 1 and VHF 1 antennas, respectively. Due to this fact, the analysis of far field radiation patterns of VHF and V/UHF antennas is performed only for V/UHF 1 and VHF 1 antennas.

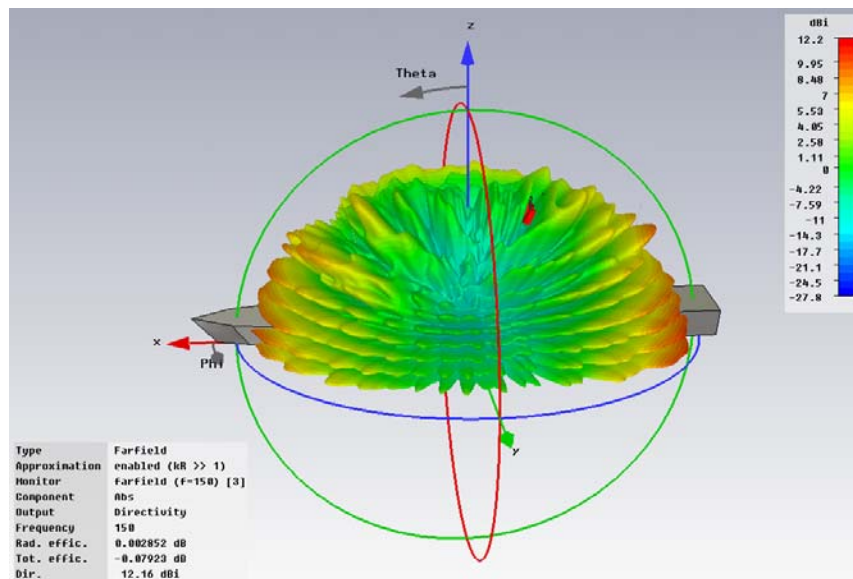


Figure 4-37 3D Radiation Pattern of V/UHF 1 Antenna at 150 MHz – Plan 4 (1st Angle of View)

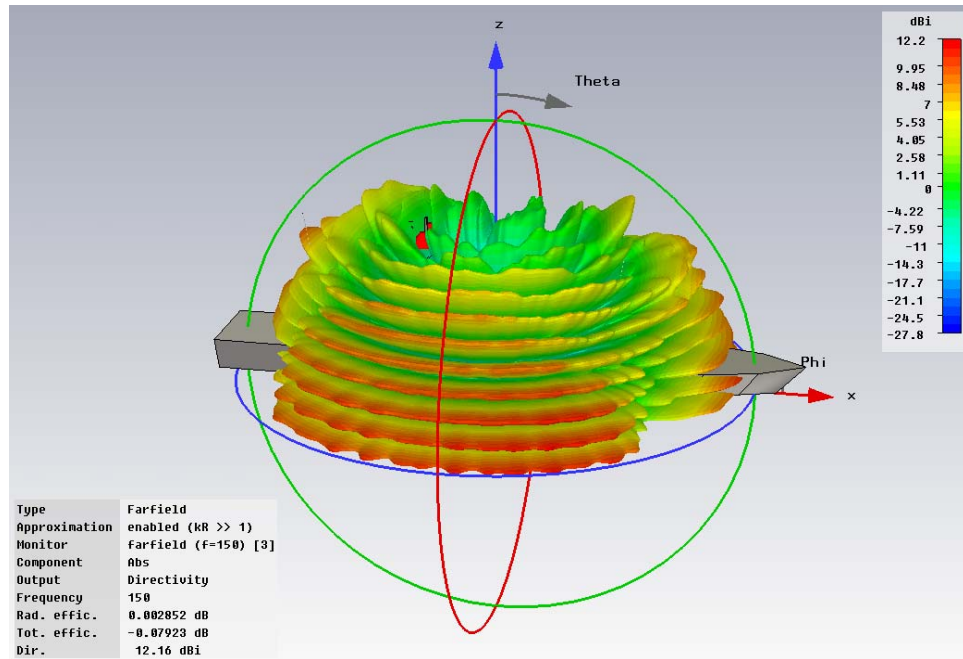


Figure 4-38 3D Radiation Pattern of V/UHF 1 Antenna at 150 MHz – Plan 4 (2nd Angle of View)

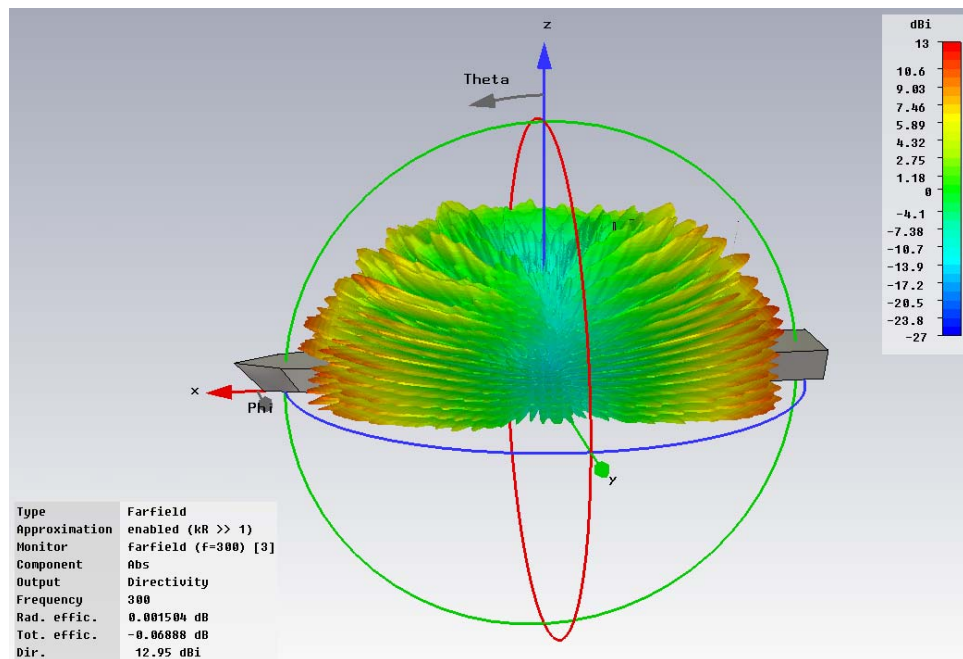


Figure 4-39 3D Radiation Pattern of V/UHF 1 Antenna at 300 MHz – Plan 4 (1st Angle of View)

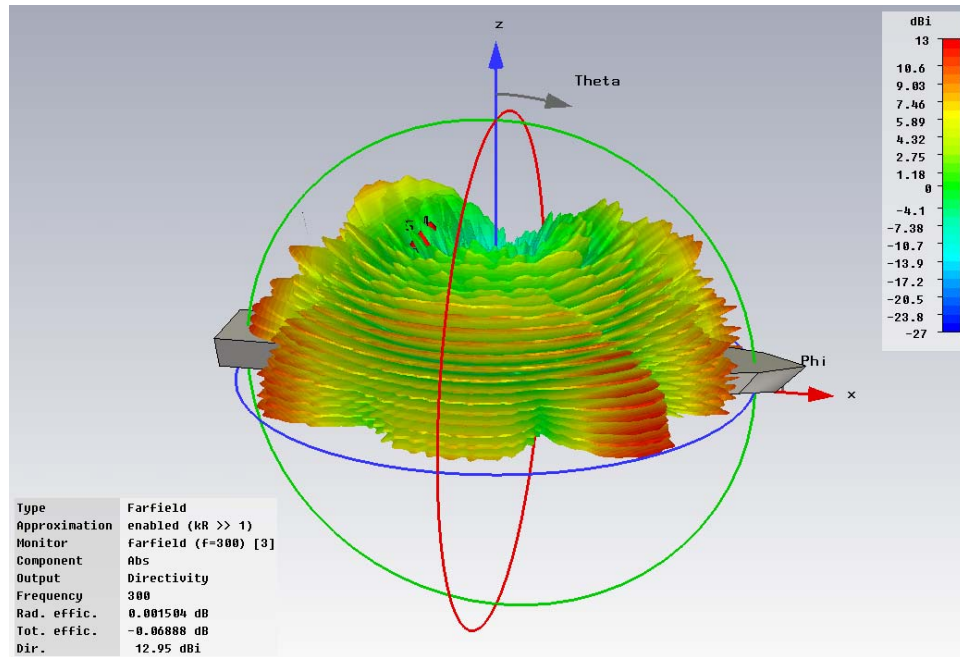


Figure 4-40 3D Radiation Pattern of V/UHF 1 Antenna at 300 MHz – Plan 4 (2nd Angle of View)

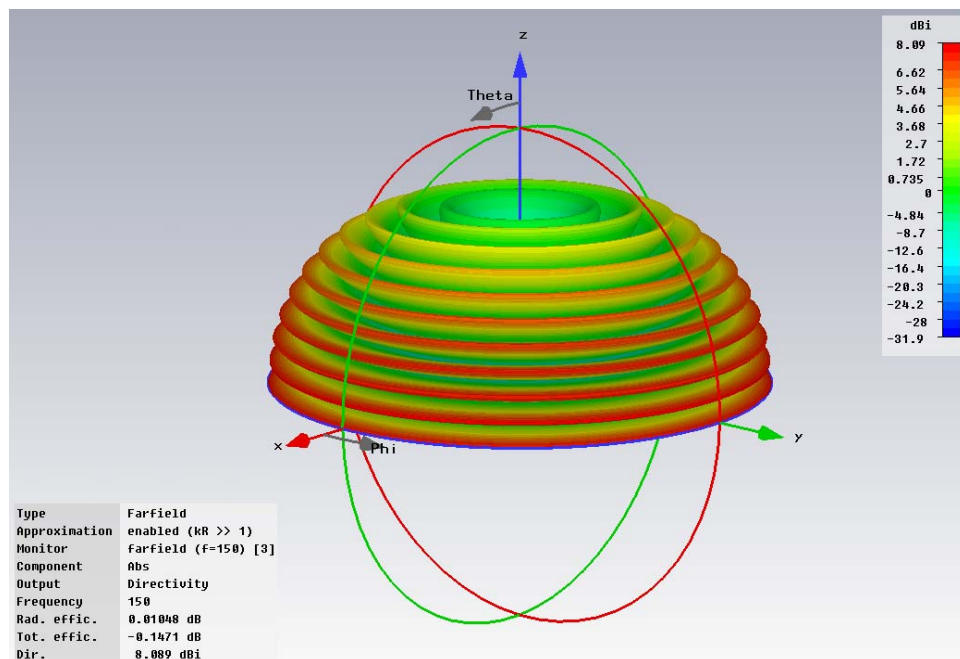


Figure 4-41 3D Radiation Pattern of V/UHF 1 Antenna at 150 MHz – Above Infinite Ground Plane

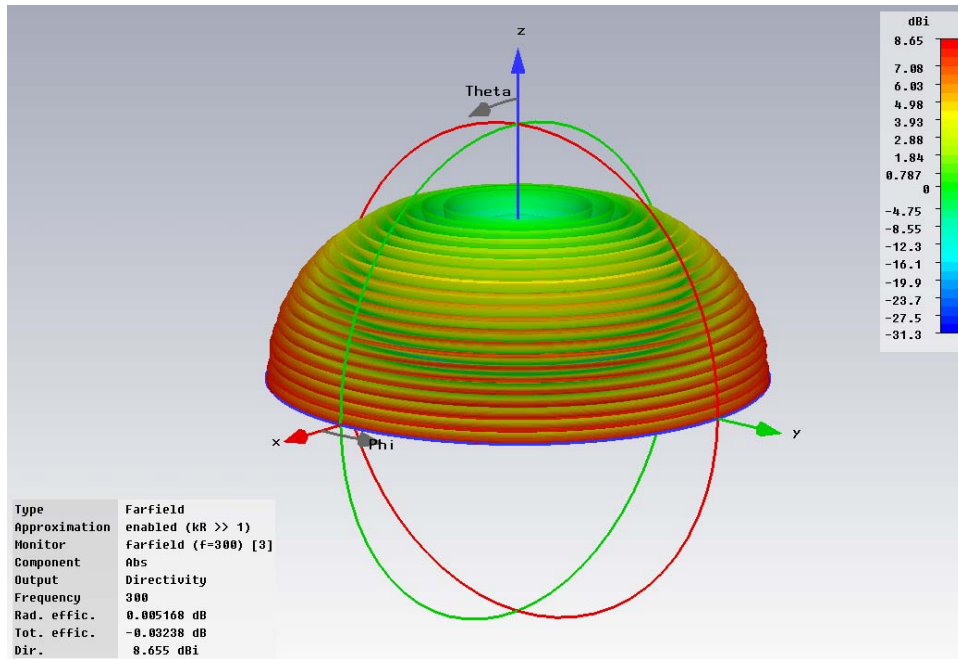


Figure 4-42 3D Radiation Pattern of V/UHF 1 Antenna at 300 MHz – Above Infinite Ground Plane

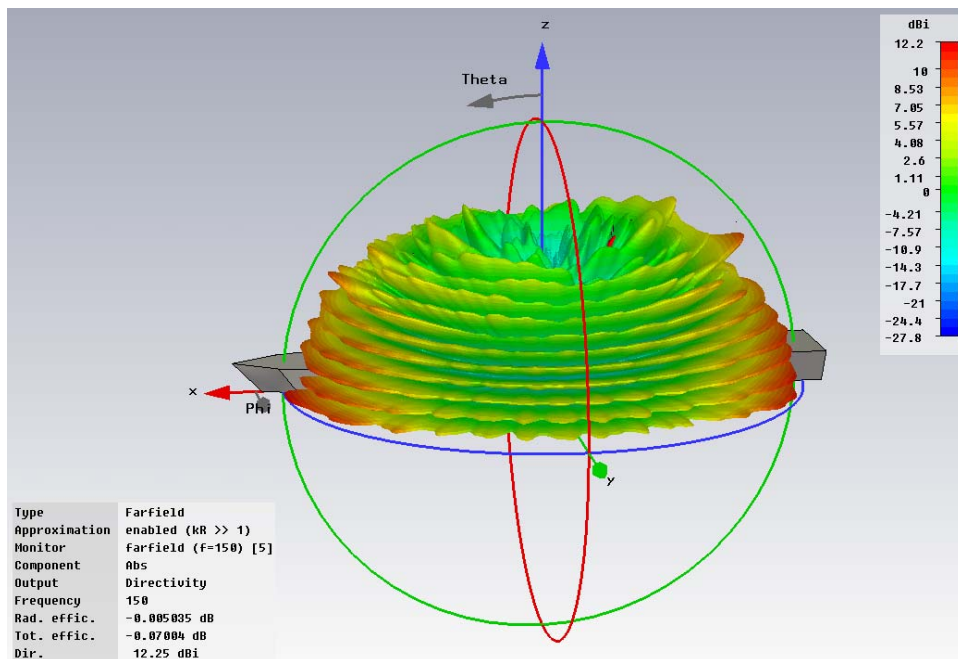


Figure 4-43 3D Radiation Pattern of VHF 1 Antenna at 150 MHz – Plan 4 (1st Angle of View)

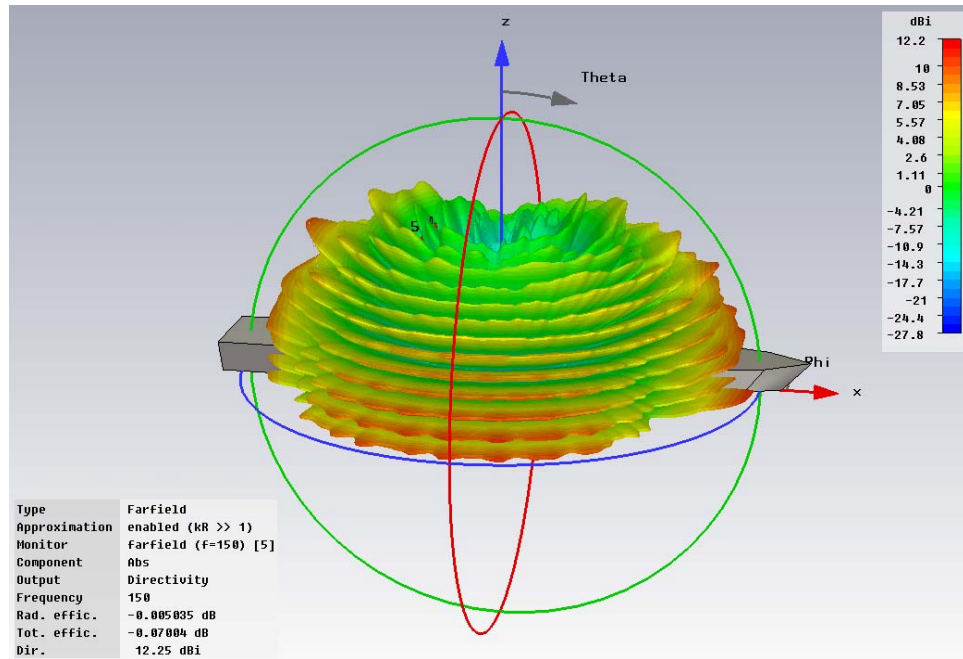


Figure 4-44 3D Radiation Pattern of VHF 1 Antenna at 150 MHz – Plan 4 (2nd Angle of View)

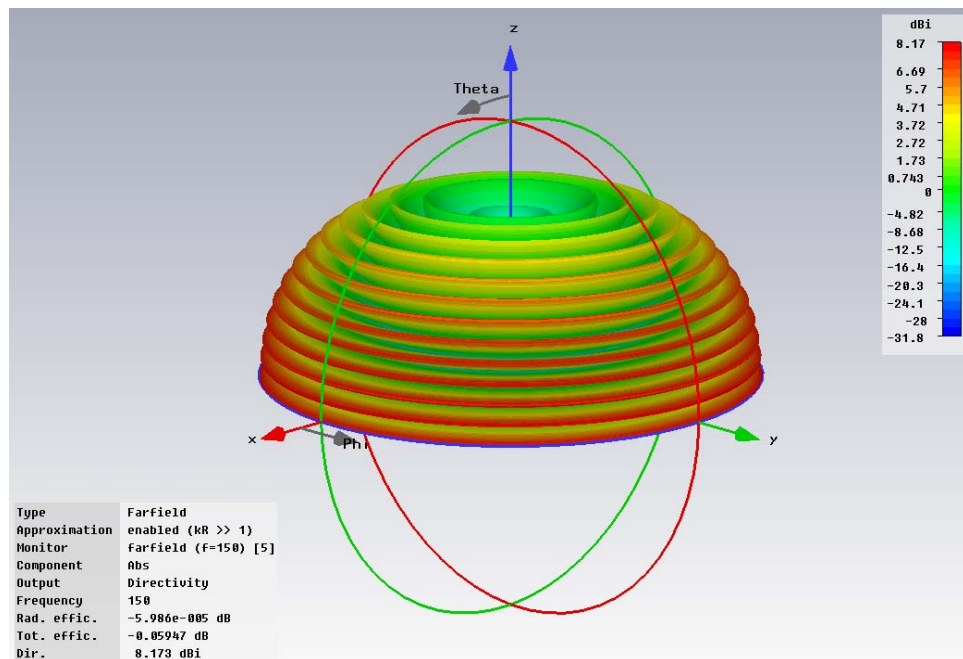


Figure 4-45 3D Radiation Pattern of VHF 1 Antenna at 150 MHz – Above Infinite Ground Plane

In consequence of the comparison done between 3D far field radiation patterns of VHF and V/UHF antennas at their optimal locations (Plan 4) and those of these antennas above infinite ground plane, the results of percentage of coverage of these antennas are obtained and given in Table 4-7.

Finally, according to these results, the far field radiation patterns of VHF and V/UHF antennas at their optimal locations have sufficient directivity values in the region where these antennas have to operate efficiently.

Table 4-7 Results of Percentage of Coverage of VHF and V/UHF Antennas for Plan 4

| Antenna Name | Frequency (MHz) | Results of Percentage of Coverage of VHF and V/UHF Antennas for Plan 4 | |
|--------------|-----------------|--|--|
| | | Comparison for 1 st Criterion | Comparison for 2 nd Criterion |
| V/UHF 1 | 150 | 99.96 % | 99.3 % |
| | 300 | 99.9 % | 97.7 % |
| V/UHF 2 | 150 | 99.96 % | 99.3 % |
| | 300 | 99.9 % | 97.7 % |
| VHF 1 | 150 | 99.98 % | 99.8 % |
| VHF 2 | 150 | 99.98 % | 99.8 % |

Moreover, as a result of the observation of the polar radiation patterns (shown in Figures 4-46, 4-47 and 4-48) of V/UHF 1 and VHF 1 antennas in y-z plane, which are obtained for placement plan 4, it can be concluded that:

- Since the sea is modeled as a conducting wall having a conductivity of 5 S/m (it functions as infinite ground plane) in the simulations, there exist virtual sources (images) of VHF and V/UHF antennas at the locations that are symmetric (with respect to x-y plane) of the locations of actual sources, because of image theory [8]. Due to this fact, the far field radiation patterns of V/UHF 1 and VHF 1 antennas have many sidelobes [8].
- Since the electrical distance between V/UHF 1 antenna and the sea at 300 MHz is greater than that at 150 MHz, the number of sidelobes of the polar radiation pattern of V/UHF 1 antenna at 300 MHz is more than that of the polar radiation pattern at 150 MHz [8]. Besides, since the electrical distance between VHF 1 antenna and the sea is greater than the electrical distance between V/UHF 1 antenna and the sea at 150 MHz, the number of sidelobes of the polar radiation pattern of VHF 1 antenna is more than that of V/UHF 1 antenna at 150 MHz.
- As it is seen in Figures 4-46 and 4-47, directivity values of the polar radiation patterns in $\Phi = 90^\circ$ plane are quite less than those in $\Phi = 270^\circ$ plane. Because, there exists electromagnetic blockage caused by the mainmast of the warship against the radiation of V/UHF 1 antenna towards the region in $\Phi = 90^\circ$ plane. As it is seen in Figure 4-48, directivity values of the polar radiation pattern in $\Phi = 90^\circ$ plane are less than those in $\Phi = 270^\circ$ plane. Because, there exists electromagnetic blockage caused by the topmast of the warship against the radiation of VHF 1 antenna towards the region in $\Phi = 90^\circ$ plane. The differences between directivity values in $\Phi = 270^\circ$ plane and those in $\Phi = 90^\circ$ plane in the polar radiation patterns of V/UHF 1 antenna are more than those in the polar radiation pattern of VHF 1 antenna. Because the electromagnetic blockage caused by the mainmast against the radiation of V/UHF 1 antenna is much more than the electromagnetic blockage caused by the topmast against the radiation of VHF 1 antenna due to the fact that the thickness of the mainmast along x axis is much more than that of the topmast.

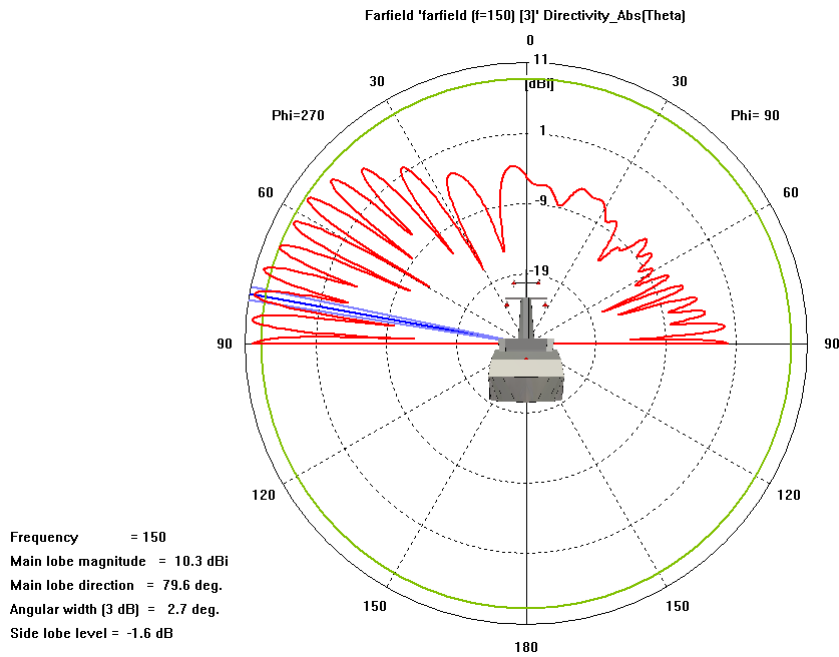


Figure 4-46 Polar Radiation Pattern of V/UHF 1 Antenna in y-z Plane – Plan 4 (at 150 MHz)

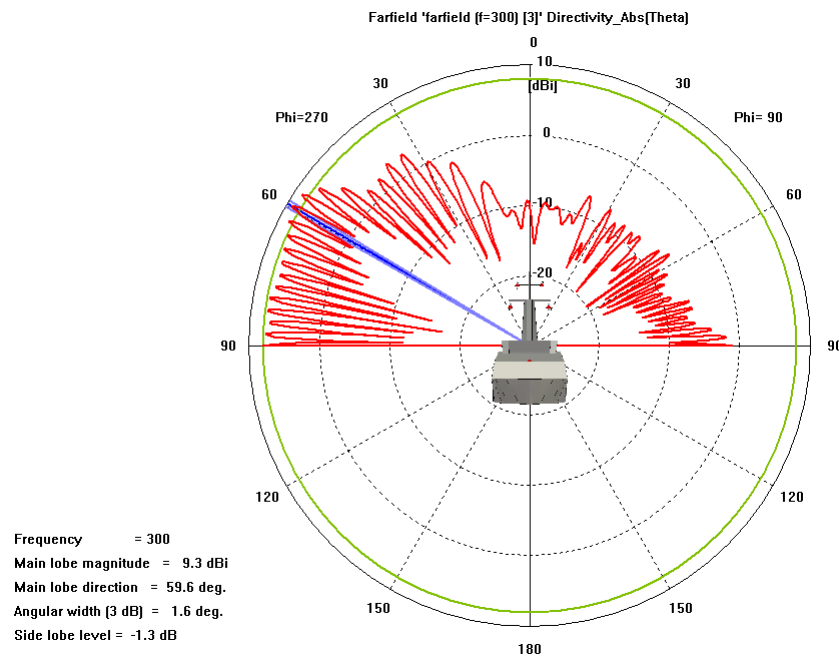


Figure 4-47 Polar Radiation Pattern of V/UHF 1 Antenna in y-z Plane – Plan 4 (at 300 MHz)

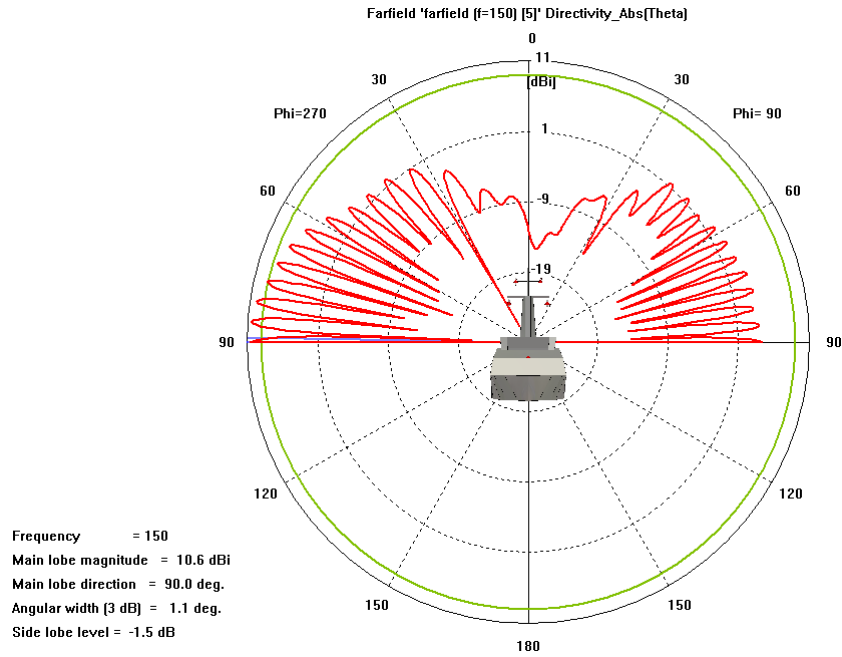


Figure 4-48 Polar Radiation Pattern of VHF 1 Antenna in y-z Plane – Plan 4 (at 150 MHz)

4.3. The Optimal Placement Plan for HF, VHF and V/UHF Antennas

The optimal placement plan for HF, VHF and V/UHF antennas is composed of these two optimal placement plans determined in sections 4.1 and 4.2, and shown in Figure 4-49.

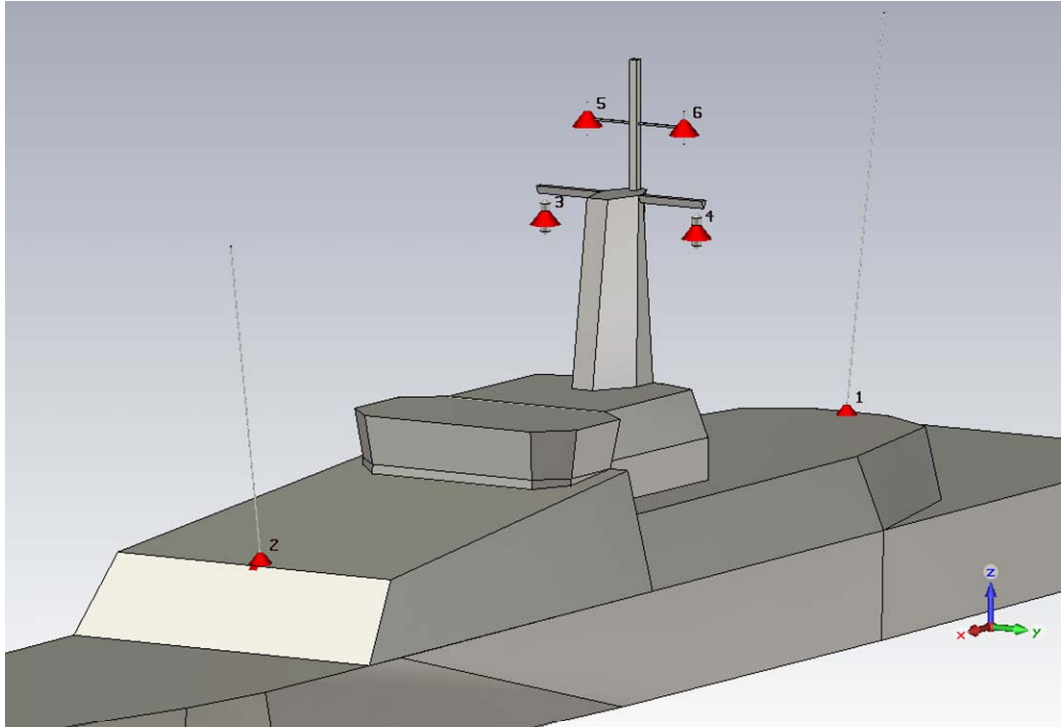


Figure 4-49 The Optimal Placement Plan for HF, VHF and V/UHF Antennas

CHAPTER 5

CONCLUSIONS AND FUTURE STUDIES

In this thesis study, the electromagnetic analysis of the communication antennas mounted on F-4 aircraft and the warship is carried out for improving the operational performance of these antennas by arranging their placements. The general conclusions obtained within the scope of this thesis study are summarized in the following items:

- Far field radiation pattern of a quarter wavelength monopole antenna mounted on a finite square ground plane is obtained by means of uniform GTD and GO.
- The change of far field radiation pattern of the monopole antenna and complex diffraction functions due to the variation of the width of a finite square ground plane is examined.
- As a result of the electromagnetic analysis of two UHF antennas mounted on simplified and original F-4 aircrafts, the location, that the mean value of the electromagnetic coupling levels between UHF antennas is minimal, is determined as the optimal location for the lower UHF antenna (newly installed antenna) among four different locations.
- It is observed that the far field radiation pattern of the lower UHF antenna at the optimal location on the original F-4 aircraft has sufficient directivity values in the region where the antenna has to operate efficiently.

- As a result of the electromagnetic analysis of UHF antennas mounted on geometrically simple structures composing simplified F-4 aircraft, the influences of geometrically simple structures and the locations of UHF antennas on the electromagnetic coupling between UHF antennas and the far field radiation patterns of the lower UHF antenna are observed.
- As a result of the electromagnetic analysis of HF antennas mounted on the warship, the placement plan, that the mean value of the electromagnetic coupling levels between HF antennas is minimal, is determined as the optimal placement plan for HF antennas among eleven different placement plans.
- As a result of the electromagnetic analysis of VHF and V/UHF antennas mounted on the warship, the placement plan, that the sum of the mean values of the electromagnetic coupling levels between VHF and V/UHF antennas is minimal, is determined as the optimal placement plan for VHF and V/UHF antennas among four different placement plans.
- The optimal placement plan for HF, VHF and V/UHF antennas is composed of these two optimal placement plans determined above.
- It is observed that the far field radiation patterns of HF, VHF and V/UHF antennas at their optimal locations on the warship have sufficient directivity values in the regions where these antennas have to operate efficiently.
- Also, the influences of the structural components such as mainmast, topmast, main yard and bridge of the warship, the locations of HF, VHF and V/UHF antennas and the sea on the electromagnetic coupling between these antennas and the far field radiation patterns of VHF and V/UHF antennas are observed.
- In order to determine the optimal locations of the communication antennas mounted on F-4 aircraft and the warship, the mean values of the electromagnetic coupling levels between the related antennas, obtained for different placement plans, are calculated over their operational frequency

bands coinciding with each other and these mean values are compared with each other. Because, there is a possibility of in-band interference between these antennas over their operational frequency bands coinciding with each other. Besides, in case these antennas are more frequently used at individual frequencies in their operational frequency bands, the minimization of the electromagnetic coupling levels at these frequencies has more priority than the minimization of the mean value of the electromagnetic coupling levels over the operational frequency bands of these antennas.

- Finally, in order to decrease the electromagnetic coupling between two communication antennas between which there is a possibility of in-band interference, the following three factors shall be taken into consideration while these antennas are located on the platform:
 - a. While these antennas are located on a ship, there shall be a structural component such as mainmast, topmast, main yard and bridge of a ship, which provides electromagnetic blockage against the radiation of these antennas towards each other, between these antennas. On the other hand, while these antennas are located on an aircraft, there shall be structural components such as fuselage, wings and nose of an aircraft, which provide electromagnetic blockage against the radiation of these antennas towards each other, between these antennas.
 - b. In case these antennas are mounted with the same polarization on the platform, the angle between the boresight of these antennas and the distance vector between these antennas shall be close to 90° as much as possible.
 - c. The physical distance between these antennas shall be large as much as possible.

Besides, future studies which can be carried out based on this thesis study are summarized in the following items:

- Radio Frequency (RF) components such as antenna tuning units, RF pre-selector filters and Intermediate Frequency (IF) filters existent in the communication system are not taken into consideration in the electromagnetic analysis of antennas performed within the scope of this thesis study. Therefore, in order to obtain more accurate results, these RF components can be taken into consideration in this analysis.
- In order to observe the influence of the mast of a ship on the far field radiation patterns of radar antennas and to decrease the electromagnetic coupling between radar antennas whose operational frequency bands coincide with each other, electromagnetic analysis of radar antennas mounted on a ship can also be performed by using CST MWS[®].
- In order to observe whether there is a risk of electromagnetic radiation hazards to ordnance and personnel due to high power transmitters such as HF antennas and radar antennas on the platform, electric field intensities generated by these transmitters can be examined in the electromagnetic analysis of antennas.

REFERENCES

- [1] G. Afacan, "The electrical characteristics of antennas in their operational environment," MSc Thesis, Middle East Technical University, Ankara, December 2007.
- [2] J. B. Keller, "Diffraction by an aperture," *Journal of Applied Physics*, vol. 28, no. 4, pp. 426-444, April 1957.
- [3] J. B. Keller, "Geometrical theory of diffraction," *Journal of the Optical Society of America*, vol. 52, no. 2, pp. 116-130, February 1962.
- [4] R. G. Kouyoumjian, "Asymptotic high-frequency methods," *Proceedings of the IEEE*, vol. 53, pp. 864-876, August 1965.
- [5] P. H. Pathak and R. G. Kouyoumjian, "The dyadic diffraction coefficient for a perfectly conducting wedge," Technical Report 2183-4 (AFCRL-69-0546), Ohio State University ElectroScience Laboratory, June 5, 1970.
- [6] P. H. Pathak and R. G. Kouyoumjian, "An analysis of the radiation from apertures on curved surfaces by geometrical theory of diffraction," *Proceedings of the IEEE*, vol. 62, no. 11, pp. 1438-1447, November 1974.
- [7] R. G. Kouyoumjian and P. H. Pathak, "A uniform geometrical theory of diffraction for an edge in perfectly conducting surface," *Proceedings of the IEEE*, vol. 62, no. 11, pp. 1448-1461, November 1974.

- [8] C. A. Balanis, *Advanced Engineering Electromagnetics*, John Wiley & Sons, New York, 1989.

- [9] C. A. Balanis, *Antenna Theory: Analysis and Design*, John Wiley & Sons, New York, 1982.

- [10] *CST MWS[®] 2009 - Workflow & Solver Overview*, CST Studio Suite[™] 2009, 2009.

- [11] S. A. Davidson and G. A. Thiele, "A hybrid method of moments-GTD technique for computing electromagnetic coupling between two monopole antennas on a large cylindrical surface," *IEEE Transactions on Electromagnetic Compatibility*, vol. EMC-26, no. 2, pp. 90-97, May 1984.